Neural Activity of 16p11.2 CNV Human and Mouse

Reem Al-Jawahiri

A thesis submitted for the degree of

Doctor of Philosophy

The University of Sheffield

Department of Psychology

Publication arising from this thesis:

Al-Jawahiri, R., Jones, M., and Milne, E. (2019). Atypical Neural Variability in Carriers of 16p11.2 Copy Number Variants. *Autism Research*. doi:10.1002/aur.2166

Acknowledgements

Abstract

Although rare in the population, individuals affected by deletions or duplications of DNA material at 16p11.2 chromosomal region (within the region '11.2' in the short arm of chromosome 16) are at higher risk of myriad clinical features and neurodevelopmental disorders including intellectual disability, developmental delays, and autism spectrum disorder. Whether inherited or appearing for the first time in the family, this 16p11.2 copy number variation (CNV) seems to impact on brain structure and function that may, in turn, drive the profile and severity of 16p11.2 associated phenotypes. As studies of 16p11.2 CNV brain function are scarce, the aim of this thesis is to investigate EEG activity in (human) 16p11.2 CNV carriers and parallel in-vivo electrophysiological activity in 16p11.2 deletion mouse model. Data-sharing platforms and collaborative efforts made it possible to access datasets of this rare population and analyse it for the purpose of this thesis. The thesis is comprised of three studies: 1) an investigation of visual-evoked neural variability, as measured by variability of intra-participant ERP and spectral power, and signal-to-noise ratio, in 16p11.2 CNV carriers; 2) a study of spontaneous neural activity, as measured by multi-scale entropy and conventional spectral power, in 16p11.2 deletion carriers; and 3) a study of spontaneous neural activity in 16p11.2 deletion mouse model. Neural variability was mostly higher in 16p11.2 deletion carriers relative to typical controls and 16p11.2 duplication carriers. Compared to typical controls, higher entropy was found in 16p11.2 deletion carriers and this was associated with certain psychiatric and behavioural traits, e.g., anxiety problems. The 16p11.2 deletion mice showed no group differences in neural activity compared to wild-type control mice. In conclusion, despite the lack of converging evidence from the mouse model, the collective 16p11.2 CNV human findings indicated that neural activity in 16p11.2 deletion carriers, especially, was altered and related to psychiatric traits found in 16p11.2 deletion carriers.

Contents

List of Figures

List of Tables

Chapter 1   16p11.2 CNV Human and Mouse

The aim of this thesis is to investigate functional brain alterations, as revealed via EEG and in-vivo electrophysiology, in 16p11.2 copy number variation (CNV) human carriers and mouse model. Prior to discussing 16p11.2 CNV characteristics and the relevant literature, the following sections outline and describe what '16p11.2' denotes.

1.1   The 16p11.2 genomic address

'16p11.2' could be thought of as a postcode that leads to a specific address in the genome. It is an abbreviated form of address that dictates the specific chromosome, chromosome-arm, region, and sub-region (as will be elaborated in the following paragraphs).

The human DNA (deoxyribonucleic acid) consists of long strands of protein-coding and non-coding material that are ~ 2 metres long when stretched. To contain DNA into the nucleus of each cell, DNA is packaged into structures called chromosomes. There are typically 23 homologous pairs of chromosomes in human cells (i.e., 46 chromosomes per cell, except for gametes which have 23 chromosomes). To refer to a particular chromosome, the pairs have been numbered from 1 to 22 (generally from largest to smallest), with the 23rd pair labelled either as 'x' and 'y' or 'x' and 'x' (which determines an individual's sex). The '16' in the genomic address of '16p11.2', therefore, refers to the 16th chromosome pair (**Figure 1.1**).
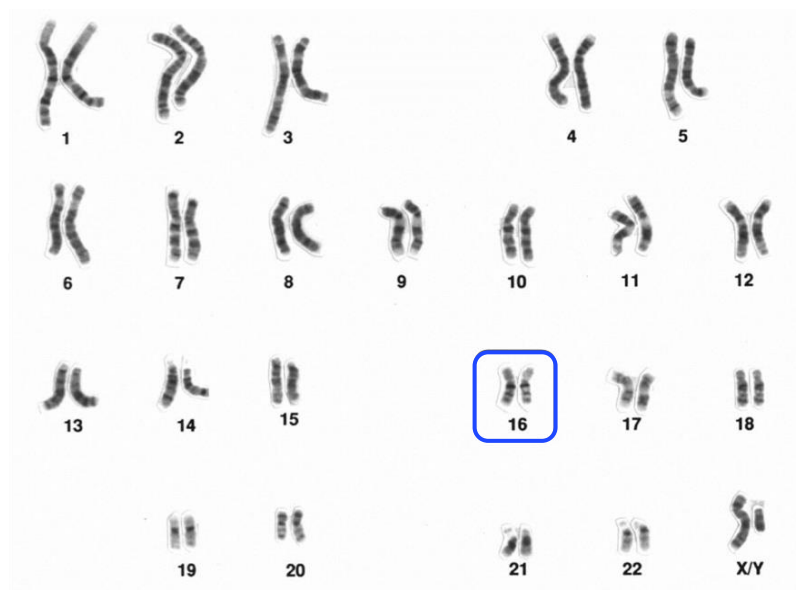
Figure 1.1: Karyotype of a human male.
The blue rectangle points out chromosome 16. *Courtesy: National Human Genome Research Institute. https://www.genome.gov/*

Whereas the 'p' in '16p11.2' narrows this down to the short arm/s of chromosome 16 (**Figure 1.2**). Finally, the '11.2' in '16p11.2' further specifies a smaller region within 'p' (shaded area in **Figure 1.3**) and close to the centromere (the narrow region near the centre that separates the chromosome into short and long arms).
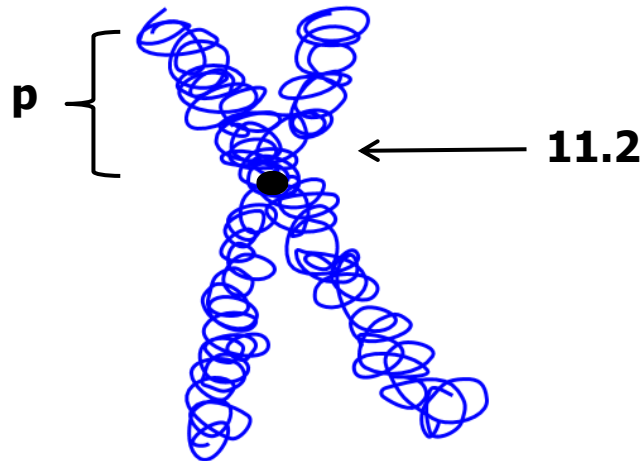
Figure 1.2: The 16p11.2 chromosomal region.
This figure represents chromosome 16. The bracket indicates the 'p' region ('p' stands for petit; meaning 'small' in French), which represents the short arm/s of chromosome 16. The arrow points to the '11.2' region. The black circle indicates the centromere.

The smaller region of interest to this thesis (area outlined in **Figure 1.3**), within the 16p11.2 region, spans ~ 600 thousand DNA building blocks, or base pairs (bp; from a total of ~ 90 million bp in chromosome 16) with start and end points at ~ 29.68 and ~ 30.21 million bp, respectively (breakpoints 4 and 5; genome reference hg18). This region encompasses ~ 29 genes (from a total of more than 800 genes in chromosome 16; http://www.ensembl.org; **Figure 1.3**); Many of which are highly expressed in the (human) brain (e.g., *KCTD13*, *TAOK2*, and *SEZ6L2*) and some play a role in regulating gene expression (e.g., *MAPK3*, *MAZ*, *TBX6*, *HIRIP3*, and *INO80E*; Nucleic Acids Research, 2016).

Henceforth, any reference to '16p11.2' will be in relation to the smaller region of interest (within 16p11.2) described here and frequently termed the 'proximal' 16p11.2 region in the literature.

~ 29.68 Mbp

SEP1
MYLPF
TBC1D10B
CD2BP2
SPN
QPRT
C16orf54
ZG16
KIF22
MAZ
PRRT2
C16orf53
MVP
CDIPT
SEZ6L2
ASPHD1
KCTD13
TMEM219
TAOK2
HIRIP3
INO80E
DOC2A
C16orf92
FAM57B
ALDOA
PPP4C
TBX6
YPEL3
GDPD3
MAPK3
CORO1A
BOLA2
SLX1B

~ 30.21 Mbp

Chromosome 16

p13.3
p13.2
p13.13
p13.12
p13.11
p12.3
p12.2
p12.1
p11.2
p11.1
q11.1
q11.2

q12.1
q12.2
q13
q21

q22.1

q22.2
q22.3
q23.1

q23.2

q24.1
q24.2
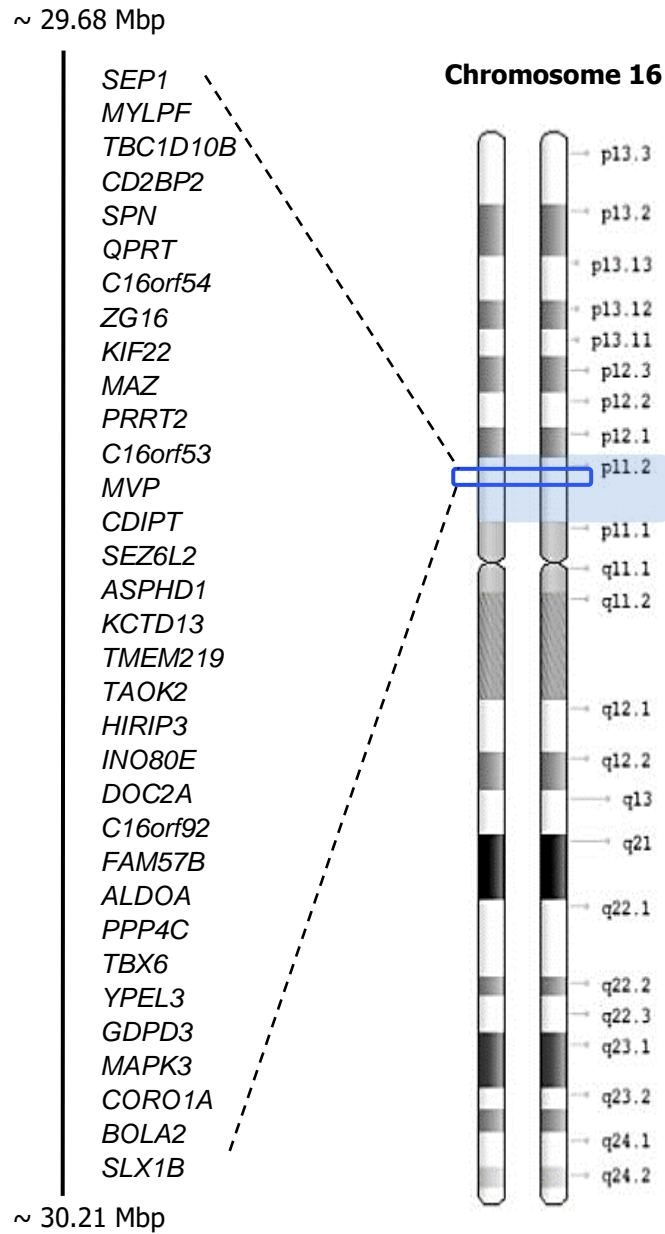
Figure 1.3: Genes within the 16p11.2 region of interest.
The 'p11.2' region is shaded in light blue. The smaller region of interest is outlined in blue,
zoomed in to show the gene content. Genes are arranged in linear order. *Courtesy: Genome
Decoration Page/National Centre for Biotechnology Information*.
https://www.ncbi.nlm.nih.gov/genome/tools/gdp

1.2 Role of key genes within the 16p11.2 region

Although the roles of the genes within the 16p11.2 region and how they contribute to the 16p11.2 CNV phenotype remain largely unknown, the likely molecular functions of certain key genes are summarised below.

The KCTD13 gene (potassium channel tetramerization domain containing 13; Abrahams et al., 2013; Escamilla et al., 2017) has been suggested to play a role in the degradation of an enzyme called RhoA (Ras homolog gene family, member A). The degradation of RhoA regulates the formation of actin cytoskeletion (the structure that supports the shape of a cell among other functions) and thus leads to the formation of dendritic spines and enhanced synaptic transmission.

The TAOK2 gene (thousand and one amino-acid Kinase 2; Abrahams et al., 2013; Richter et al., 2019) also affects RhoA activity, similar to KCTD13 – although in an opposing manner: TAOK2 enhances RhoA activity, whereas KCTD13 degrades RhoA. Thus, TAOK2 and KCTD13, together, regulate RhoA activity and promotes dendritic spine formation and neural communication. Loss of TAOK2 was found to lead to reduced RhoA activity, particularly in the cerebral cortex, and reduced the formation of dendritic spines.

The MAPK3 gene (mitogen-activated protein kinase 3; also known in the literature as extracellular signal-regulated kinases (ERK1); Abrahams et al., 2013; Pucilowska et al., 2015) encodes for the MAPK/ERK pathway, which is a cascade of protein interactions in a cell that transfer the signal from the cell's receptor to the cell's DNA. In response to various extracellular signals, the MAPK/ERK pathway regulates cellular processes including the progression of the cell cycle, cell proliferation, and cell differentiation.

The MVP gene (major vault protein; Stelzer et al., 2016; Jacque et al., 2018) encodes for a protein required for vault structure – a structure that carries RNA, proteins, and other molecules between the nucleus and cytoplasm. MVP also regulates other genes including STAT1 (signal transducer and activator of transcription 1 – a gene involved in immune function). MVP/STAT1 interactions were suggested to play a role in homeostatic plasticity, which is the ability of neural connections to adapt to changes in experience.

The roles of the individual genes within the 16p11.2 region are useful to elucidate the link from genotype to phenotype, however, it is important to note that gene interactions

within the CNV region and outside may contribute to the complex and heterogeneous 16p11.2 CNV phenotypes.

1.3 Copy number variation at the 16p11.2 region

Usually, a typically developing individual would carry two copies of the 16p11.2 region (and indeed the rest of the DNA). However, in the event of a deletion, cells would only have one copy of the 16p11.2 region, while in the event of a duplication, there would be three copies (**Figure 1.4**). When the deleted or duplicated regions are large (>1000 nucleotide base pairs, often spanning many genes and non-encoding regions), they are referred to as copy number variations (CNVs). Deletions and duplications occurring at the same chromosomal region (e.g., proximal 16p11.2) are termed reciprocal CNVs. CNVs, therefore, are a type of structural variation that can be pathogenic as is the case in 16p11.2 CNVs.
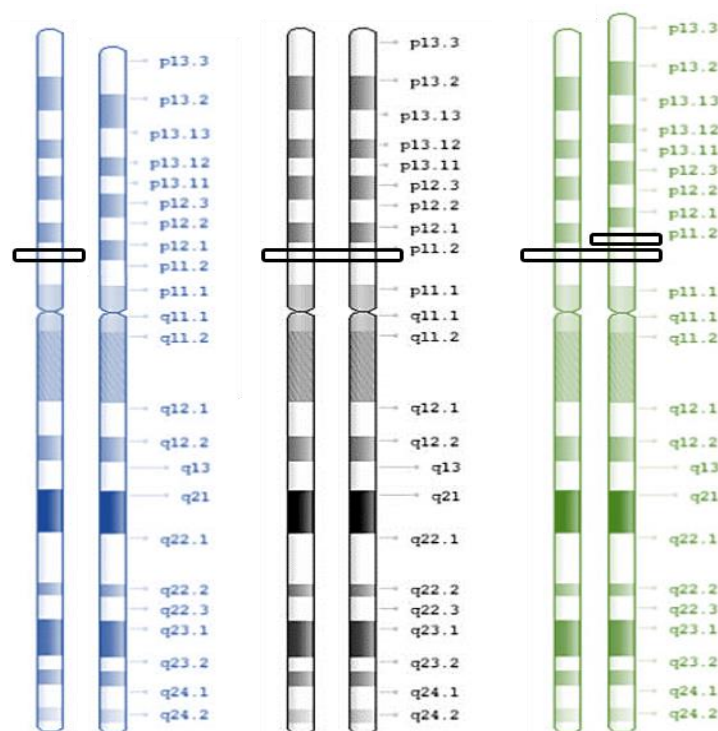
Figure 1.4: 16p11.2 CNV.
Rectangles indicate the '16p11.2' region. The colours blue, black, green indicate deletion, typical, and duplication, respectively. *Courtesy: Genome Decoration Page/National Centre for Biotechnology Information.* https://www.ncbi.nlm.nih.gov/genome/tools/gdp

CNVs may be inherited or may appear for the first time in one family member. A newly occurring CNV is termed a de-novo CNV. One mechanism that gives rise to de-novo CNVs is non-allelic homologous recombination (NAHR). Homologous recombination is the

process by which broken strands of DNA join with other homologous (i.e., similar or identical) strands of DNA. During meiosis (i.e., the process of cell division of gametes), homologous chromosomes, e.g., maternally- and paternally-derived chromosome 16, align together prior to undergoing homologous recombination. In this example, a particular region in the maternal chromosome 16 is exchanged with the same region in the paternal chromosome 16. However, in the event of a NAHR, homologous chromosomes misalign and therefore lead to non-allelic exchange of DNA material (i.e., exchange of similar DNA between two different regions in the same or different chromosome). Thus, the resulting daughter gametes, that underwent NAHR, have chromosomal imbalances in the form of either a deletion or duplication (in other words, a CNV) of the affected genetic region. Notably, there are certain hotspots in the genome where NAHR are more likely to occur. These tend to be in regions with highly similar base sequences (98.5-99%) within the genome, termed low copy repeats (LCRs, also known as segmental duplications). Due to this high sequence similarity, there is more susceptibility for errors to occur in the normal event of meiotic recombination.

1.4 16p11.2 CNV prevalence and pathogenicity

16p11.2 CNVs are rare in the population as only ~ 5 in 10,000 people carry a deletion, and only ~ 4 in 10,000 people carry a duplication (Kirov et al., 2014). Notably, a 16p11.2 CNV is not sufficient for carriers to develop difficulties and disorders, as some carriers seem unaffected by the CNV (i.e., 16p11.2 CNVs have incomplete penetrance; Kirov et al., 2014). Nevertheless, the risk for developing one or more of the possible associated disorders is relatively high for 16p11.2 CNV carriers (Shinawi et al., 2010; D'Angelo et al., 2016; Hanson et al., 2015; Niarchou et al., 2019). In addition, the consequences of this CNV are quite heterogenous as they vary from one individual to another in their severity and phenotypes (i.e., showing a high degree of pleiotropy; Girirajan and Eichler, 2010; Niarchou et al., 2019). This heterogeneity can be obvious in carriers within the same family and across families irrespective of inheritance status (i.e., inherited vs. de novo CNV).

When inherited, the inheritance pattern is autosomal dominant (Miller et al., 2009), which means that there is a 50% chance that the offspring of a carrier would inherit this CNV. Interestingly, when comparing 16p11.2 deletion vs duplication carriers, the latter group are more frequently identified as inheriting the CNV. While the former group (deletion

carriers) have more frequent de-novo cases, i.e., a new 16p11.2 deletion case appearing in the family for the first time (Duyzend et al., 2016; D'Angelo et al., 2016).

1.5 16p11.2 CNV detection

Although studies suggest that 16p11.2 CNVs are rare in the population, it is possible that the frequency of these CNVs is underestimated. This is because certain people with this genotype may not exhibit severe or obvious phenotypes, therefore they are not detected. Whereas those with more severe phenotypes, especially in relation to developmental delays and psychiatric phenotypes such as autism spectrum disorder (ASD)[1], are more likely to be referred for genetic screening and detected for 16p11.2 CNV. This is especially true in de-novo cases, as when an inherited case is detected, further screening is normally recommended for first-degree relatives.

1.5.1 Karyotyping

There are several techniques for detecting CNVs in the DNA. Conventional karyotyping is the process of detecting CNVs involving at least several megabase pairs (Mbp; million base pairs) through a microscope (Sinclair, 2002). The chromosomes are first stained using standardised staining procedures that reveal characteristic dark and light bands of each chromosome (**Figure 1.1** and **Figure 1.3**). However, 16p11.2 CNVs are too small to be visible using karyotyping alone (16p11.2 CNV = ~ 600 Kbp; thousand base pairs). Therefore, 16p11.2 CNVs are typically detected by fluorescent in situ hybridization (FISH), comparative genomic hybridization (CGH), or a combination of the aforementioned techniques.

1.5.2 Fluorescent in situ hybridisation

Fluorescent in situ hybridisation (FISH) is a technique that uses fluorescent single strands of DNA (i.e., probes) that are complementary to the DNA sequence of interest: the 16p11.2 region (O'Connor, 2008). Under certain conditions, these probes then bind only with their target matched DNA sequences, i.e., the 16p11.2 region from the DNA sample of the individual suspected to have a 16p11.2 CNV. Based on the absence or presence of a fluorescent signal, 16p11.2 deletions or duplications are identified under a microscope.

---

[1] There is some controversy regarding the terminology used to refer to ASD (Kenny et al., 2016). For this thesis, I made the decision to use the terms/acronym 'ASD' because Kenny et al. (2016) showed that it is among the most endorsed term across ASD communities.

1.5.3 Comparative genomic hybridisation

With the comparative genomic hybridisation (CGH) technique (Theisen, 2008), the DNA sample of the suspected 16p11.2 carrier (i.e., target sample) is compared with the DNA sample from a typical control (i.e., reference sample) for CNVs. Probes (i.e., a single-stranded DNA) from the target sample are labelled with green fluorescence, whereas probes from the reference sample are labelled with red fluorescence. The two samples are mixed and applied to the microarray (i.e., DNA chip; a collection of DNA probes, complementary to those in the two samples, attached to a solid surface typically a glass slide). The target and reference sample then compete to bind to the microarray. This process of binding two complementary single-stranded DNA and forming a double-stranded DNA via base pairing is termed hybridisation. The fluorescent signals are then measured by the microarray scanner and analysed with a dedicated computer software. Higher intensity of red indicates deletions; Conversely, higher intensity of green indicates duplications. A net colour of yellow indicates equilibrium: the target sample and reference sample bind in equal amounts to the microarray.

1.5.4 Single nucleotide polymorphism array

A single nucleotide polymorphism (SNP) refers to a variation at a single nucleotide base (adenine, cytosine, guanine, or thymine) in a specific locus in the genome in the population (with the rarer variant found in at least 1% of the population). The SNP array technique shares the same basic principles as CGH: 1) the use of probes marked with fluorescent dyes; 2) hybridisation of probes to the microarray; 3) and the use of algorithms to interpret the intensity of fluorescent signals. Here, the target DNA sample (i.e., DNA probe from the suspected 16p11.2 CNV carrier) is hybridised to the SNP array. The SNP array consists of probes, from a reference human genome, known to contain multiple alleles[2]. The array contains two probes to represent the different alleles (AA, BB, or AB) and the location on the array indicates the locus of the SNP in the genome. If the target DNA sample is homozygous for either the A or B alleles, then the sample will hybridise to the A or B alleles, respectively (AA, BB). Otherwise, the sample will hybridise to the A and B alleles (AB). In the event of a deletion or duplication (i.e., CNVs), the alleles will be missing (A-, or -B) or duplicated (AAAA, AAAB, ABBB, or BBBB). As the different alleles are labelled with particular

---

[2] An allele is a variant form of a gene. If an individual carries the same variant on both chromosomes, then this individual is homozygous for the respective allele, typically denoted as AA or the alternative allele BB. If an individual carries one copy of each allele, then this individual is heterozygous for the allele AB.

fluorescent colours, SNPs and CNVs may be inferred via quantification of the fluorescent signal intensities.

1.5.5 Next-generation sequencing

Next-generation sequencing (NGS) refers to methods that determine the order of nucleotide bases in the DNA using advanced sequencing technologies and bioinformatics. There are various NGS methods, however, they share certain basic principles. These methods sequence sections of DNA of millions of nucleotides long in parallel. Basic steps generally involve the following; 1) The target DNA is fragmented into sections (the length depends on the technology used); 2) amplification of DNA fragments via clustering of individual fragments; 3) The clustered/amplified fragments are then sequenced; 4) The sequences are aligned to the reference genome. CNVs can then be identified. In summary, 16p11.2 CNVs are rare deletion or duplication events of the '16p11.2' region implicating approximately 29 genes. Whether inherited or de-novo, 16p11.2 CNV carriers present with a spectrum of traits and difficulties (although the clinical profile and severity vary from one individual to another). 16p11.2 CNVs are detected, using techniques such as CGH, predominantly in clinically referred cases with intellectual disability. However, 16p11.2 CNV carriers are associated with numerous disorders, which fall under the ESSENCE umbrella acronym, as will be explained in the following section.

1.6 The ESSENCE Framework

The current section will introduce the ESSENCE approach and its relevance to 16p11.2 CNVs, forming the basis for my rationale for adopting this approach in the current thesis.

1.6.1 Defining ESSENCE

It is not uncommon for a person presenting trait characteristics of one psychiatric disorder to also show traits and difficulties characteristic of another disorder or even partial traits relating to numerous other disorders. In fact, comorbidities and shared traits among neurodevelopmental and psychiatric disorders seem to be the rule rather than the exception (e.g., Kadesjö and Gillberg, 2001). Evidence showing overlaps between these heterogeneous disorders, in terms of clinical symptoms and genetic and environmental risk factors, is mounting (Doherty and Owen, 2014; Gandal et al., 2018; The Brainstorm Consortium, 2018). This gave rise to the conceptual framework behind the 'ESSENCE' umbrella acronym, which refers to Early Symptomatic Syndromes Eliciting Neurodevelopmental Clinical Examinations

(Gillberg, 2010). Rather than considering individual neurodevelopmental/psychiatric disorders as unique conditions, ESSENCE refers to them as a whole group, typically presenting with early impairments in some or all of the fields of 1) general development, 2) communication and language, 3) social inter-relatedness, 4) motor coordination, 5) attention, 6) activity, 7) behaviour, 8) mood, and/or 9) sleep. Some examples of disorders that would fall under the ESSENCE umbrella acronym include ASD, attention deficit hyperactivity disorder (ADHD), oppositional-defiant disorder, early-onset bipolar disorder, early-onset schizophrenia (although it is possible that some later-onset psychiatric disorders should qualify as ESSENCE disorders), etc. It is important to clarify that while the ESSENCE framework supports merging these disorders into one large group, it is not against segregating these disorders into meaningful subgroups per se; Rather, it is a renewed call for researchers and clinicians to first approach these disorders as a large group prior to segregating them into meaningful ways (when it is possible to do so) for refined research and specialised intervention.

1.6.2 16p11.2 CNV and ESSENCE

In light of this, the current thesis conceptualises 16p11.2 CNVs as presenting with ESSENCE traits/disorders (as will be described in detail in later sections). This is especially suitable as individuals with 16p11.2 CNV vary widely in their clinical profile and impairment severity in ESSENCE-related traits (Girirajan and Eichler, 2010; Shinawi et al., 2010; Hanson et al., 2015; Niarchou et al., 2019). In addition, comorbidities are common in 16p11.2 CNV carriers (Niarchou et al., 2019): E.g., deletion carriers were found to have an average of ~3 diagnoses (Hanson et al., 2015). Accordingly, it would be accurate to describe 16p11.2 CNV as generally relating to ESSENCE as a whole. Considering 16p11.2 CNV in this way serves as a useful reminder of the heterogeneous nature of this CNV, and draws attention to the potential relevance of literature in relation to any one of the ESSENCE disorders. Therefore, I will consider 16p11.2 in the context of the ESSENCE framework, in this thesis.

Another distinction can be made between studies that adopt a phenotype-first approach vs a genotype-first approach to studying ESSENCE traits and disorders. A phenotype-first approach consists of recruiting participants based on their clinical diagnosis; This is contrary to the genotype-first approach, which involves grouping individuals based on a shared genetic mutation or deleterious variation (e.g., The Simons VIP Consortium, 2012, see **chapter 2, Section 2.2.1**) regardless of the presented variability in phenotype and diagnoses. This approach is consistent with the conceptual framework behind the ESSENCE

umbrella acronym. In that context, the current thesis follows a genotype-first approach to studying a group screened for 16p11.2 CNVs irrespective of their ESSENCE profile and severity.

1.7 Consequences of 16p11.2 CNV

Unlike other mutations, a CNV is a gene-dosage problem (i.e., having a smaller or larger number of genes than typical cells); which could result in an imbalance in the expression of the genes in the CNV region. For reciprocal CNVs (i.e., deletions and duplications occurring in the same region), it is intuitive to presume that gene-expression changes would follow a linear relationship (deletion < control < duplication), which ultimately leads to opposing phenotypes. Indeed, for 16p11.2 CNVs, gene expression in the CNV region was in line with gene dosage: deletions resulted in under-expression, whereas duplications resulted in over-expression of the genes in the 16p11.2 region – with no evidence of dosage compensation (Blumenthal et al., 2014). Although some phenotypes associated with 16p11.2 CNV might exhibit a linear relationship with gene-dosage, this is probably a simplistic view. The effects of 16p11.2 CNVs extend beyond the genes within its region; E.g., associations were found between 16p11.2 CNVs and altered expression patterns outside the CNV region (Blumenthal et al., 2014). Additionally, the overall genetic background and environmental factors also play an enhancer and/or suppressive role towards the presented phenotypes and their directionality.

Consequences of 16p11.2 CNV have been studied on multiple levels (e.g., chromatin looping interactions, Loviglio et al., 2017). However, for the purpose of this thesis, the focus in the following sections will be on describing 16p11.2 CNV clinical phenotypes, brain structure, and brain function, in addition to the relationship between these levels where possible.

1.7.1 Genotype-phenotype models

Despite the complexity of the impact of 16p11.2 CNVs on phenotypes, it is useful to categorise the relationship between 16p11.2 reciprocal CNVs and their phenotypes into the following theoretical models (**Figure 1.5**; Deshpande and Weiss, 2018).

1.7.1.1 Additive model: opposing phenotypes

This model represents the phenomenon, described earlier, by which 16p11.2 deletions and duplications, respectively, contribute to opposing phenotypes (**Figure 1.5a**). This relationship

has been observed regarding the physical features of 16p11.2 CNV carriers, as will be described later.

1.7.1.2 Dominant model: unique phenotypes

In this model, a change in the copy number in only one direction, e.g., either a deletion or duplication, leads to a deleterious phenotype (**Figure 1.5b**). Indeed, some ESSENCE traits/disorders seem to be mainly associated with either 16p11.2 deletion or duplication.

1.7.1.3 U-shaped model: shared phenotypes

In this model, the deleterious phenotype is shared between the 16p11.2 reciprocal CNVs (**Figure 1.5c**). The U-shaped model is as such because both deletions and duplications are associated with either an increase (U-shape) or decrease (inverted U-shape) of the same phenotype (therefore leading to a pathological state as it deviates from the average). As will be described in the later sections, there is a large overlap in many ESSENCE traits.
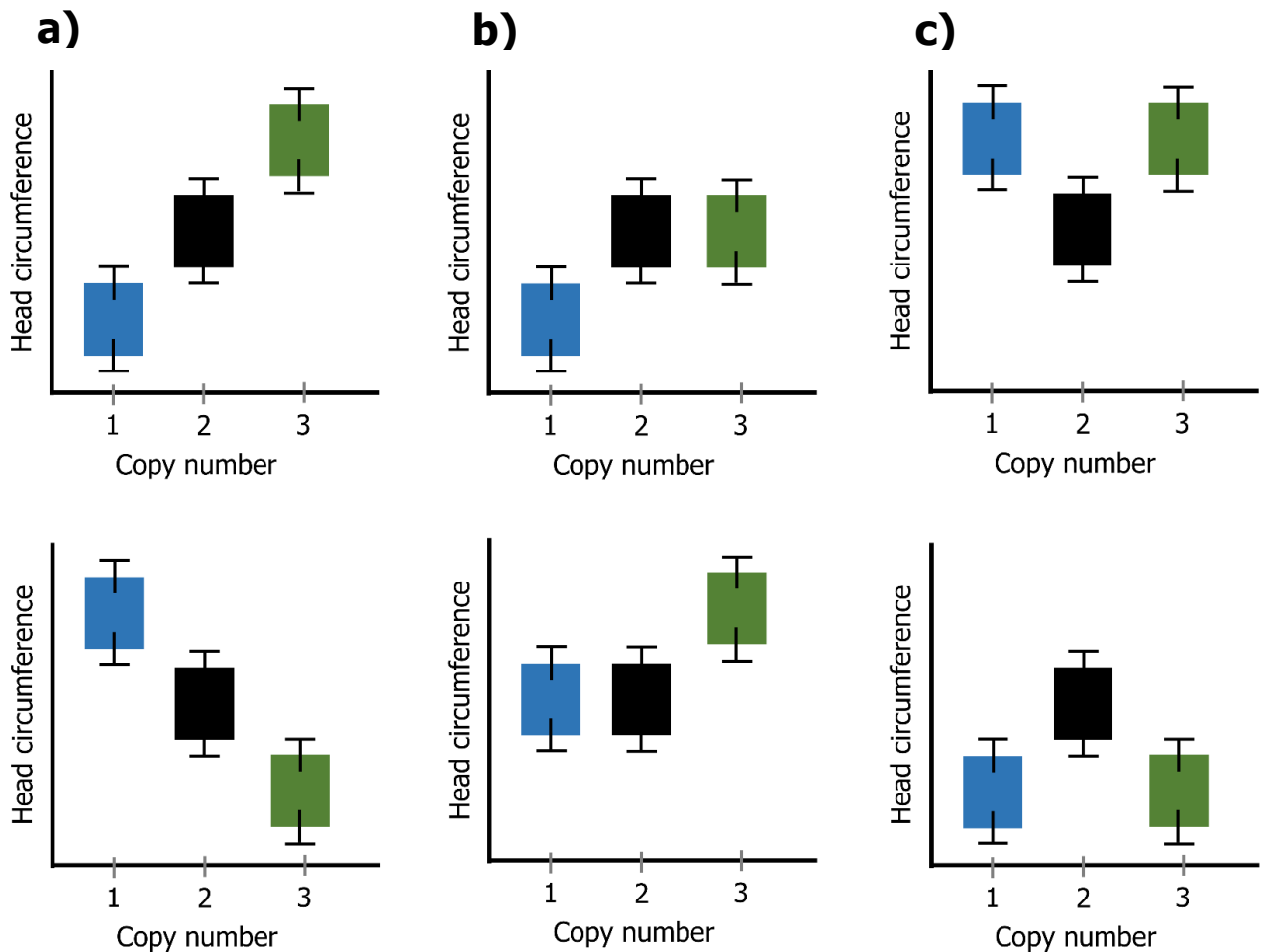
Figure 1.5: Theoretical models of the impact of copy number on phenotypes.
Here, head circumference (HC) is used as an example of a quantitative phenotype. Extreme forms of this phenotype are microcephaly (decreased HC) and macrocephaly (increased HC). X-axis indicates the deletion group (1 copy number of the '16p11.2' region), control group (the typical amount of 2 copy numbers), duplication group (3 copies). Boxplots representing a) the additive model: Copy number impacts HC in an opposing manner leading to microcephaly in deletions and macrocephaly in duplications, vice versa. b) The dominant model: Copy number change in only one direction (e.g., deletion) leads to micro- or macrocephaly, whereas the outcome of a change in the other direction (e.g., duplication) is a HC in the typical range, or vice versa. c) The U-shaped model: Both deletions and duplications lead to the same atypical phenotype, e.g., either macro- or microcephaly.

1.7.2 16p11.2 CNV ESSENCE traits and disorders

As mentioned earlier, 16p11.2 CNV carriers can be characterised as presenting with myriad ESSENCE traits and disorders. Evidence is drawn from 1) studies that investigate the prevalence of CNVs in psychiatric populations (phenotype-genotype approach); and 2) studies that conduct phenotypic characterisation of individuals with 16p11.2 CNV (i.e., genotype-phenotype approach). From the first approach, 16p11.2 CNVs were frequently identified in psychiatric/ESSENCE populations, including intellectual disability and

developmental delay (deletion and duplication, Kaminsky et al., 2011; Weiss et al., 2008; Cooper et al., 2011), ASD (deletion and duplication, Walsh and Bracken, 2011; Sanders et al., 2011; Weiss et al., 2008; deletion, Kumar et al., 2008), schizophrenia (duplication, Zhou et al., 2018, Marshall et al., 2017; McCarthy et al., 2009), bipolar disorder (duplication, Green et al., 2016), and depression (duplication, Kendall et al., 2019; deletion and duplication, Degenhardt et al., 2012). From the second approach (i.e., genotype-phenotype approach), deep phenotypic characterisation of 16p11.2 CNV carriers also revealed high frequencies of a range of ESSENCE disorders and traits.

To summarise the results of studies using the second approach, a systematic review was conducted in this thesis. The Scopus database was used to search for the term "16p11.2" within the title, abstract, and keywords of the journal articles. In addition, the reference lists/citations of all articles identified as highly relevant were manually checked for other potentially relevant papers. Abstracts of the search results (and reference list manual search) were screened and classified as relevant if they included the terms relating to ESSENCE disorders/traits such as "psychiatric", and/or key terms relating to the process of phenotyping and determining disorder prevalence, such as "frequency". Full text articles of relevant papers were then inspected prior to formulating the optimal inclusion criteria for the review in this thesis.

A few observations were made, which formed the basis of the inclusion criteria. 1) Most studies lacked data of 16p11.2 CNV adults. Studies typically reported the genotype-phenotype associations in children with 16p11.2 CNVs (Chawner et al., 2019; Niarchou et al., 2019; D'Angelo et al., 2016; Snyder et al., 2016; Hanson et al., 2015; Hippolyte et al., 2015; Zufferey et al., 2012; Hanson et al., 2010; Shinawi et al., 2010; Fernandez et al., 2010; Rosenfeld et al., 2010). Therefore, this review only included studies reporting results relating to 16p11.2 CNV children. 2) Generally, the more recent the study, the larger the sample size; This is due to larger projects, but also due to studies combining data from previous studies and collaborative efforts. To avoid overlaps, the data sources and sample sizes of relevant studies were noted (**Table 1.1**). Based on this information, this review only included the most recent findings and prioritised reporting results of studies with larger sample sizes. Duplications in information between the studies mentioned in **Table 1.1** were avoided (e.g., ADHD data reported in studies prior to Niarchou et al. (2019) including Hanson et al. (2015) were not presented in this review); Data regarding the specific diagnoses reported in **Table**

1.1 were extracted from the respective studies. The Search was last carried out in December 2019. Therefore, any studies post this date are not included.

Table 1.1: 16p11.2 CNV genotype-phenotype data sources and sample sizes.

Data source		*del %*	*del (n)*	*dup %*	*dup (n)*
Niarchou et al. (2019)	ADHD	29	63	42	48
ECHO study	Psychotic symptoms	4	5	11	7
16p11.2 European Consortium	ODD/CD	7	15	12	14
IMAGINE-ID	ASD	22	41	26	26
Simon's VIP	ID	30	61	34	36
	Any anxiety disorder	9	20	12	14
	Total (N)		**217**		**113**
D'Angelo et al. (2016)	Epilepsy/ all seizure types	19	73	14	37
16p11.2 European Consortium ECHO study Simon's VIP	**Total (N)**		**390**		**270**
Hanson et al. (2015)	Phonological Processing Disorder	56	44		
Simon's VIP	Language Disorders	46	36		
	Coordination disorder	58	45		
	Learning disorders	13	10		
	Tic Disorder	6	5		
	Total (N)		**78**		
Snyder et al. (2016)	Phonological (articulation) Disorder			19	12
Simon's VIP	Language Disorders			10	6
	Coordination disorder			47	29
	Learning disorders			3	2
	Mood disorder			3	2
	Tic Disorder			3	2
	Total (N)				**62**

The results of the systematic review consisting of the latest findings relating to the prevalence of ESSENCE disorders in 16p11.2 CNV children are presented in **Figure 1.6** (Niarchou et al., 2019; D'Angelo et al., 2016; Snyder et al., 2016; Hanson et al., 2015).
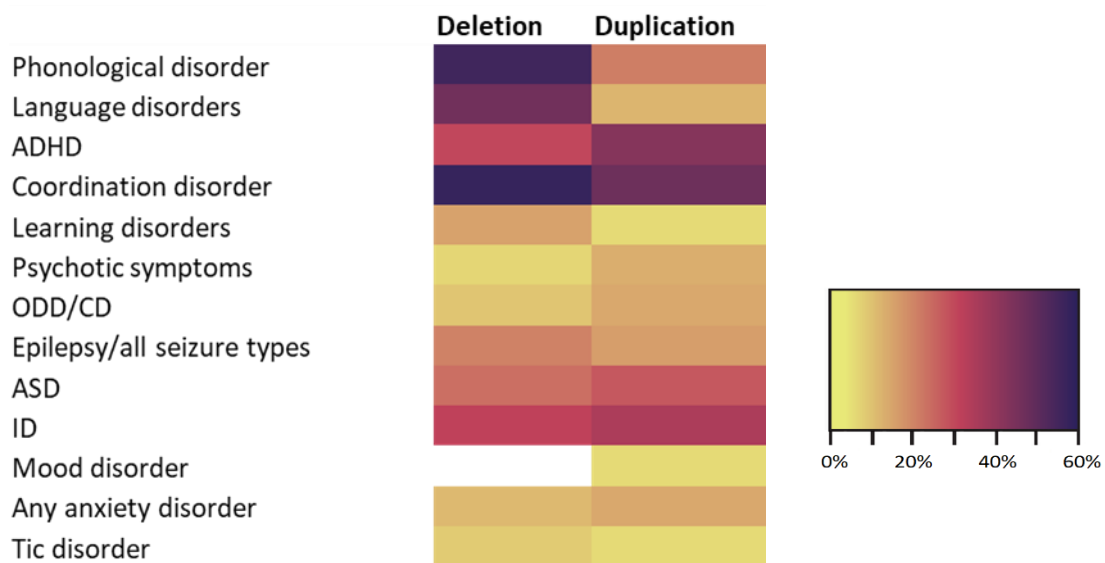
Figure 1.6: Frequency of ESSENCE disorders in 16p11.2 CNV carriers.
The lighter the colour, the lower the frequency of diagnoses. Note that the colour white indicates data is not available. The disorders are ordered in descending order in terms of the contrast in the frequency of diagnoses between deletion and duplication carriers (i.e., the prevalence of disorders at the top largely differ between deletion and duplication carriers, whereas disorders at the bottom are similarly prevalent in both deletion and duplication carriers. *ADHD, attention deficit hyperactivity disorder; ASD, autism spectrum disorder; ODD/CD oppositional defiant disorder/conduct disorder; ID intellectual disability.*

As shown in **Figure 1.6**, deletion carriers have a high frequency (> 30%) of phonological and language disorders, coordination disorder, intellectual disability, and ADHD. ASD was also prevalent (22%). Duplication carriers have high frequencies (> 30%) of coordination disorder, ADHD, and intellectual disability. ASD was similarly prevalent in duplication carriers as deletion carriers (26%). Based on the contrast in the frequencies of ESSENCE disorders present in 16p11.2 deletion vs duplication carriers, a dominant model (unique phenotypes) is more likely to apply to the following disorders (ordered in the top of the list of disorders in **Figure 1.6**), phonological disorders and language disorders. Although not presented in **Figure 1.6** (due to the lack of data), schizophrenia is a possible phenotype that could be regarded as common in 16p11.2 duplication carriers (as it was not frequently found in deletion carriers; Zhou et al., 2018, Marshall et al., 2017; McCarthy et al., 2009).

Most disorders, however, seem to be presenting a U-shaped model demonstrating shared phenotypes between 16p11.2 deletions and duplications (although examination of the severity of the manifested disorders would further inform the shape of this model). Due to the nature of this data, it is not suitable to infer any opposing phenotypes that would fall under the additive model.

A recent study (Chawner et al., 2019) examined the quantitative effect of numerous pathogenic CNVs collectively on ESSENCE traits. However, as the focus of this thesis is on 16p11.2 CNVs, relevant data from supplementary files in Chawner et al. (2019) were extracted and presented in **Figure 1.7**.

Deletion **Duplication**

Subclinical psychotic experiences (child CAPA)
Anxiety CAPA subscale
Total CAPA symptom count
ADHD CAPA subscale
SDQ total (caregiver report)
ODD CAPA subscale
Hyperactivity SDQ subscale (teacher report)
Mood CAPA subscale
OCD CAPA subscale
Hyperactivity SDQ subscale (caregiver report)
Conduct SDQ subscale (caregiver report)
Emotional SDQ subscale (teacher report)
Emotional SDQ subscale (caregiver report)
Spatial planning
SDQ total (teacher report)
Sleep CAPA subscale
Prosocial SDQ subscale (caregiver report)
Peer SDQ subscale (caregiver report)
Conduct SDQ subscale (teacher report)
General functioning
Social functioning
Verbal reasoning
ASD traits
Non-verbal reasoning
VIQ
PIQ
Sustained attention
Processing speed
Verbal knowledge
Peer SDQ subscale (teacher report)
Set-shifting
Motor coordination

Severity

-3   -2   -1   0

Z-score

Figure 1.7: Severity of ESSENCE traits in 16p11.2 CNV carriers.
The lighter the colour, the less severe the phenotypic trait (i.e., a z-score difference of zero between the CNV group and controls). The traits are ordered in descending order in terms of the contrast of severity between deletion and duplication carriers (i.e., traits at the top have greater differences in trait severity between deletion and duplication carriers, whereas traits at the bottom have more similar severity levels, or z-scores). *CAPA, child and adolescent psychiatric assessment; ADHD, attention deficit hyperactivity disorder; SDQ, strengths and difficulties questionnaire; ODD, oppositional defiant disorder; OCD, obsessive-compulsive disorder; ASD, autism spectrum disorder; VIQ, verbal intelligence quotient; PIQ, performance intelligence quotient.*

Extensive cognitive and psychiatric assessments were conducted, including the Wechsler Abbreviated Scale of Intelligence (WASI), Child and Adolescent Psychiatric Assessment (CAPA), and Social Communication Questionnaire (SCQ), etc. As can be observed in **Figure 1.7**, various traits are severe for deletion carriers, including hyperactivity, ASD traits, IQ, and verbal and motor ability. For duplication carriers, severe traits include psychotic traits, anxiety, ADHD, ASD, IQ, general functioning, and verbal and motor ability. Overall, traits are more severe in duplication carriers compared to deletion carriers. The contrast in trait-severity is most prominent in psychotic, anxiety, and ADHD, and oppositional defiant disorder (ODD). Considering both diagnoses and traits, psychosis traits/ schizophrenia might be unique to duplication carriers, in line with the dominant model. Whereas numerous overlaps in trait severity and profile are present in 16p11.2 reciprocal CNVs, including social behaviour, IQ, working memory, motor coordination, etc. However, deep characterisation of the cognitive profile of 16p11.2 reciprocal CNVs revealed opposing phenotypes (Hippolyte et al., 2016). Deletion carriers showed severe deficits in phonology and verbal inhibition skills. Whereas, duplication carriers performed better in these skills than deletion carriers and intrafamilial controls, with the same IQ level.

Other common characteristics identified in 16p11.2 reciprocal CNVs are mirrored BMI and microcephaly/macrocephaly phenotypes: 16p11.2 deletion is associated with obesity (Crawford et al., 2019; Owen et al., 2018; Walters et al., 2010) and macrocephaly (large head circumference; Shinawi et al., 2010), whereas duplication is associated with being underweight (Owen et al., 2018; Jacquemont et al., 2011) and microcephaly (small head circumference; Jacquemont et al., 2011; Shinawi et al., 2010). Animal models of 16p11.2 CNV identified the *KCTD13* gene (one of the genes within the 16p11.2 region) as a major driver in inducing the reciprocal head size phenotype (Golzio et al., 2012). Micro- and macrocephaly were attributed to decreased and increased progenitor cell proliferation (i.e., the process by which cells increase in number and are governed by the balance between cell divisions and cell loss), respectively (Golzio et al., 2012). Based on these outcomes, 16p11.2 CNVs were suggested to impact brain structure, possibly in an opposing manner.

1.7.3 16p11.2 CNV brain structural alterations

Indeed, numerous studies reported macro-and micro brain structural alterations in 16p11.2 CNV carriers (**Table 1.2**, Ahtam et al., 2019; Blackmon et al., 2018; Owen et al., 2018; Martin-brevet et al., 2018; Chang et al., 2016; Maillard et al., 2015; Berman et al., 2015; Qureshi et al., 2014; Owen et al., 2014). Altogether, the structural MRI and diffusion MRI

analyses (including diffusion tensor imaging techniques) demonstrate the pervasiveness of brain structural alterations in 16p11.2 CNV carriers. Global and regional brain areas are implicated, whether white matter or grey matter.

Table 1.2: 16p11.2 CNV Brain structural alterations.

	CNV	Modality	Age group	Tissue	Results (del)	Results (dup)	Additive model
Ahtam et al. (2019)	del	dMRI	Children	White matter	del > ctrl: MD, AD, RD (language pathways).		
Blackmon et al. (2018)	del; dup	sMRI	Children and adults (collapsed)	N/A	del > ctrl: Cortical thickness (left bank of the superior temporal sulcus, left cuneus, left postcentral, right pericalcarine, and right postcentral regions).		
Owen et al. (2018)	del; dup	sMRI	Children and adults (collapsed)	White matter; Grey matter	del > ctrl: Thickness of corpora callosa; Cerebellar tonsillar ectopia, and Chiari I malformations.	dup < ctrl: Thickness of corpora callosa; Global white matter volume. dup > ctrl: Brain ventricular volume.	Thickness of corpora callosa.
Martin-brevet et al. (2018)	del; dup	sMRI	Children and adults (collapsed)	White matter; Grey matter	del > ctrl: Global white matter volume; Global grey matter volume; Grey matter volume and surface area (insula, calcarine cortex, transverse temporal gyrus). del < ctrl: Grey matter volume and surface area (superior and middle temporal gyri).	dup < ctrl: Global white matter volume; Global grey matter volume; Grey matter volume (caudate and hippocampus); Grey matter volume and surface area (superior and middle temporal gyri).	Global white matter volume; Global grey matter volume; Regional grey matter volume (insula).
Chang et al. (2016)	del; dup	dMRI	Children and adult (split)	White matter	del > ctrl [children]: MD, FA, AD (pervasive); del > ctrl [adults]: AD (internal capsules).	dup < ctrl [children]: FA (pervasive). dup < ctrl [adult]: FA, AD (pervasive). dup > ctrl [children]: MD, RD (pervasive). dup > ctrl [adult]: RD (pervasive).	AD.

	CNV	Imaging	Sample	Tissue	del findings	dup findings	Overlap
Maillard et al. (2015)	del; dup	sMRI; dMRI	Children and adults (collapsed)	White matter; Grey matter	del > ctrl: White matter volume (forceps, longitudinal fasciculus, thalamic radiation, cingulate); Grey matter volume (anterior insula, putamen, caudate, superior temporal gyrus, supramarginal gyrus, area triangularis, calcarine sulcus, cuneus, inferior and middle occipital gyrus, lingual gyrus); FA (grey matter: middle temporal gyrus, lateral fusiform gyrus); Cortical thickness (inferior pre- and postcentral gyrus and supramarginal gyrus, superior parietal gyrus, superior postcentral gyrus).	dup < ctrl: Global white matter volume; Grey matter volume (caudate, putamen).	Grey matter volume (putamen).
					del < ctrl: Grey matter volume (lobule VIII of cerebellar hemisphere, crus II of cerebellar hemisphere, middle temporal gyrus); Cortical thickness (middle temporal, fusiform gyrus).	dup > ctrl: MD (grey matter: caudate); Cortical thickness (medial orbitofrontal cortex); Surface area (rostral middle frontal gyrus and frontal pole, insula).	
Berman et al. (2015)	del	dMRI	Children	White matter	del > ctrl: MD (arcuate fasciculus), MD and AD (auditory radiation).		
Qureshi et al. (2014)	del; dup	sMRI	Children	White matter; Grey matter	del > ctrl: Global white matter volume; Global grey matter volume; Subcortical volume (thalamus); Cerebellum volume; Surface area (brainstem).	dup < ctrl: Global white matter volume; Global grey matter volume; Subcortical volume (thalamus, hippocampus); Cerebellum volume; Surface area (brainstem); Cortical thickness.	Global white matter volume; Global grey matter volume; Thalamus volume; Cerebellum volume; Surface area (brainstem).
Owen et al. (2014)	del	dMRI; NODDI	Children	White matter	del > ctrl: FA (white matter: corpus callosum, superior corona radiata, internal capsule), AD (corpus callosum, internal capsule, external capsule, brainstem), MD (internal capsule, external capsule).		
					del < ctrl: Fibre orientation dispersion.		

CNV, copy number variant; del, deletion carriers; dup, duplication carriers; ctrl, controls; dMRI, diffusion MRI or diffusion tensor imaging; sMRI, structural MRI; NODDI, neurite orientation dispersion and density imaging; MD, mean diffusivity; FA, fractional anisotropy; RA, radial diffusivity; AD, axial diffusivity.

1.7.3.1 Structural MRI findings

Morphological measures detecting macro-alterations include brain volume, cortical thickness, and cortical surface area. Overall, the general directionality of results relating to these measures are consistent and point toward a gene-dosage effect (deletion > control > duplication): Deletion carriers have increased brain volume, cortical thickness, and surface area compared to controls and duplication carriers. Numerous studies (**Table 1.2**) found trends that suggest a linear relationship between copy number and brain structure; However, here, I only consider results that are significant for both reciprocal CNVs (i.e., deletion > control and control > duplication) and corrected for multiple comparisons. These results fall under the additive model described earlier, which demonstrates opposing phenotypes. Structural features in line with the additive model include thickness of corpus callosum, global white matter volume, global grey matter volume, surface area of the brainstem, regional grey matter volume in the insula and putamen, subcortical volume of thalamus, and cerebellum volume (see **Table 1.2** for more detail). Notably, most of the aforementioned studies focused on finding opposing effects on brain structure between deletion and duplication carriers. Consequently, there was less emphasis on disentangling the unique features from the shared features in the reciprocal CNVs. Therefore, it is less clear whether structural alterations in other regions are in line with the dominant model (unique phenotypes to either deletion or duplication) or U-shaped model (shared phenotypes between deletion and duplication). Nevertheless, the overall findings point to pervasive structural alterations with overlaps (e.g., decreased grey matter volume in the superior and middle temporal gyri) and some unique features (e.g., Chiari type I malformation and the anatomically milder cerebellar tonsillar ectopia in deletions) problematic to either deletion or duplication carriers.

1.7.3.2 Diffusion MRI findings

In relation to micro-structural alterations detected using diffusion MRI or diffusion tensor imaging techniques, only two (out of five) studies examined duplication carriers in addition to deletion carriers (Chang et al., 2016; Maillard et al., 2015). Diffusivity metrics detecting micro-alterations include mean diffusivity (MD), fractional anisotropy (FA), radial diffusivity (RD), and axial diffusivity (AD). Diffusion MRI techniques are more sensitive to white matter architecture, although Maillard et al. (2015) also reported findings relating to the integrity of grey matter. Overall, deletion carriers consistently showed increased diffusivity compared to controls (**Table 1.2**), regardless of the diffusivity metric, implicating language pathways and major white matter tracts such as internal capsules and corpus callosum.

Whereas duplication carriers showed widespread increased and decreased diffusivity compared to controls, depending on the metric used: E.g., FA was decreased, and RD was increased regardless of age group (Chang et al., 2016). However, the metric that showed changes in line with the additive model is AD: Deletion carriers showed increased AD, whereas duplication carriers showed decreased AD. However, due to the small number of studies, it is unclear whether the reciprocal CNVs are indeed showing AD-related opposing effects and also whether there are alterations that fit the other models.

1.7.3.3 Links between 16p11.2 CNV, brain structural alterations, and ESSENCE traits

Although the consequences of 16p11.2 CNV are due to complex and indirect interactions between many levels, studies have found certain relationships between 16p11.2 CNV, brain structure, and ESSENCE traits (**Table 1.3**). In relation to macro-structural brain alterations, there were certain links with IQ, non-verbal, daily living, language, communication, and social skills for 16p11.2 CNV carriers (Ahtam et al., 2019; Blackmon et al., 2018; Owen et al., 2018). Specifically, for deletion carriers, the presence of any atypical brain structural feature indicated worse daily living, communication, and social skills compared with deletion carriers without any structural abnormality. For duplication carriers, the presence of decreased white matter, callosal volume, and/or increased ventricle size was associated with lower IQ compared with duplication carriers without these features (Owen et al., 2018). In addition, cortical thickness, for deletion and duplication carriers, was inversely related to language skills and IQ, respectively (Blackmon et al., 2018).

In relation to microstructural alterations, associations were found with non-verbal IQ and language abilities for 16p11.2 CNV carriers (Chang et al., 2016; Berman et al., 2015; Owen et al., 2014). All the diffusivity metrics, at respective regions, showed an inverse relationship with non-verbal IQ in 16p11.2 CNVs. For language ability, an inverse relationship was found with MD and RD (diffusivity metrics of mean and radial diffusivity), in respective regions, for deletion carriers in particular.

Table 1.3: Links between 16p11.2 CNV, brain structural alterations, and ESSENCE traits.

	CNV	Modality	Age Group	Tissue	Correlations (del)	Correlations (dup)
Ahtam et al. (2019)	del	dMRI	Children	White matter	Positive correlation between the special nonverbal composite (DAS-II) scores and the volume of the left long arcuate fasciculus (findings from additional volume analyses).	
Blackmon et al. (2018)	del; dup	sMRI	Children and adults (collapsed)	N/A	Cortical thickness (abnormally thin) and cortical thickness (abnormally thick) were negatively correlated with CELF-4 core language composite scores in the left pars opercularis and middle temporal region, respectively.	Negative relationship between total cortical thickness and full-scale IQ. (This result was similar even when the data was segmented into abnormally thick and thin cortices).
Owen et al. (2018)	del; dup	sMRI	Children and adults (collapsed)	White matter; Grey matter	The presence of any imaging feature indicated worse daily living, communication, and social skills compared with deletion carriers without any radiologic abnormalities.	The presence of decreased white matter, callosal volume, and/or increased ventricle size was associated with decreased full-scale and verbal IQ scores compared with duplication carriers without these findings.
Chang et al. (2016)	del; dup	dMRI	Children and adult (split)	White matter	(Both CNV groups combined): For the children, negative relationship with non-verbal IQ, MD, and RD in the callosal, association, and projection tracts, as well as FA in the callosal tracts, and MD in the global white matter.	
Berman et al. (2015)	del	dMRI	Children	White matter	Negative relationship between MD, RD (left-hemisphere arcuate fasciculus), and CELF-4 core language scores.	
Owen et al. (2014)	del	dMRI; NODDI	Children	White matter	Negative relationship between global AD and non-verbal IQ.	

CNV, copy number variant; del, deletion carriers; dup, duplication carriers; ctrl, controls; dMRI, diffusion MRI or diffusion tensor imaging; sMRI, structural MRI; NODDI, neurite orientation dispersion and density imaging; MD, mean diffusivity; FA, fractional anisotropy; RA, radial diffusivity; AD, axial diffusivity; DAS-II, differential ability scales-early years and school age-second edition; CELF-4, the clinical evaluation of language fundamentals.

1.7.4 16p11.2 CNV brain functional alterations

Other features of 16p11.2 CNV carriers are functional brain alterations (**Table 1.4**; Hudac et al., 2015; Steinman et al., 2016; Berman et al., 2016; Jenkins et al., 2016; LeBlanc and Nelson, 2016; Bertero et al., 2018; Hinkley et al., 2019). Evidence of functional brain alterations in 16p11.2 CNVs come from functional neuroimaging studies, including fMRI, MEG, and EEG, and from clinical evaluations of EEG activity.

Table 1.4: 16p11.2 CNV brain functional alterations.

	Modality	Age Group	Paradigm	Feature	del / ctrl	dup / ctrl	del / dup	Region
Hinkley et al. (2019)	MEG	Children and adults (split)	Speech and motor	Beta power suppression	del > ctrl	-	del > dup	Vocal production task: MOG, PoCG. Manual production task: MiFG, MeFG, and SFG.[1]
				Laterality index	del < ctrl	-	del < dup	IFG, MiFG, PrCG.
Bertero et al. (2018)	fMRI	Children	Resting-state	Functional connectivity (global)	del < ctrl	-	-	Medial PFC, temporal and parietal areas (superior and medial temporal gyrus, and temporo-parietal junctions).
				Functional connectivity (PFC-seed region)	del < ctrl	-	-	Latero-temporal cortex, inferior parietal lobule, superior and inferior frontal cortex and paracentral gyrus.
LeBlanc and Nelson (2016)	EEG	Children	Visual	P1 amplitude	-	-	del > dup	Occipital area.
Jenkins et al. (2016)	MEG	Children	Auditory	M100 latency	del > ctrl	-	-	Left and right STG auditory cortex.
Hudac et al. (2015)	EEG	Children and adults (collapsed)	Social	mu power suppression	del > ctrl[2]	dup > ctrl[2,3]	-	Centro-parieto-occipital areas.

del, deletion carriers; dup, duplication carriers; ctrl, controls; PFC, prefrontal cortex; PoCG, post-central gyrus (primary somatosensory cortex); PrCG, pre-central gyrus (primary motor cortex); STG, superior temporal gyrus; MOG, middle occipital gyrus; MiFG, middle frontal gyrus; MeFG, medial superior frontal gyrus; SFG, superior frontal gyrus; IFG, inferior frontal gyrus.

[1] For deletion adult carriers, neural responses to both tasks were observed mainly in the PoCG (somatosensory cortex).

[2] For del and dup, there were no group differences per se, compared to controls. However, group by context interactions were observed. Del and dup showed an increase in mu suppression for non-social stimuli, as opposed to social stimuli as is the case in controls.

[3] Additional analysis showed that mu power suppression was initially in the typical range for duplication carriers in response to social stimuli, however, mu suppression decreased over time more rapidly compared to controls.

1.7.4.1 Clinical-focused EEG

Based on clinical EEG reports of 16p11.2 CNV carriers, various EEG abnormalities were reported, e.g., generalised sharps (i.e., widespread amplitude spikes that last up to 200 ms; **Figure 1.8**; Steinman et al., 2016). Fifty-four percent and 40 percent of deletion and duplication carriers, respectively, present with at least one abnormal EEG feature (as detected by clinical neurophysiologists; **Figure 1.8**; Steinman et al., 2016).

	Deletion (n = 39)	Duplication (n = 30)
Carrier with at least one abnormal EEG	54%	40%
Focal sharps	8%	27%
Generalized sharps	8%	7%
Focal slowing	8%	13%
Generalized slowing	8%	13%
Other abnormalities	15%	3%
Abnormalities not described	15%	7%
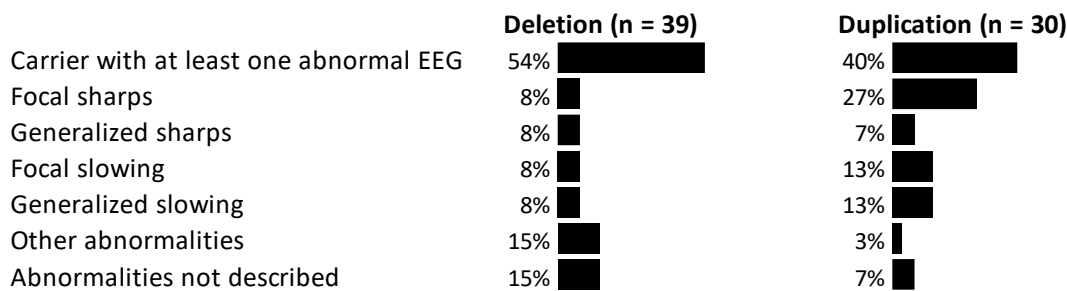
Figure 1.8: Prevalence of abnormal EEG based on clinical reports.
Frequencies presented here were reported in Steinman et al. (2016).

1.7.4.2 Research-focused EEG

Even though relatively little is known in this area as only a few studies have been conducted on 16p11.2 CNV brain function, these studies reported atypical neural activity in response to different conditions (i.e., sensory, social, and speech and motor) and at fMRI resting-state (**Table 1.4**; Hudac et al., 2015; Jenkins et al., 2016; LeBlanc and Nelson, 2016; Bertero et al., 2018; Hinkley et al., 2019).

1.7.4.2.1 Sensory neural activity

Sensory neural responses were examined via passive auditory (Jenkins et al., 2016) and visual stimuli (LeBlanc and Nelson, 2016): Tones and alternating black and white checkerboards were presented, respectively, to 16p11.2 CNV carriers. The outcome revealed some findings and trends that resemble the additive model (i.e., opposing neural activity in deletion vs duplication), albeit in a preliminary sense. Specifically, Jenkins et al. (2016) found a significant delay in the M100 response (i.e., a typical waveform elicited at ~100 ms post-stimulus onset in response to auditory events) in deletion carriers compared to controls, whereas duplication carriers showed an earlier (nonsignificant) M100 response compared to controls. To examine whether this delayed M100 response in deletion carriers is associated with white matter microstructural alterations, Berman et al. (2016) conducted secondary

analyses of the MEG and DTI datasets previously analysed by Jenkins et al. (2016) and Berman et al. (2015), respectively. The authors found no relationship between brain structure and function, supporting the view that factors other than microstructural alterations may be contributing to atypical auditory neural responses in 16p11.2 deletion.

Examining the amplitude of the P1 component (i.e., the equivalent of the M100 response, but to visual events), LeBlanc and Nelson (2016) similarly found opposing neural activity in deletion and duplication groups. In this case, a trend (albeit nonsignificant) of higher P1 amplitude in deletion compared to controls and lower P1 amplitude in duplication compared to controls was found. Notably, when deletion and duplication groups were compared to each other directly, a significant difference in P1 amplitude was found: Deletion carriers showed higher P1 amplitude than duplication carriers.

1.7.4.3 Social neural activity

In relation to neural responses to social stimuli, Hudac et al. (2015) were the first to examine functional brain alterations in 16p11.2 CNV carriers. The authors studied power changes in the mu frequency band (8–12 Hz) in response to viewing social and non-social motion. Typically, increased suppression of mu power is expected in response to social stimuli as opposed to non-social stimuli. Contrary to controls, neural responses to social and non-social stimuli were modulated in a reversed manner in CNV carriers; I.e., Increased mu suppression was observed to non-social as opposed to social stimuli, in centro-parieto-occipital areas. Crucially, this study (Hudac et al., 2015) also conducted a trial-to-trial analysis to examine whether the level of mu suppression varied over time between groups. They found that unique to duplication carriers, there was an initial typical mu response (to social stimuli), which then decreased over time more rapidly compared to controls. In contrast, deletion carriers consistently showed the pattern described earlier (i.e., increased mu suppression to non-social stimuli vs social stimuli). Although these results revealed ongoing dynamic changes to mu activity that differed between the reciprocal CNVs, it seems that both 16p11.2 deletion and duplication impair social neural responses generally in the same direction. This perhaps suggests a U-shaped model of gene-dosage effects on social neural responses.

1.7.4.4 Speech / motor neural activity

Hinkley et al. (2019) similarly examined neural features of power suppression in 16p11.2 CNV carriers, but in this case, the focus was on beta power suppression in response to speech and motor tasks. When preparing for overt speech or hand movements, beta power is

typically suppressed over the sensorimotor cortex. The authors found increased beta suppression in deletion carriers compared to controls and duplication carriers, in response to both tasks. In addition, left-hemispheric dominance for language (i.e., left-lateralised beta suppression during speech) was examined and found to be decreased in deletion carriers compared to controls and duplication carriers.

1.7.4.5 Resting-state neural activity

Using resting-state fMRI, Bertero et al.'s (2018) study further contributed to characterising functional brain alterations in 16p11.2 deletion carriers[3]. Functional connectivity (global and region-specific seed-based analyses) was altered in 16p11.2 deletion carriers compared to controls (duplication carriers were not included in this study). Specifically, deletion carriers showed decreased global connectivity and prefrontal connectivity with several tempo-parietal regions, indicating long-range neural dysfunction.

1.7.4.6 Links between 16p11.2 CNV, brain functional alterations, and ESSENCE traits

Links between 16p11.2 CNV, neural activity, and ESSENCE traits remain largely unexplored, except for a few studies focusing on certain ESSENCE traits (**Table 1.5**; Hinkley et al., 2019; Bertero et al., 2018; LeBlanc and Nelson, 2016; Jenkins et al., 2016, Berman et al., 2016). Unique to Hinkley et al.'s (2019) study are reports of significant correlations between M/EEG activity and ESSENCE traits in deletion carriers. Specifically, increased task-induced beta power, over region-specific sensorimotor cortices (see **Table 1.5**), was positively associated with phonological and motor impairments. The remaining 16p11.2 CNV studies of evoked-neural activity either did not perform brain-behaviour correlation analyses (i.e., Hudac et al., 2015) or did so, but found no significant results (i.e., Jenkins et al., 2016; Berman et al., 2016; LeBlanc and Nelson, 2016). Namely, no significant correlations were found between the auditory M100 latency and non-verbal IQ (Jenkins et al., 2016; Berman et al., 2016), social, and language skills (Jenkins et al., 2016) in 16p11.2 deletion carriers. Similarly, no significant links were found between visual-evoked neural activity (i.e., N1, P1, and N2 amplitude and latency) and IQ in deletion carriers. In contrast, using a resting-state fMRI paradigm, the decreased prefrontal connectivity found in deletion carriers was associated with social and cognitive deficits (Bertero et al., 2018). Certainly, future studies should focus on examining further links between these levels, especially in relation to

---

[3] Bertero et al. (2018) and Hinkley et al. (2019) were focused on deletion carriers, possibly due to the small number of duplication participants in the case of Hinkley et al.'s (2019) study (duplication vs control comparisons were not conducted).

spontaneous neural activity as it is possible that these links are more easily observed in a resting-state paradigm.

Indeed, further 16p11.2 CNV studies are necessary to investigate neural activity, whether in response to sensory or other contexts, to verify gene-dosage effects on neural activity, and associations with behavioural and ESSENCE traits. Functional brain features could serve as an intermediary phenotype, or endophenotype, bridging the gap between genotype (i.e., 16p11.2 CNV) and phenotypes (e.g., behavioural and psychiatric traits found in 16p11.2 CNV carriers). In addition, using animal models of this CNV, future efforts could further verify findings, facilitate interpretations of the link between different levels of analyses, and shed light into the underlying pathophysiology.

Table 1.5: Links between 16p11.2 CNV, brain functional alterations, and ESSENCE traits.

	CNV	Modality	Age Group	ESSENCE traits	Neural activity	Direction of correlation
Hinkley et al. (2019)	del	MEG	Children and adults (split)	CTOPP	Task-induced beta power (picture naming task) over PoCG.	Positive
	del			PPB	Task-induced beta power (picture naming task) over MiFG.	Positive
	del			CTOPP; PPB	Task-induced beta power (picture naming task) over left and right MOG; SFG and MeFG.	N/A (non-significant)
	dup			CTOPP; PPB	Task-induced beta power (picture naming task) over PoCG, left and right MOG; MiFG, SFG, and MeFG.	N/A (non-significant)
Bertero et al. (2018)	del	fMRI	Children	IQ, NVIQ	PFC connectivity strength	Positive
				SRS	PFC connectivity strength	Negative
LeBlanc and Nelson (2016)[1]	del	EEG	Children	IQ	N1, P1, and N2 amplitude and latency	N/A (non-significant)
Jenkins et al. (2016)	del	MEG	Children	NVIQ, SRS, CELF-4 core language index, CTOPP	M100 latency	N/A (non-significant)
Berman et al. (2016)	del	MEG	Children	NVIQ	M100 latency	N/A (non-significant)

CNV, copy number variant; del, deletion carriers; dup, duplication carriers; ctrl, controls; CTOPP, Comprehensive Test of Phonological Processing; PPB, Perdue Pegboard test; SRS, Social Responsiveness Scale; NVIQ, non-verbal IQ; CELF-4, the clinical evaluation of language fundamentals; PoCG; postcentral gyrus (primary somatosensory cortex); MiFG, middle frontal gyrus (over the representation of the hand in pre-motor cortex); MOG, middle occipital gyrus; SFG, superior frontal gyrus; MeFG, medial superior frontal gyrus; PFC, prefrontal cortex.
[1] For duplication carriers, correlation analyses between IQ and neural activity were not conducted due to the small sample size.

1.8 16p11.2 CNV mouse model

Among the animal models used to study 16p11.2 CNVs are mouse models generated by three independent groups (Horev et al., 2011; Portmann et al., 2014; Arbogast et al., 2016). Genes in the (human) 16p11.2 region are conserved in the mouse, thus permitting the generation of genotype-based mouse models of 16p11.2 CNV (as opposed to models designed to recapitulate certain cognitive and behavioural deficits common to 16p11.2 CNV human carriers). These mouse models were engineered to carry a hemideletion or duplication of the mouse chromosomal region 7qF3 - which corresponds to the 16p11.2 region in humans (**Figure 1.9**).
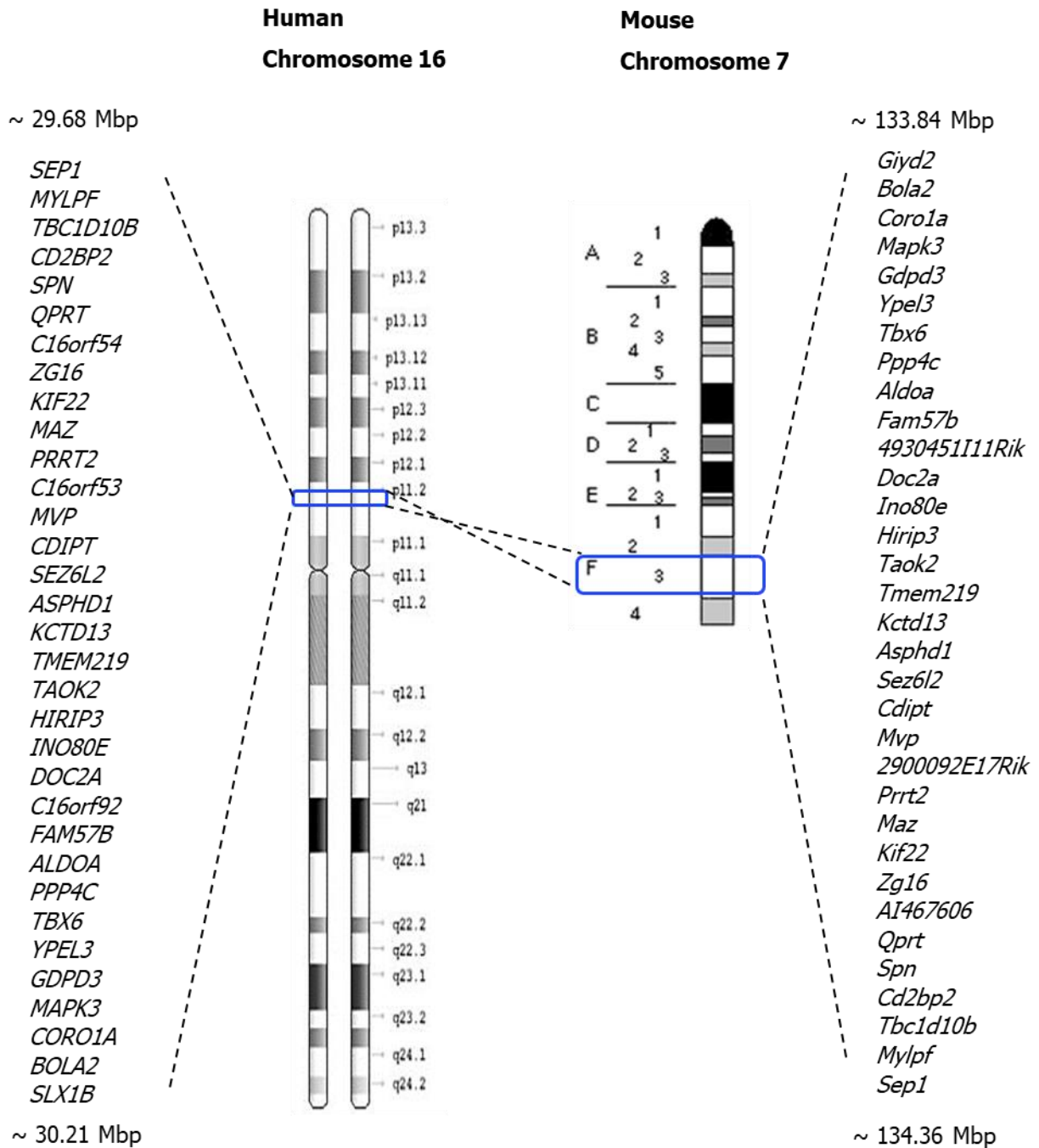
Figure 1.9: The mouse chromosomal region homologous to the human 16p11.2 region.
Courtesy*: Adler, D. (1994). Mouse Idiogram. University of Washington, Seattle.*

Although highly similar, there are some small differences between the three mouse models with regards to their genotype and genetic background/strain. Specifically, for each mouse model, the particular intervals targeted to be deleted or duplicated are respectively flanked by the following genes, Slx1b-Sept1 (Horev et al., 2011), Coro1a-Spn (Portmann et al., 2014), and Sult1a1-Spn (Arbogast et al., 2016). In terms of the genetic background /

strain, all three models were maintained on hybrid backgrounds (i.e., C57BL/6NxSv; Horev et al., 2011; C5BL/6NxP2; Portmann et al., 2014; and C57BL/6NxC3B; Arbogast et al., 2016), the latter study additionally generated 16p11.2 CNV mice on an inbred genetic background (i.e., C57BL/6N; Arbogast et al., 2016). Despite these differences, these models show similar phenotypes of relevance to 16p11.2 human CNVs. However, it is useful to keep in mind these differences in genotype and genetic background as possible factors that may influence findings.

Although both 16p11.2 deletion and duplication mouse models were generated, the focus of this thesis is on the former, i.e., 16p11.2 deletion model. Henceforth, key behavioural, brain structural, and brain functional attributes of this model will be introduced with particular emphasis on the latter (i.e., mouse fMRI and in-vivo electrophysiology) and its relevance to 16p11.2 CNV human findings.

1.8.1 16p11.2 deletion mouse model behavioural and ESSENCE traits

Overall, 16p11.2 deletion mouse model display phenotypes similar to human 16p11.2 deletion. The presented phenotypes and assessments as described by the independent groups that engineered these models are summarised in **Figure 1.10**.

Genetic background	C57BL/6NxSv	C5BL/6NxP2	C57BL/6N	C57BL/6NxC3B
Diurnal activity	H			V
Nocturnal activity	H		V	V, H
Open field activity	H	H	TC	
Repetitive behaviour	C	C, Ci	R, J	C
Recognition memory		1 hr	0.5 hr, 3 hrs	3 hrs
Social interaction				
Social preference				

Horev et al. (2011)   Portmann et al. (2014)   Arbogast et al. (2016)

Figure 1.10: Behavioural and ESSENCE phenotypes of the three 16p11.2 deletion mouse models.

Green and red boxes respectively indicate higher, or lower, level of the particular phenotype in 16p11.2 deletion mice compared to wild-type controls. Grey box indicates no group difference. White box indicates no available data. H, horizontal locomotor activity; V, vertical locomotor activity; C, climbing; Ci, circling; J, jumping; R, rearing; TC, time in Centre; hr, hour; 0.5, 1, and 3 hours retention delays for the recognition memory assessments.

Further studies conducted additional assessments on these models, which supplemented and confirmed some of the findings shown in **Figure 1.10**. Altogether, behavioural and cognitive phenotypes observed in 16p11.2 deletion mice include altered sleep architecture, and nocturnal and diurnal hyperactivity (Lu et al., 2019; Horev et al., 2011; Portmann et al., 2014; Arbogast et al., 2016), motor control deficits (Horev et al., 2011; Portmann et al., 2014; Yang et al., 2015a; Brunner et al., 2015; Arbogast et al., 2016; Angelakos et al., 2017), recognition and memory deficits (i.e., deficits in novel object recognition, object location memory, social recognition, and fear memory; Portmann et al., 2014; Pucilowska et al., 2015; Yang et al., 2015b; Tian et al., 2015; Arbogast et al., 2016), social behavioural deficits (i.e., atypical ultrasonic vocalization behaviour in social settings; Yang et al., 2015a; duration of sniffing and other social behaviours; Arbogast et al., 2016), and impaired learning and cognitive flexibility (Yang et al., 2015b).

Certain phenotypes are observed in 16p11.2 deletion mice, but not in human carriers. 16p11.2 deletion mice tend to show metabolic deficits opposite to that of humans (Horev et al., 2011; Portmann et al., 2014; Arbogast et al., 2016). Although at early postnatal age, both 16p11.2 deletion humans and mice are born underweight, adult humans undergo a drastic increase in BMI (Jacquemont et al., 2011; Zufferey et al., 2012) - whereas mice either remained underweight or recovered to normal weight in adulthood. In addition, unique to Portmann et al.'s (2014) 16p11.2 deletion mouse model, hearing deficits were observed, whereas hearing problems were not found to be frequent in human deletion carriers. Despite differences in certain phenotypes between 16p11.2 deletion mice and humans, there are overall similarities in ESSENCE traits, and brain structural and functional alterations.

1.8.2 16p11.2 deletion mouse model brain structural alterations

Similar to human 16p11.2 deletion, alterations in brain structure have been identified in 16p11.2 deletion mice (**Figure 1.11**; Horev et al., 2011; Portmann et al., 2014; Bertero et al., 2018).

		C57BL/6NxSv	C5BL/6NxP2	
Macrostructure	Brain volume			
	Cortical thickness			
Microstructure	Fractional anisotropy			
		Horev et al. (2011); Bertero et al. (2018)	Portmann et al. (2014)	
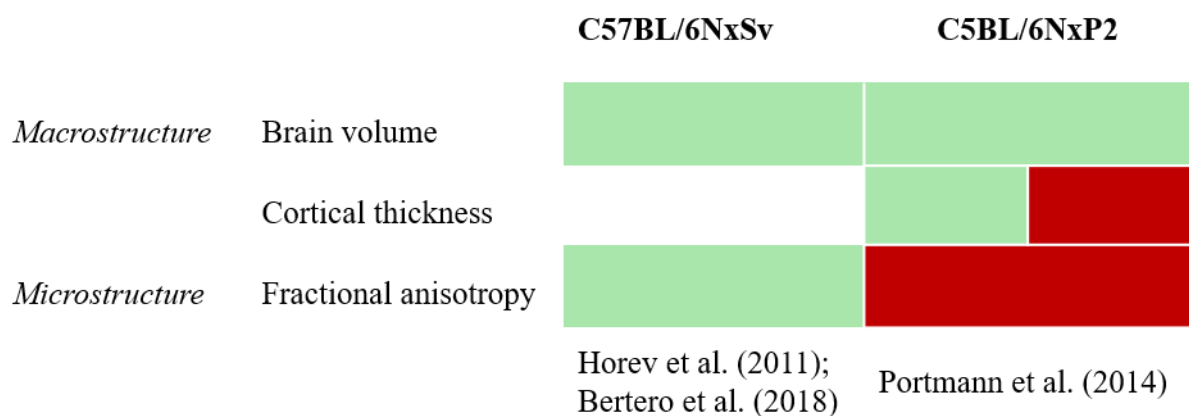
Figure 1.11: 16p11.2 deletion mouse model brain structural alterations.
Green and red boxes, respectively, indicate a higher or lower level of the particular brain structural feature in 16p11.2 deletion mice compared to wild-type controls. White box indicates no available data. Green + red indicates the presence of both higher and lower level of the respective feature.

Using MRI, Horev et al. (2011) found increased brain volume in 16p11.2 deletion mice relative to wild-type mice in many brain regions including superior colliculus, fornix, hypothalamus, mammillothalamic tract, midbrain, and periaqueductal grey. Another study (Bertero et al., 2018) found widespread white matter microstructural alterations, i.e., increased fractional anisotropy (FA) in major white matter tracts, detected by DTI. These

results could be reflecting increased axonal thickness of corpus callosal neurons as observed in the same study via an electron microscope. In contrast, Portmann et al. (2014) reported decreased FA in the corpus callosum, although this was only observed for male 16p11.2 deletion mice. In addition, the authors observed changes in brain volume and cortical thickness: increased volumes of the nucleus accumbens and globus pallidus; and increased and decreased cortical thickness at respective regions, e.g., motor and sensory cortices. Overall, these studies (Horev et al., 2011; Portmann et al., 2014; Bertero et al., 2018) provide converging evidence to the human 16p11.2 deletion studies (Owen et al., 2018; Chang et al., 2016; Qureshi et al., 2014) that macro- and microstructural changes in these multiple brain regions are implicated in 16p11.2 deletion.

1.8.3 16p11.2 deletion mouse model brain functional alterations

Functional brain alterations have also been observed in 16p11.2 deletion mice (**Table 1.5**; Bertero et al., 2018; Lu et al., 2019). Key findings from Bertero et al.'s (2018) resting-state study point to fMRI functional connectivity impairments in the prefrontal cortex of 16p11.2 deletion mice, similar to 16p11.2 deletion human findings (reported in the same study). The authors identified reduced long-range prefrontal connectivity with parieto-temporal areas, retrosplenial cortex, and thalamus in these mice (Bertero et al., 2018). The same study also analysed local field potential (LFP) coherence between the prefrontal and retrosplenial cortex. Coherence is a common EEG/LFP measure of functional connectivity between brain regions (i.e., this analysis measures the similarity in power spectra (power at different frequencies) between electrodes). The authors found reduced long-range (i.e., prefrontal and retrosplenial) coherence in the delta band in 16p11.2 deletion mice compared to control.

Power spectral analysis (see **Chapter 2**, **Section 2.2.10.2**, and **Chapter 3**, **Section 3.2.6.3** for more detail about power spectral analysis) conducted by another study (Lu et al., 2019) similarly found atypical neural activity in the delta frequency band in 16p11.2 deletion mice. Specifically, Lu et al. (2019) examined EEG activity from the parietal region during vigilant and sleep states (i.e., wakefulness, NREM sleep, and REM sleep) in the day-time and night-time. 16p11.2 deletion mice showed lower delta power during day-NREM, but higher delta power during night-NREM compared to wild-type mice. However, this was not restricted to delta frequency as atypical neural activity were also found in other frequency bands in Lu et al.'s (2019) study: lower theta power during day-wake, day-REM, night-wake, and night-REM; and higher beta power during wake-REM.

Altogether (based on Bertero et al.'s (2018) and Lu et al.'s (2019) studies), functional brain activity seems to be altered in 16p11.2 deletion mice at multiple frequency bands and brain regions. More studies are required to verify and expand on this, especially as only fMRI (prefrontal) long-range connectivity has been implicated in both 16p11.2 deletion humans and mice (Bertero et al., 2018).

Table 1.6: 16p11.2 deletion mouse model brain functional alterations.

	Analysis	**Feature**	**Results**	**Regions**
fMRI	Functional connectivity	Global	del < ctrl	PFC
		PFC-seed region	del < ctrl	Parieto-temporal areas, retrosplenial cortex, and thalamus; Also along the rostro-caudal axis of the cingulate and retrosplenial cortex.
LFP	Coherence			
		Delta	del < ctrl	Prefrontal and retrosplenial cortices.
EEG	Power			
		Delta	del < ctrl (day-NREM); del > ctrl (night-NREM)	Parietal cortex.
		Theta	del < ctrl (day-wake, day_REM, night-wake, night-REM)	
		Beta	del > ctrl (wake-REM)	

del, deletion carriers; ctrl, controls; PFC, prefrontal cortex.

1.9 Outstanding questions and thesis aim

Accordingly, the outstanding questions that this thesis aims to answer are below:

1.9.1 Is neural activity altered, as revealed via EEG variability, power, and entropy metrics, in 16p11.2 CNV carriers?

Overall, prior work (**Table 1.4**) suggest a neural dysfunction in 16p11.2 CNV, which is more prominent in 16p11.2 deletions compared to duplications, in the above-mentioned contexts. However, other metrics of neural activity, i.e., neural variability, entropy, and power (for human studies), have not been investigated in 16p11.2 CNV, yet they are likely to be relevant. These metrics were implicated in ESSENCE disorders and might serve as reliable endophenotypes informing prognosis and treatment progression in 16p11.2 CNV carriers. In addition, no study has characterised resting-state neural activity at temporal resolutions higher than that of fMRI for human 16p11.2 CNV carriers, even though the resting-state paradigm is the most practical and feasible for clinical settings and populations. Therefore, work in this thesis aims to determine the nature of neural activity in 16p11.2 CNV through the lens of various neural dynamics unexplored in previous studies (i.e., neural variability, entropy, and power) yet found to be of relevance to ESSENCE disorders (e.g., ASD, ADHD). As such, EEG neural activity in response to visual stimuli (**Chapter 2**) and at rest (**Chapter 3**) will be investigated in human 16p11.2 CNV.

1.9.2 Does 16p11.2 dosage have an opposing effect on neural activity as per the additive model?

Previous work suggest certain trends, albeit non-significant, that indicated a gene-dosage opposing effect (i.e., additive model) on neural activity, specifically involving the visual-evoked P1 and auditory evoked M100 (**Section 1.6.4.2.1**). Therefore, research in this thesis aims to establish whether reciprocal 16p11.2 CNVs do indeed present with opposing neural activity (**Chapter 2**).

1.9.3 Is there a relationship between neural activity and ESSENCE traits in 16p11.2 deletion carriers?

Two studies reported brain-behaviour associations (i.e., beta suppression and connectivity vs phonological, motor, and social impairments; Hinkley et al., 2019; Bertero et al., 2018; **Table 1.5**) in 16p11.2 deletion. The current thesis will expand on this by examining associations between 16p11.2 deletion neural activity and numerous ESSENCE traits, e.g., anxiety problems (**Chapter 3**).

1.9.4 Is neural activity in 16p11.2 deletion mouse model similar to that of 16p11.2 deletion humans?

The only neural feature that was found to be similar between 16p11.2 deletion humans and mice was atypical fMRI long-range prefrontal connectivity (**Section 1.7.3**; Bertero et al., 2018). This is most likely due to the small number of 16p11.2 deletion human and mouse studies, respectively, and the lack of parallel human-mouse studies (other than Bertero et al.'s (2018) fMRI study). Therefore, work in this thesis aims to establish whether 16p11.2 deletion humans and mice show similar brain functional features, as revealed via EEG/LFP (**Chapter 4**).

Chapter 2   Atypical Neural Variability in Carriers of 16p11.2 Copy Number Variants

2.1 Introduction

As mentioned in **Chapter 1**, many studies have consistently drawn the conclusion that the number of 16p11.2 copies (i.e., 1 copy = deletion, 2 copies = typical control, 3 copies = duplication) may lead to observed opposing effects in certain phenotypes in deletion (del) versus duplication (dup) carriers (e.g., Shinawi et al., 2010; Jacquemont et al., 2011; Qureshi et al., 2014; Hippolyte et al., 2016; LeBlanc & Nelson, 2016). For example, 16p11.2 del is associated with atypically large brain volume, whereas dup is associated with atypically small brain volume (Qureshi et al., 2014). This is in line with the additive model described in **Chapter 1**; i.e., reciprocal CNVs (copy number variants) contributing to opposing phenotypes (see **Figure 1.5a**). Investigating whether particular 16p11.2 CNV phenotypes fit the additive, dominant, or U-shaped model (**Section 1.6.1**, **Figure 1.5**) is important because it connects genotype to phenotype, enabling a deeper understanding of the pathological effects of 16p11.2 CNVs.

Further evidence to indications of 16p11.2 CNV additive effects on phenotypes come from phenotypes in the form of M/EEG activity (Jenkins et al., 2016; LeBlanc and Nelson, 2016; Hudac et al., 2015). As mentioned earlier (**Section 1.6.4.2.1**), trends, albeit non-significant, suggesting opposing neural activity, involving atypical P1-visual (LeBlanc and Nelson, 2016) and M100-auditory responses (Jenkins et al., 2016), were found in the reciprocal 16p11.2 CNVs. Alternatively, neural activity involving mu-power (8-12 Hz) social responses (described in detail in **Section 1.6.4.3**) revealed atypical mu suppression to non-social stimuli (as opposed to social stimuli) in the same direction, i.e., increased mu suppression, in both 16p11.2 del and dup compared to controls (Hudac et al., 2015). Hence, suggesting a U-shaped model of copy number effects on neural responses, specifically in a social context. Interestingly, trial-to-trial analyses conducted in the same study, examining changes to mu-suppression across time, revealed subtle neural differences between the reciprocal 16p11.2 CNVs, countering the U-shaped model. Specifically, an initial typical mu response to social stimuli (i.e., increased mu) was found in dup, whereas a consistent atypical mu response was found in del (i.e., decreased mu to social stimuli). Indeed, further research using other measures of neural activity, especially trial-to-trial variability measures, is

warranted to verify distinct and potentially reciprocal EEG responses in 16p11.2 CNV carriers.

In the ESSENCE (early symptomatic syndromes eliciting neurodevelopmental clinical examinations) literature (e.g., Haigh et al., 2015; Dinstein et al., 2012; Milne, 2011), variability measures for both M/EEG and fMRI responses have been computed to study intra-participant trial-to-trial neural variability via visual, somatosensory, and auditory paradigms. Despite finding no differences in the mean measures of stimulus-response amplitude, these studies identified neural responses that were variable across single trials in the autism spectrum disorder (ASD) group relative to the typical group. Conducting trial-to-trial variability analyses, therefore, is useful in identifying these subtle yet significant differences in neural responses between ESSENCE and typical populations, which would have been unnoticed in measures of averaged-trial responses. Neural variability has been increasingly studied in ESSENCE populations and recognized as a useful sign of atypical brain function and development (Pernet et al., 2011; Garrett et al., 2013; Dinstein et al., 2015; David et al., 2016). Overall, intra-individual variability measures and analyses (e.g., multiple M/EEG and fMRI variability metrics) could present a possibly unifying multimodal approach to studying subtle differences in heterogeneous disorders that vary in their symptomology and severity from one person to another, such as 16p11.2 CNVs.

The purpose of the current study is to further determine the nature of the putative atypical and reciprocal EEG activity in 16p11.2 del and dup carriers. To our knowledge, no existing study has investigated neural variability in this population. As such the current study conducts novel analyses of the dataset obtained from Simons Foundation Autism Research Initiative (SFARI) and previously published by LeBlanc and Nelson (2016). Neural variability was measured via the following metrics: intra-participant response variability of visual evoked components (i.e., across-trial variability in the amplitude and latency of C1, P1, and N1), timecourse variability, spectral power variability (i.e., across-trial variability in absolute alpha power, relative alpha power, absolute beta power, and relative beta power), and mean signal-to-noise ratio (SNR). Further to these measures, we analysed mean visual evoked potentials and spectral power (both absolute and relative alpha and beta frequencies) to facilitate comparisons with other studies relating to associated disorders and similar CNVs (e.g. ASD, 15q, 1q).

2.2 Materials and Methods

2.2.1 Data source

The findings in this study represent the analyses of a previously collected dataset (LeBlanc and Nelson, 2016). The dataset was obtained from the Simons Foundation Autism Research Initiative (SFARI), which provides funding and resources to support research relating to ASD (https://www.sfari.org/; see Al-Jawahiri and Milne, 2017 for a review on resources available for autism research). SFARI's Simons Variation in Individuals Project (SVIP; The Simons VIP Consortium, 2012) specifically aims to "identify and study large numbers of individuals sharing recurrent genetic variants known to increase the risk of developing autism spectrum and other neurodevelopmental disorders" (https://www.sfari.org/resource/simons-vip/). Datasets collected as part of SVIP, which include 16p11.2 CNV data, are available to approved researchers via their data request process.

For this study, data of individuals with 16p11.2 deletion, the reciprocal duplication, and typically developing individuals were obtained from SFARI. Participant identification, recruitment, and inclusion/exclusion criteria of the SVIP have been described previously (see The Simons VIP Consortium, 2012; Jenkins et al., 2016; LeBlanc & Nelson, 2016). Briefly, eligibility criteria consisted of having a deletion or duplication of the 16p11.2 region (as described in **Section 1.1** and **Section 1.2**, although note that CNVs at smaller regions within 16p11.2 than that described in these sections are also eligible). Exclusion criteria consisted of having any other pathogenic CNVs or known genetic syndromes.

The control participants analysed in this study did not undergo the Simon's VIP battery of assessments. LeBlanc and Nelson (2016) recruited the control group independently through the Boston Children's Hospital participant registry. The group consisted of typical individuals without any neurological or developmental disorders.

2.2.2 Participants

Data from a total of 46 participants were obtained for the current study. Seven participants were then excluded. Reasons for exclusions were EEG data contaminated by artefacts (n = 2) based on visual inspection, and/or EEG datasets with fewer than 24 clean trials. The final dataset analysed contained 39 participants: 20 del, 8 dup, and 11 typical controls.

Phenotypic data including IQ scores, diagnoses, current medications, and vision problems were accessed from the Simons VIP Phase 1 16p11.2 dataset at SFARI Base

(http://www.sfari.org/resources/sfari-base). Participant information relating to age, sex, CNV inheritance, ASD diagnosis, Autism Diagnostic Observation Schedule -Calibrated Severity Score (ADOS-CSS), and IQ scores are reported in **Table 2.1**. Note that the reported IQ scores were not adjusted for prematurity.

Table 2.1: Participant information.

Group	N	Age mean in months (SD)	Age range in months	Sex	CNV inheritance			ASD diagnosis[c]			ADOS-CSS mean (SD)[a c d]	FSIQ mean (SD)[b c d]	VIQ mean (SD)[b c d]	NVIQ mean (SD)[b c d]
					De novo	Inherited	unknown	Yes	No	unknown				
del	20	69.05 (36.93)	12 - 163	M 12	7	2	3	2	8	2	4.29 (2.87)	78.32 (14.23)	72.84 (16.22)	83.58 (14.93)
				F 8	6	1	1	2	6	0				
dup	8	110 (86.22)	40 - 256	M 4	0	4	0	1	3	0	2.71 (1.50)	82.25 (13.29)	83.63 (17.61)	84.88 (10.23)
				F 4	1	3	0	0	4	0				
Control	11	68.36 (23.31)	39 - 109	M 5	-	-	-	-	-	-	-	-	-	-
				F 6	-	-	-	-	-	-	-	-	-	-

ADOS-CSS, Autism Diagnostic Observation Schedule - Calibrated Severity Score; *FSIQ*, full-scale IQ, *VIQ*, verbal IQ, *NVIQ*, nonverbal IQ.

[a]Missing data from del carriers (n = 6), dup carriers (n =1), control (n = 11).

[b]Missing data from del carriers (n = 1), control (n = 11).

[c]IQ and diagnosis data were extracted from diagnosis_summary.csv

[d]The reported IQ scores were not adjusted for prematurity.

Other diagnoses and comorbidities are reported in **Table 2.2**. Information regarding current medication was extracted from the SFARI medication questionnaire (med_child.csv); two del carriers were reported to have been currently taking antiepileptic medication (i.e., Keppra and Topamax). Additionally, vision problems were reported for eight del and four dup carriers in the SFARI development and medical history form (mhi_ped.csv).

Kruskal–Wallis tests revealed that there were no significant age or sex differences among the three groups (χ^2 (2) = 1.46, P = 0.481; χ^2 (2) = 0.65, P = 0.724). Also, there were no significant differences in IQ scores (full-scale IQ: χ^2 (1) = 2.97, P = 0.085; verbal IQ: χ^2 (1) = 2.34, P = 0.126; nonverbal IQ: χ^2 (1) = 1.71, P = 0.191) between del and dup groups. Comparisons with the control group were not possible as, other than age and sex, participant details and phenotypic data were not available for the control group.

Table 2.2: Diagnoses summary[a].

Diagnoses[b]	del (n = 20)	dup (n = 8)
ADHD	4	1
Anxiety disorders including OCD and phobia	-	2
Articulation disorder	9	1
Other disruptive behaviour disorder (conduct/oppositional)	3	2
Developmental coordination disorder	12	3
Enuresis disorder	2	-
Language disorders	8	4
Learning disorder	1	1
Intellectual disability	4	-
Seizures/epilepsy	3	1

[a]Comorbidities or more than one diagnoses are present in this sample.

[b]Seizure / epilepsy diagnoses data were extracted from the nrrg.csv file; all other diagnoses data were found in the diagnosis_summary.csv file.

2.2.3 Ethical approval

The local institutional ethical review board reviewed and approved the secondary analyses presented here. Our request to obtain access to phenotypic and imaging data on SFARI Base was approved after submitting the required information and signing the joinder to the researcher distribution agreement (https://www.sfari.org/resource/sfari-base/). SFARI obtained initial ethical approval for the SVIP (IRB of record: Columbia University Medical Center; the Simons VIP Consortium, 2012). As part of the SVIP, approval was obtained for data collection on individuals with 16p11.2 deletions or duplications and for their de-identified data to be shared with approved researchers.

2.2.4 Psychometric assessments (CNV groups only)

The Autism Diagnostic Observation Schedule-Calibrated Severity (ADOS-CSS) and IQ scores for 16p11.2 CNV groups were accessed from the Simons VIP Phase 1 16p11.2 dataset at SFARI Base (http://www.sfari.org/resources/sfari-base).

2.2.4.1 Autism Diagnostic Observation Schedule-Calibrated Severity Score (ADOS-CSS)

The Autism Diagnostic Observation Schedule-2 (ADOS-2; Gotham et al., 2007) is a semi-structured assessment for diagnosing and describing autism core symptoms, based on observation of the individual's behaviour in response to a series of activities. Depending on the individual's chronological age and language ability, one of five ADOS modules is administered (e.g., toddler module is appropriate for toddlers who do not consistently use phrase speech, while module 4 is for verbally fluent adolescents and adults). The observed behaviour is then coded by a trained examiner and scored based on an algorithm to yield classifications of 'non-spectrum', 'autism spectrum disorder', and 'autism'. A calibrated severity score (CSS; (Gotham et al., 2009) is a new metric developed from raw ADOS-2 scores, which estimates core autism symptom severity independent of language, age, and intellectual ability. CSS ratings are classified as follows: 'non-spectrum' (ratings 1-3), 'autism spectrum disorder' (ratings 4-5), and 'autism' (ratings 6-10). Data from six del and one dup carriers are missing.

2.2.4.2 IQ

Based on the participants' age, intellectual and cognitive ability was measured either with the Wechsler Abbreviated Scale of Intelligence (WASI; Wechsler, 1999), the Mullen Scales of Early Learning (Mullen, 1995), or the Differential Ability Scales – Early Years & School

Age (DAS-II; Elliott, 2007). Standard scores for full-scale IQ, verbal IQ, and non-verbal IQ were obtained from SFARI. Data from one del carrier is missing.

2.2.5 Stimuli and procedure

The stimuli and procedure were as described in previous studies (LeBlanc and Nelson, 2016; LeBlanc et al., 2015; Varcin et al., 2016). Specifically, the presented stimuli consisted of black and white high contrast checkerboards of 99% with an average luminance of 80 cd/m^2, and a phase reversal rate of 2 Hz (i.e. phase reversing from black to white and white to black twice per second). The size of the checker was ~60 arcminute with a spatial frequency of 0.5 cycles/degree. Participants were seated ~60 cm from a Tobii T60 eye-tracking monitor (Tobii Technology, Sweden) that was 34.7 cm wide. Infant participants were seated on their caregiver's lap. The stimulus was presented on the monitor by running the E-Prime software (Psychology Software Tools, Pittsburgh, PA) in a dark room that was sound-attenuated and electrically shielded. Binocular eye gaze was monitored to ensure phase-reversal occurred as long as the participant's fixation gaze on the stimulus lasted for a minimum of 100 ms. Phase-reversal was paused when the participant's gaze was not fixated towards the stimulus. Depending on the participants' attentiveness and patience during the sessions, up to 150 trials were presented.

2.2.6 EEG recording and pre-processing prior to the current study

EEG was continuously recorded using a 128 channel HydroCel Geodesic Net-Version 1 (Electrical Geodesics Inc., Eugene, OR, USA). The signal was amplified with a NetAmps 300 amplifier and digitised at a sampling rate of 500 Hz. A total offset of 34 ms was present and consistent for all participants. The offset resulted from both an 18 ms amplifier offset (due to the anti-alias filters within the amplifier) and 16 ms DIN offset (due to a delay between the stimulus trigger and stimulus visual onset on the monitor). Because this offset was consistent for all participants, it is not expected to drive group differences. In addition, the time window for the P1 component used for this study has a wide range (56–132 ms post-stimulus onset), which accounted for this offset and captured the P1 response.

A number of pre-processing steps were conducted offline using NetStation software prior to obtaining the data for the current study. Firstly, the data were filtered with a bandpass of 0.3-30 Hz. Secondly, the data were segmented into epochs 400 ms long (100 ms baseline and 300 ms post-stimulus). Baseline correction was applied. 'Bad' channels, i.e. channels which recorded a noisy EEG signal, were removed. Channels were defined as bad if they:

were missing; measured EOG from around the eyes, had amplitude ± 150 µV; contained artefacts in 100% of trials. By hand-edit, trials were marked bad if more than 12 channels were bad (not including missing or eye channels). Trials with eye blinks, eye movements, large clusters of bad channels, muscle artefacts, or excessive drift, were rejected. Bad channels were replaced using interpolation techniques. Channels (including interpolated channels) were referenced to an average reference.

2.2.7 EEG pre-processing conducted in the current study

Additional pre-processing steps were conducted in the current study after obtaining the dataset, which consisted of rejecting obvious bad trials (three trials in total) based on manual visual inspection. In addition, the number of trials selected for analysis was adjusted per group in order to control the average number of trials analysed per group and avoid bias in analysis outcomes (original trial number range after participant exclusions: 24–147; original mean trial number for control = 67, original mean for del = 49, original mean for dup = 71; new trial number range: 24–97; new mean = 49 trials per group). This was done via an algorithm that applied a different number of trial limits per participant depending on the group the respective participant belonged to, which in turn was designed to result in the same trial number averages for all groups.

2.2.8 EEG channel selection

In accordance with previous studies (e.g., Foxe and Simpson, 2002; Milne, 2011; Gonen-Yaacovi et al., 2016; Arazi et al., 2017), for each participant, the channel within the occipital and parietal regions with the highest amplitude within the time window 60–140 ms post-stimulus onset was selected for timecourse variability analyses and C1, P1, and N1 analyses (both mean and variability analyses; **Table 2.3**). This will be referred to as criterion 1 for channel selection.

Table 2.3: Channels selected for C1, P1, N1, and timecourse variability primary analyses based upon criterion 1 (peak channel for P1 responses).

All three groups (n = 39)	Control (n = 11)	del (n = 20)	dup (n = 8)
58 [1]	62 [1]	58 [1]	71 [1]
62 [1]	71 [2]	69 [1]	73 [1]
69 [1]	74 [2]	70 [1]	74 [1]
70 [1]	75 [3]	71 [1]	75 [1]
71 [4]	76 [2]	74 [2]	81 [1]
73 [1]	99 [1]	75 [4]	82 [1]
74 [5]		76 [2]	84 [1]
75 [8]		81 [1]	99 [1]
76 [4]		82 [4]	
81 [2]		83 [2]	
82 [5]		90 [1]	
83 [2]			
84 [1]			
90 [1]			
99 [2]			

The frequency of subjects for which each channel was selected is noted in brackets. Reported as channel number [frequency].

We also analysed the data based on an alternative criterion (criterion 2) of selecting the channel with the lowest C1 amplitude, highest P1 amplitude, and lowest N1 amplitude for the respective C1, P1, and N1 analyses (both mean and variability analyses; **Table 2.4**); this analysis produced identical variability results, in addition to certain minor differences in the mean ERP results (see Results **Section 2.3**).

Table 2.4: Channels selected for C1, P1, N1, and timecourse variability supplementary analyses based upon criterion 2 (peak channel unique for each component).

Control (n = 11)	del (n = 20)	dup (n = 8)

C1	P1	N1	C1	P1	N1	C1	P1	N1
91 [1]	99 [1]	89 [1]	97 [1]	90 [1]	99 [2]	94 [1]	99 [1]	99 [1]
81 [1]	76 [2]	85 [1]	96 [2]	83 [2]	96 [1]	83 [1]	84 [1]	94 [2]
75 [2]	75 [3]	83 [1]	94 [1]	82 [4]	94 [2]	82 [1]	82 [1]	90 [1]
74 [1]	74 [2]	82 [1]	91 [1]	81 [1]	93 [1]	75 [1]	81 [1]	88 [1]
73 [1]	71 [2]	81 [1]	88 [1]	76 [2]	88 [1]	73 [1]	75 [1]	76 [1]
71 [2]	62 [1]	75 [1]	83 [2]	75 [4]	84 [2]	65 [1]	74 [1]	56 [2]
57 [1]		71 [1]	82 [1]	74 [2]	82 [1]	60 [1]	73 [1]	
56 [1]		68 [1]	74 [1]	71 [1]	76 [1]	56 [1]	71 [1]	
		65 [1]	73 [2]	70 [1]	74 [1]			
		56 [2]	71 [1]	69 [1]	73 [2]			
			68 [3]	58 [1]	71 [1]			
			57 [1]		70 [2]			
			56 [2]		65 [1]			
			51 [1]		56 [2]			

The frequency of subjects for which each channel was selected is noted in brackets. Reported as channel number [frequency].

For power analyses and SNR analyses, the average of a set of channels positioned above the occipital cortex was computed (**Figure 2.1**).
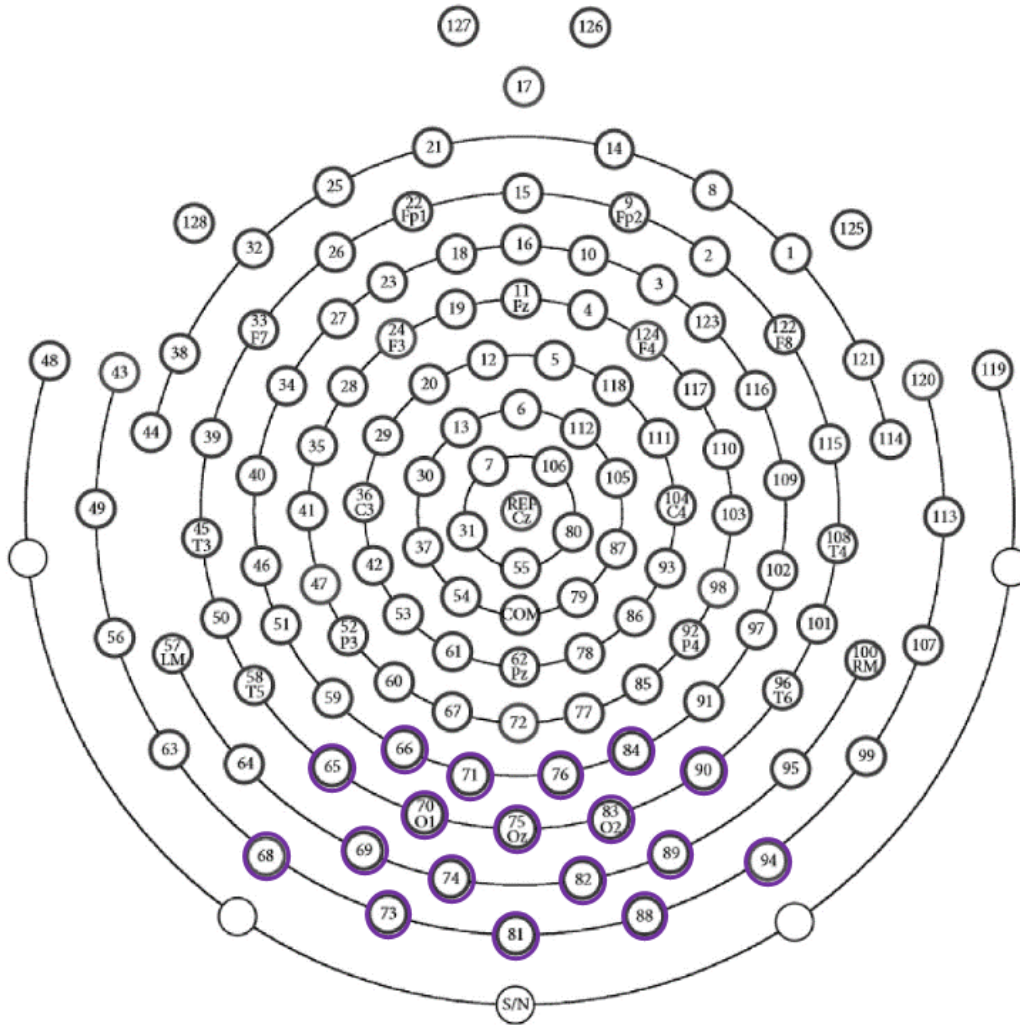
Figure 2.1: Electrical Geodesics Inc. (EGI) 128-channel hydrocel sensor net – version 1. The correspondence between the EGI 128 sensor net and the international 10–20 system. For power and SNR analyses, the channels circled in purple were averaged.

2.2.9 Extracting C1, P1, and N1 amplitude and latency

C1, P1, and N1 were identified for each trial and participant. Using a peak-picking algorithm, which identified either the maximum or minimum amplitude within a given time window, negative and positive deflection points were identified in overlapping period ranges consistent with those previously reported by LeBlanc and Nelson (2016). C1 was identified as the minimum amplitude occurring in the post-stimulus period range of 0–70 ms; P1 was the highest amplitude in the period range of 56–132 ms; N1 was the lowest amplitude in the 108–266 ms range. The amplitude and latency of C1, P1, and N1 were first extracted from every trial. Respectively, the C1, P1, and N1 average single-trial amplitudes were then given by computing the median of all the single-trial C1, P1, and N1 amplitude deflection points. Similarly, C1, P1, and N1 average single-trial latencies were given by the median of all the

single-trial time points at which the C1, P1, and N1 amplitude peaks (therefore, following the approach of Milne (2011)).

2.2.10 Measures of neural variability

Because there are many variables that have been suggested to indicate neural variability (e.g., Milne, 2011; Weinger et al., 2014; Haigh et al., 2016; Arazi et al., 2017; Butler et al., 2017), it is good practice to apply more than one measure and examine whether there is concordance between the metrics. Measures of neural variability examined in the current study were C1, P1, and N1 variability; inter-trial variability in ERP amplitude across the timecourse (henceforth referred to as timecourse variability); alpha and beta power variability; and EEG SNR. Although it could be argued that SNR is not a true reflection of inter-trial variability, it is often used as a proxy measure of variability, with lower SNRs interpreted as higher neural variability (Dinstein et al., 2012; Butler et al., 2017). Thus, SNR is provided in the current study for comparison with previous research.

2.2.10.1 C1, P1, N1, and timecourse variability

For each participant, C1, P1, and N1 variability were given by computing the median absolute deviation (MAD) of the single trial amplitude and latency values. Timecourse variability was given by computing the MAD of all 2 ms interval amplitudes across trials for the full length of the signal in order to investigate the precise timing of any differences in variability between the three groups. In other words, we computed the MAD of single-trial amplitudes of each individual datapoint in the signal (encompassing all the pre-stimulus and post-stimulus periods; range: $-100\,\mathrm{ms}$, $300\,\mathrm{ms}$).

2.2.10.2 Alpha and beta power variability

Power variability was given by computing the MAD of single-trial absolute and relative alpha (8–14 Hz) and beta power (14–30 Hz) for each participant (see more detailed description below). These were computed from the average input of a set of occipital channels as indicated in **Figure 2.1**.

The fast Fourier transform of the full length of each single trial data (200 datapoints) for each participant was computed using the 'fft' MATLAB function and divided by the number of datapoints. The signal was first zero-padded, to form a total of 1000 timepoints, and subtracted from the mean signal amplitude (this is done to remove the direct current signal). In addition, a taper was applied to the data, specifically, a hanning window, using the 'hann' MATLAB function. Power spectral density (PSD) was then computed by squaring the

absolute of the Fourier coefficients then multiplying by two to account for the negative frequencies. Given the parameters of the data, i.e. sampling rate of 500 Hz and 200 datapoints (corresponding to 400 ms) epoch lengths, the frequency resolution was 2.5 Hz. Absolute and relative power were computed for the alpha (8-14 Hz) and beta (14-30 Hz) frequency ranges. Using the 'trapz' MATLAB function, trapezoidal integration for each range was conducted to obtain the absolute power of single trials. Prior to obtaining the relative power, the total spectral power was defined as the entire range between 1-30 Hz. Relative alpha and relative beta power were subsequently calculated as the ratio of alpha and beta power, respectively, to total power on each trial. To analyse power variability, again the MAD of single-trial absolute and relative alpha and beta power was found for each participant. Mean absolute and relative alpha and beta power were also measured to facilitate comparisons with other studies. These analyses were conducted using in-house code (code available upon request) derived from codes shared by Dr Mike X. Cohen (Cohen, 2014) with functions from the EEGlab toolbox (Delorme and Makeig, 2004).

2.2.10.3 Signal-to-noise ratio

SNR is the ratio of post-stimulus signal (i.e., 0 to 100 ms in the current study) strength to the pre-stimulus signal (i.e., −100 to 0 ms relative to stimulus time) strength (the latter traditionally termed as noise) and is usually expressed in decibels. The current study followed the same SNR formula used in Butler et al. (2017) to compute SNRs (see more detailed description below).

To compute the visual evoked potential SNR, the squared root-mean-square-amplitude (rms) of the post-stimulus signal was divided by the squared rms of the pre-stimulus signal and converted into decibels. The 'post-stimulus period' was taken from 0 ms to 100 ms post-stimulus onset, and the 'pre-stimulus period' was from -100 ms to 0 ms relative to stimulus time. This ensured that equal temporal segments of data before and after stimulus presentation necessary to compute the SNR were obtained. The SNR formula is as follows;

$$SNR_{db} = 10 * log_{10} \left(\frac{rms_{post-stimulus}}{rms_{pre-stimulus}} \right)^2$$

Where *rms* is the root-mean-square amplitude.

This formula is also embedded as a function in MATLAB 'snr' version R2016a (The MathWorks Inc.). The SNR from the mean of a set of channels positioned above the occipital cortex (**Figure 2.1**) was computed for each trial and then averaged across trials and compared between groups.

2.2.11 Statistical Analysis

As sample sizes were small and the data were skewed, permutation tests (Rodgers, 1999) were conducted to investigate whether there were group differences in neural activity between the three groups. The advantage of this technique is it makes no a priori assumptions about the distribution of the data and uses the actual data to conduct the test. For each group comparison (i.e., del/control, dup/control, and del/dup), the whole group data were randomly permuted, this new permuted data were assigned to two groups with identical sample sizes to the respective original dataset. The mean difference between these two new groups was calculated; this procedure was then repeated 10,000 times. The actual absolute mean difference was compared to the randomized distribution of absolute mean differences. The P-value is the number of (absolute) mean differences' values above the actual (absolute) mean difference obtained and divided by the number of iterations (10,000). This was conducted for each EEG averaged and variability metric described in earlier sections. To account for multiple comparisons, the false discovery rate (FDR) was controlled using the Benjamini–Hochberg procedure, with $q < 0.05$.

The permutation approach was also applied to correlation analyses to examine whether age, IQ, and autistic traits impact neural responses in 16p11.2 CNV carriers. For each group, the null hypothesis ($r = 0$) is tested by holding the X-variable (e.g., age) constant and permuting the Y-variable (e.g., P1 amplitude variability) against it. In other words, the r-coefficient for the respective actual X-variable and the random permutated Y-variable pair is computed, with the expectation of $r = 0$. This process is repeated 10,000 times, where only the Y-variable is permuted. The actual absolute r-coefficient of the respective variables were then compared to the randomized distribution of absolute r-coefficients, which were produced by the 10,000 correlation permutations. The P-value is the number of (absolute) r-

coefficients' values above the actual (absolute) r-coefficients obtained and divided by the number of iterations (10,000). All the outcomes were corrected by controlling FDR using the Benjamini–Hochberg procedure, with $q < 0.05$.

2.3 Results

2.3.1 C1, P1, N1, and timecourse variability

Del, dup, and control group averages and differences in the variability of C1, P1, and N1 amplitude and latency are presented in **Table 2.5** and **Table 2.6**. Significant differences were found in P1 amplitude variability (**Figure 2.2A**) between del and controls. Specifically, del showed significantly higher variability in P1 amplitude compared to controls. Also, del showed significantly lower variability in P1 latency compared to dup (**Figure 2.2B**). No other significant differences were found between the three groups in C1, P1, and N1 intra-participant variability.

Table 2.5: Variability and averaged measures of neural activity of 16p11.2 CNVs.

		del	Control	dup
C1, P1, N1 variability	C1 amplitude (μV)	15.2 [6 17.75]	12.18 [3.91 14.39]	12.11 [4.5 17.8]
	C1 latency (ms)	21.5 [10 31]	16 [2 26]	16 [6 24]
	P1 amplitude (μV)	**17.67 [10.17 26.27]**	**11.01 [5.48 19.4]**	13.62 [3.11 25.25]
	P1 latency (ms)	**8 [4 16]**	10 [4 24]	**13 [8 26]**
	N1 amplitude (μV)	19.4 [9.52 25.88]	14.54 [6 26]	17.56 [4.02 30.51]
	N1 latency (ms)	34.5 [12 56]	32 [23 40]	42 [22 52]
Power variability	Absolute alpha (μV^2)	**13.39 [7.36 44.27]**	9.01 [2.78 34.85]	**8.10 [1.49 14.28]**
	Relative alpha (%)	0.09 [0.05 0.17]	0.11 [0.07 0.14]	0.08 [0.04 0.09]
	Absolute beta (μV^2)	**5.36 [1.93 19.74]**	3.15 [0.54 10.55]	**2.28 [1.25 5.35]**
	Relative beta (%)	0.04 [0.02 0.09]	0.05 [0.03 0.06]	0.04 [0.01 0.07]
SNR	(dB)	4.73 [3.22 6.29]	4.89 [3.93 7.87]	4.83 [4.40 6.35]
C1, P1, N1 mean	C1 amplitude (μV)	**0.03 [-10.23 6.48]**	**-6.49 [-20.1 0.52]**	-4.54 [-7.91 -1.41]
	C1 latency (ms)	40 [2 72]	64 [20 70]	52 [2 72]
	P1 amplitude (μV)	**23.13 [8.08 43.06]**	14.42 [1.47 28.73]	**10.41 [3.21 16.76]**
	P1 latency (ms)	98 [78 126]	98 [68 134]	92 [88 134]
	N1 amplitude (μV)	-10.05 [-24.53 5.83]	-7.8 [-13.08 -1.34]	-7.3 [-11.79 -0.53]
	N1 latency (ms)	213 [144 268]	210 [136 250]	199 [162 268]
Power mean	Absolute alpha (μV^2)	**31.62 [18.01 98.28]**	24.52 [5.95 51.55]	**18.18 [3.60 35.93]**
	Relative alpha (%)	0.20 [0.14 0.35]	**0.23 [0.18 0.33]**	**0.16 [0.12 0.23]**
	Absolute beta (μV^2)	**15.48 [6.09 66.96]**	10.08 [1.81 22.92]	**6.78 [3.40 13.38]**
	Relative beta (%)	0.10 [0.04 0.24]	0.11 [0.08 0.16]	0.09 [0.05 0.20]

The data are reported as median [range]. Descriptives relating to significant results are in bold.

Table 2.6: Group differences in variability and averaged measures of neural activity of 16p11.2 CNVs.

		del/Control		dup/Control		del/dup	
		Actual difference	P-value	Actual difference	P-value	Actual difference	P-value
C1, P1, N1 variability	C1 amplitude (µV)	2.92	0.048	1.45	0.437	1.48	0.330
	C1 latency (ms)	7.25	0.010	1.45	0.702	5.80	0.020
	P1 amplitude (µV)	6.16	**0.001**	2.79	0.282	3.37	0.100
	P1 latency (ms)	0.80	0.650	5.05	0.108	5.85	**0.003**
	N1 amplitude (µV)	4.01	0.080	3.15	0.368	0.86	0.724
	N1 latency (ms)	5.61	0.154	9.66	0.021	4.05	0.372
Power variability	Absolute alpha (μV^2)	4.67	0.226	4.80	0.231	9.47	**0.004**
	Relative alpha (%)	0.01	0.510	0.03	0.016	0.02	0.064
	Absolute beta (μV^2)	2.28	0.085	1.17	0.325	3.45	**0.002**
	Relative beta (%)	< 0.01	0.599	<0.01	0.950	<0.01	0.687
SNR	(dB)	0.23	0.556	0.04	0.931	0.27	0.400
C1, P1, N1 mean	C1 amplitude (µV)	6.50	**0.006***	2.75	0.349	3.75	0.025
	C1 latency (ms)	18.07	0.022	9.52	0.277	8.55	0.323
	P1 amplitude (µV)	8.65	0.010	3.06	0.359	11.71	**0.0003**
	P1 latency (ms)	0.45	0.926	1.45	0.862	1.00	0.836
	N1 amplitude (µV)	0.98	0.702	0.63	0.728	1.61	0.565
	N1 latency (ms)	20.41	0.191	20.91	0.284	0.50	0.975
Power mean	Absolute alpha (μV^2)	13.87	0.067	8.22	0.225	22.09	**0.003**
	Relative alpha (%)	0.02	0.208	0.07	**0.003**	0.04	0.019
	Absolute beta (μV^2)	7.51	0.053	2.78	0.289	10.29	**0.003**
	Relative beta (%)	0.01	0.731	<0.01	0.892	0.01	0.681

Significant results of permutation tests after correcting for FDR (significance threshold at p < 0.006) are in bold. *This result becomes non-significant in the secondary analysis of channel selection criterion.
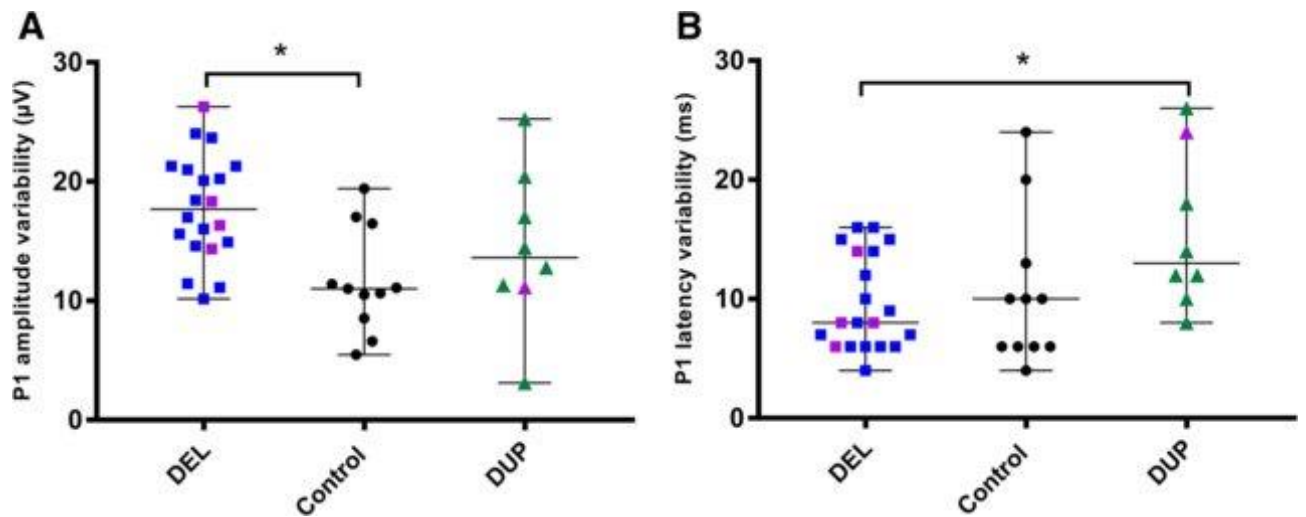
Figure 2.2: P1 variability in 16p11.2 CNV.
All three groups are presented similarly in both subfigures with the del group shown in blue, the dup group shown in green, and the typical control groups shown in black. In addition, participants within the CNV groups with a diagnosis of autism spectrum disorder are indicated in purple. (A) The left graph shows scatter plots representing the distributions (median and range) of intra-participant amplitude variability (MAD) of the peak P1 component, averaged across groups. (B) The right graph shows group distributions of latency variability of peak P1.

Timecourse variability, that is, trial-to-trial variability in the amplitude of each individual datapoint (2 ms) in the signal (range: −100 ms, 300 ms), was also compared between the three groups. Compared to controls, del showed higher 2 ms-interval trial-to-trial variability almost consecutively for the whole period between −100 and 172 ms (length of gaps <31 ms) and at 286 ms (see **Figure 2.3** for a precise illustration of the timepoints during the epoch where timecourse variability was significantly greater in del than controls). No other differences were found in timecourse variability between the three groups.
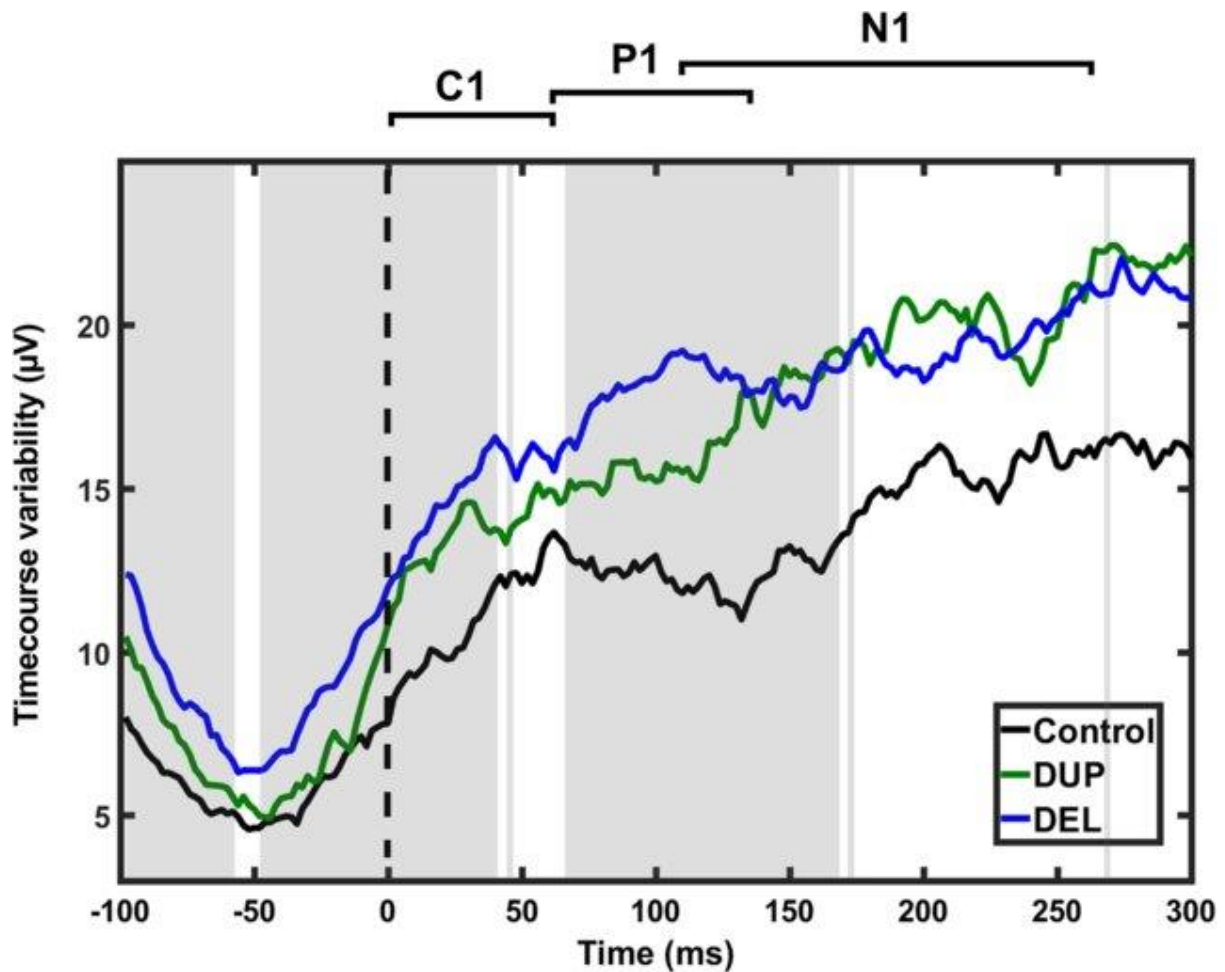
Figure 2.3: Timecourse variability in 16p11.2 CNV.
Timecourse variability in 16p11.2 CNV. The del group is indicated with blue, dup group with green, and control group with black. The figure shows the timecourse variability (i.e., variability in amplitude at each time-point, 2 ms interval, throughout the signal) for all three groups. The grey shaded areas represent the durations by which del significantly differed from controls in amplitude (significance threshold at $P < 0.029$).

Mean amplitude and latency of C1, P1, and N1 were compared between the three groups (**Table 2.5** and **Table 2.6**). del showed higher C1 (i.e., lower negative peak) amplitude compared to controls. Note that when the channel selected for analysis was based on the alternative criterion of selecting the electrode showing the lowest C1 and N1 amplitude for the respective C1 and N1 analyses, this group difference was no longer significant and a new result of increased C1 latency in dup compared to controls was found. In line with LeBlanc and Nelson (2016), del showed higher P1 amplitude compared to dup. No other significant differences were found.

2.3.2 Alpha and beta power variability

Trial-to-trial variability in absolute and relative power within the alpha and beta frequency bands were compared between the three groups (**Table 2.5** and **Table 2.6**). Variability in absolute alpha and beta power was significantly higher for del compared to dup (**Figure 2.4A** and **Figure 2.4B**). No other significant group differences were found in alpha or beta power variability.
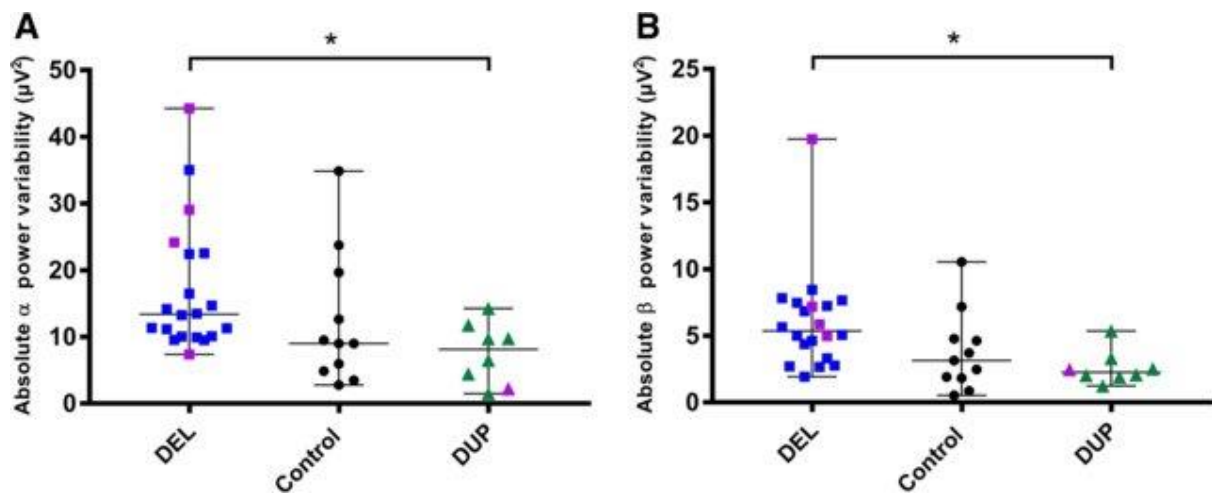
Figure 2.4: Alpha and beta power variability in 16p11.2 CNV.
All three groups are presented similarly in both subfigures with the del group shown in blue, the dup group shown in green, and the typical control groups shown in black. In addition, participants within the CNV groups with a diagnosis of autism spectrum disorder are indicated in purple. **(A)** The left subfigure shows scatter plots representing the group distributions of intraparticipant variability of absolute alpha power (8–14 Hz). **(B)** The right subfigure shows group distributions of absolute beta variability (14–30 Hz).

Mean absolute and relative power in the alpha and beta frequency bands were also compared between the three groups (**Table 2.5** and **Table 2.6**). Relative alpha power was lower for dup compared to controls. Additionally, absolute alpha and absolute beta power were higher for del compared to dup. No significant group differences were found in mean alpha or beta power.

2.3.3 Signal-to-noise ratio

The analysis revealed no significant differences in SNR between the three comparisons (**Table 2.5** and **Table 2.6**).

2.3.4 Correlations between IQ, ADOS-CSS, and EEG measures in 16p CNV

For each of the del and dup groups, correlation permutation tests were performed between IQ and ADOS-CSS against EEG measures of interest (C1, P1, and N1 variability; alpha and beta

power variability; SNR; C1, P1, and N1 mean; alpha and beta power mean), respectively. No significant correlations were found (**Table 2.7**).

Table 2.7: Correlations between IQ, ADOS-CSS, and EEG measures in 16p11.2 CNV.

		del		dup	
		IQ	**ADOS-CSS**	**IQ**	**ADOS-CSS**
C1, P1, N1 variability	C1 amplitude (µV)	-0.45	0.38	-0.30	-0.64
	C1 latency (ms)	0.06	0.08	0.54	-0.03
	P1 amplitude (µV)	-0.42	< 0.001	-0.49	-0.76
	P1 latency (ms)	-0.27	0.07	-0.70	0.06
	N1 amplitude (µV)	-0.59	0.11	-0.51	-0.52
	N1 latency (ms)	-0.37	-0.01	-0.4	0.52
Power variability	Absolute alpha (µV^2)	-0.67	0.29	-0.07	-0.88
	Relative alpha (%)	-0.10	-0.09	-0.04	-0.70
	Absolute beta (µV^2)	-0.13	0.17	-0.54	-0.39
	Relative beta (%)	0.21	0.05	0.16	0.70
SNR	(dB)	0.02	0.26	0.01	0.33
C1, P1, N1 mean	C1 amplitude (µV)	-0.01	0.23	0.14	0.21
	C1 latency (ms)	-0.49	0.74	-0.09	0.27
	P1 amplitude (µV)	< 0.001	-0.11	0.18	-0.21
	P1 latency (ms)	-0.39	-0.02	0.05	0.12
	N1 amplitude (µV)	0.02	0.10	0.17	0.64
	N1 latency (ms)	-0.18	-0.39	-0.46	0.28
Power mean	Absolute alpha (µV^2)	-0.64	0.18	-0.24	-0.88
	Relative alpha (%)	-0.19	-0.14	0.16	-0.70
	Absolute beta (µV^2)	-0.13	0.36	-0.71	-0.76
	Relative beta (%)	0.32	-0.01	0.05	0.76

The reported values correspond to the r coefficient. All results are non-significant. Significance threshold at $p < 0.003$.

2.3.5 The impact of age on neural activity

For each of the three groups, correlation permutation tests were performed between age and the EEG measures of interest (C1, P1, and N1 variability; alpha and beta power variability; SNR; C1, P1, and N1 mean; alpha and beta power mean), respectively. No significant correlations were found (**Table 2.8**).

Table 2.8: Correlations between age and EEG variability and averaged metrics in 16p11.2 and control groups.

		del	Control	dup
		Age		
C1, P1, N1 variability	C1 amplitude (μV)	0.26	-0.06	-0.23
	C1 latency (ms)	0.27	-0.36	0.02
	P1 amplitude (μV)	-0.37	<0.01	-0.57
	P1 latency (ms)	-0.47	-0.12	0.25
	N1 amplitude (μV)	-0.60	-0.16	-0.51
	N1 latency (ms)	-0.36	-0.18	-0.12
Power variability	Absolute alpha (μV^2)	-0.47	0.11	-0.42
	Relative alpha (%)	-0.30	-0.01	0.14
	Absolute beta (μV^2)	0.47	0.05	-0.38
	Relative beta (%)	0.53	0.28	0.36
SNR	(dB)	-0.15	-0.20	-0.55
C1, P1, N1 mean	C1 amplitude (μV)	0.10	-0.57	0.24
	C1 latency (ms)	-0.39	0.05	0.12
	P1 amplitude (μV)	0.04	0.36	-0.41
	P1 latency (ms)	-0.20	-0.02	0.49
	N1 amplitude (μV)	-0.19	-0.15	0.25
	N1 latency (ms)	-0.25	0.32	0.28
Power mean	Absolute alpha (μV^2)	-0.34	0.11	-0.40
	Relative alpha (%)	-0.25	0.23	0.08

Absolute beta (μV^2)	0.47	0.05	-0.47
Relative beta (%)	0.50	0.05	0.54

The reported values correspond to the r coefficient. All results are non-significant.
Significance threshold at p < 0.006.

The number of trials available for analysis differed for each participant which could potentially influence estimates of variability. Thus, to investigate whether the number of trials per participant was associated with variability, SNR, and/or averaged EEG measures, permutation correlation tests were conducted, and the outcomes were corrected using the Benjamini–Hochberg procedure, with $q < 0.05$. The results showed that there were no significant relationships between the EEG measures and trial number (**Table 2.9**). In the current study, the number of retained trials in the three groups were the same on average (mean = 49 trials per group, Kruskal–Wallis (χ^2 (2) = 0.58, $P = 0.748$, indicates no difference in median). Therefore, the variable trial number per participant is unlikely to explain any observed group differences in any of the EEG measures of interest.

Table 2.9: Correlations between EEG measures and trial number.

		Trial number
C1, P1, N1 variability	C1 amplitude (μV)	-0.38
	C1 latency (ms)	-0.07
	P1 amplitude (μV)	-0.43
	P1 latency (ms)	0.02
	N1 amplitude (μV)	-0.43
	N1 latency (ms)	-0.25
Power variability	Absolute alpha (μV^2)	-0.14
	Relative alpha (%)	0.09
	Absolute beta (μV^2)	-0.23
	Relative beta (%)	0.13
SNR	(dB)	-0.09
C1, P1, N1 mean	C1 amplitude (μV)	0.14
	C1 latency (ms)	0.05
	P1 amplitude (μV)	-0.06
	P1 latency (ms)	-0.05

	N1 amplitude (µV)	0.28
	N1 latency (ms)	-0.19
Power mean	Absolute alpha (µV^2)	-0.20
	Relative alpha (%)	0.20
	Absolute beta (µV^2)	-0.25
	Relative beta (%)	0.02

The reported values correspond to the r coefficient. All results are non-significant. Significance threshold at $p < 0.006$.

2.4 Discussion

The aim of the study was to determine whether 16p11.2 CNVs show opposing atypical EEG signals, which could broadly indicate gene-dosage effects (i.e., additive model) playing a differential role in cognitive processes and neural plasticity. Multiple measures of neural variability were estimated from EEG data, most of which were single-trial intraparticipant analyses. Overall, our results suggest that 16p11.2 del carriers showed highly variable neural responses to visual stimuli, compared to controls. Variability of timecourse amplitude (i.e., variability in amplitude at time-points throughout the epoch; **Figure 2.3**) and variability of P1 peak amplitude were higher in del compared to controls. Compared to dup, del showed higher variability in absolute alpha and beta power but lower variability in P1 latency variability. Overall, it is unclear from our findings whether 16p11.2 dosage has an opposing effect on neural activity following the additive model. Despite finding significant differences in neural variability between del and dup, we did not find any differences between dup and controls (although note that we did find dup-control group differences in mean relative alpha power). Differences in neural activity between del and dup are not sufficient evidence of an opposing effect. For a true opposing effect to be seen, we would need to show that both groups differ in opposing directions from the control group (i.e., del > control and control > dup, or vice versa).

2.4.1 Is atypical neural variability unique to 16p11.2 CNVs?

Atypical neural variability has been shown in several ESSENCE disorders including ASD (Milne, 2011; Dinstein et al., 2012; Weinger et al., 2014; Edgar et al., 2015; Haigh et al., 2015, 2016; but see Coskun et al., 2009; and Butler et al., 2017), ADHD (Woltering et al., 2012; McLoughlin et al., 2014; Gonen-Yaacovi et al., 2016; Sørensen et al., 2016), and schizophrenia (Shin et al., 2015; Haigh et al., 2016). For example, similar to the current

study's finding with respect to P1 variability found in del, atypically high visual evoked P1 amplitude variability was also reported for ASD (Milne, 2011) and ADHD groups (Gonen-Yaacovi et al., 2016). However, Milne (2011) also found atypical P1 latency variability in ASD, whereas here, neither the del nor dup group showed latency variability that differed from the control group, although, P1 latency variability was decreased in del compared to dup. Further group differences between del and dup in neural variability were found in EEG spectral power; here, del showed higher absolute power variability, in beta and alpha bands, compared to dup (again, neither CNV groups differed in power variability when compared to controls). Woltering et al. (2012) similarly reported lower (absolute) alpha and beta power variability in ADHD compared to controls (Woltering et al., 2012).

Previous studies also found higher timecourse variability in ADHD, time window: 0–500 ms (Gonen-Yaacovi et al., 2016), and time window: 0–600 ms (Myatchin et al., 2012), similar to our finding in relation to timecourse variability in del. Gonen-Yaacovi et al. (2016) also computed baseline variability (pre-visual stimulus onset; time window: −200-0 ms) and reported higher variability in ADHD—again consistent with our del findings. There is an extensive literature on the putative interactions between evoked and ongoing activity raising the possibility that the increased variability prior to stimulus onset contributed to that observed post-stimulus (Busch et al., 2009). Standard approaches to correct baseline simply subtract the average of the pre-stimulus period from each trial and do not take into account variability both in the pre-stimulus timeseries of single trials or variability across trials. As such, it is important to examine both ERP amplitude and variability before and after stimulus onset.

Evidently, it would not be plausible to regard atypical neural variability, whether in the form of P1 variability, timecourse variability, or other, as distinct to 16p11.2 CNVs in light of the several heterogeneous disorders that show general similar variability dynamics. Rather, this study highlights that 16p11.2 CNVs—specifically deletions—should be added to the list of clinical conditions which show increased neural variability. The overall picture alludes to certain similarities in the behaviour of neural responses, which would be informative and useful for further investigations.

2.4.2 Interpreting neural variability

Although, neural variability has become a topic of interest in many research areas including clinical populations (Pernet et al., 2011; Garrett et al., 2013; Dinstein et al., 2015; Butler et

al., 2017; David et al., 2016), the interpretation of neural variability remains a challenge. Nevertheless, it has been widely recognized that optimal neural variability is a characteristic of typical and healthy brain function, facilitating learning, adaptation to a changing environment, and other cognitive processes (Basalyga and Salinas, 2006; Faisal et al., 2008; McDonnell and Abbott, 2009; Heisz et al., 2012). Deviations from the typical levels of neural variability in the 16p11.2 del group, therefore, could be regarded as a signature of neuropathology and cognitive dysfunction, as was similarly indicated in the aforementioned studies of related ESSENCE disorders. IQ and autism symptom severity did not relate to any of the neural variability and averaged measures in the current study's 16p11.2 CNV sample (**Table 2.7**). Although consistent with previous studies (LeBlanc and Nelson, 2016; Jenkins et al., 2016) this lack of relationship could simply be due to sample size and needs to be further validated in future studies with larger samples. Furthermore, neural variability could be related to other 16p11.2 CNV symptoms and traits, which could not be revealed via the phenotypic assessments used in the current and previous studies.

Of note, a recent study suggested that neural variability (on a macro-level as measured by intertrial variation of the BOLD signal) is negatively related to dopamine concentration levels, quantified using PET (Guitart-Masip et al., 2016). In a mouse model of 16p11.2 CNV (Portmann et al., 2014), dopamine-related deficits were found in the striatum, therefore indicating the potential role of certain genes within the 16p11.2 region in establishing typical dopaminergic synaptic activity. Specifically, after tissue dissociation, single-cell gene expression analysis was used to first identify cell types in predefined brain regions (including the striatum) based on their gene expression pattern (of genes within the 16p11.2 region and outside). Next, the composition of the identified cells was studied and compared between 16p11.2 del mice and control. Increased numbers of striatal medium spiny neurons with the dopamine D2 receptor and decreased neurons with dopamine D1 receptors in deeper cortical layers were found. Accordingly, a potential factor driving atypical neural variability in the CNV groups could be the dysregulation of dopamine levels; this, in turn, would lead to deficits in processes mediated by dopamine such as motivation and learning processes, movement, and social behaviour (Wise, 2004; Portmann et al., 2014), all of which are seen in 16p11.2 CNV carriers and related disorders.

The observed atypical EEG activity in 16p11.2 CNV carriers could also reflect cellular electrophysiological and synaptic abnormalities that influence excitatory/inhibitory

(E/I) neural processes. To examine cellular characteristics of 16p11.2 CNV carriers, a recent study used fibroblasts obtained from 16p11.2 CNV carriers and generated induced pluripotent stem cells, which were then differentiated into (forebrain cortical) neurons (Deshpande et al., 2017). Compared to neurons derived from typical controls, the authors found an increase in the amplitude of miniature excitatory postsynaptic currents in both del and dup (excitatory) neurons. As the authors suggest, the increase in amplitude may be compensating for the reduced density of synapses in the CNV neurons. These altered cellular properties could affect overall neural plasticity and connectivity, which ultimately leads to the behavioural symptoms related to 16p11.2 CNV carriers and possibly to the activity recorded by EEG.

Relatedly, EEG alpha power has been associated with a mechanism that modulates neural E/I activity via pulsed-inhibition of on-going visual and other neural processing (for a review see Mathewson et al., 2011). Therefore, the observed lower (mean) relative alpha in dup compared to controls (in the current study) could be reflecting atypical perturbations to the E/I balance. Indeed, our EEG findings of atypical neural variability and alpha power in 16p11.2 CNV carriers could signify an E/I imbalance possibly due to synaptic impairment of excitatory neurons (Deshpande et al., 2017), and dopaminergic neurons (Portmann et al., 2014).

2.4.3 Limitations

Although we addressed the issue of small sample size with randomisation techniques, larger datasets would have been desirable to enable examination of confounding variables, such as epilepsy, than was possible here. In addition, given the small sample size and the multiple correlational analyses (i.e., numerous metrics of neural activity vs IQ and ADOS-CSS), the threshold for significance was set at a conservative $p < 0.003$, as per the Benjamini–Hochberg method. Consequently, there is a risk of committing a type II error, especially as certain correlations with large effect sizes were present, such as between P1 amplitude variability and ADOS-CSS ($r = -0.76$) for dup (**Table 2.7**). Nevertheless, a conservative approach is necessary and appropriate for the current study given the small sample size. A further limitation is the lack of IQ data for the control group. As participant IQ data were not available for the typical control participants, it was not possible to adequately account for cognitive ability in this study. Although in our current sample there were no IQ differences between del and dup, other larger-scale phenotypic studies have reported differing IQ profiles, with the dup group tending to show higher IQ (Hippolyte et al., 2016) and a wider

range of IQ scores (D'angelo et al., 2016). A further limitation concerns the wide age ranges of the participants in the three groups. Consistent with LeBlanc and Nelson (2016), we found no effect of age on any of the EEG measures of interest (**Table 2.8**). Furthermore, our sample showed no significant group differences in age. This, however, does not preclude the possibility of some minor effect of maturational changes on neural variability, which might be better expressed in a different 16p11.2 CNV sample.

2.4.4 Concluding remarks.

The overall results, drawn from multiple measures of neural variability, strongly suggest that 16p11.2 del carriers, in particular, show visual-evoked neural responses that are highly variable compared to controls. Levels of neural variability were atypical and, thus, were postulated to have deviated from the optimal variability levels necessary for healthy brain function and cognitive processing. (Of note, despite dup carriers showing neural variability levels in the typical range, secondary analyses showed that relative (mean) alpha power was atypical and, therefore, might be indicating a related dysfunction).

The following study (**Chapter 3**) will focus on 16p11.2 del carriers. Neural activity and potential associations with ESSENCE difficulties will be more extensively assessed. In order to assess this in an alternative context, the following study will analyse spontaneous neural activity (i.e., resting-state EEG), as opposed to evoked neural activity. This will further enable 16p11.2 human-mouse comparisons in relation to EEG-LFP activity at rest (**Chapter 4**).

Chapter 3 Spontaneous neural activity relates to psychiatric traits in 16p11.2 deletion carriers: a joint analysis of EEG spectral power and multi-scale entropy.

3.1 Introduction

Evidence from the study presented in **Chapter 2** and indeed the 16p11.2 literature (Al-Jawahiri et al., 2019; Hinkley et al., 2019; Bertero et al., 2018; LeBlanc and Nelson, 2016; Jenkins et al., 2016; Berman et al., 2016; Steinman et al., 2016; Hudac et al., 2015) suggest that a loss of the 16p11.2 region impacts neural activity relevant to multiple contexts, e.g., sensory, social. Despite this, the alteration in evoked neural activity did not seem to relate to any of the cognitive/psychiatric ESSENCE (early symptomatic syndromes eliciting neurodevelopmental clinical examinations) traits in 16p11.2 deletion carriers (del; **Table 1.5**) - although Hinkley et al. (2019) reported otherwise. Unlike the aforementioned studies, Hinkley et al. (2019) found that the reported increased task-induced beta power in del, over sensorimotor cortices, was associated with phonological and motor deficits. Conversely, as reported in **Chapter 2** and previous studies (see **Table 1.5**), no links were found between visual and auditory evoked neural activity (i.e., neural variability measures; N1, P1, and N2 amplitude and latency; M100 latency) and IQ, autistic-traits, and social and language ability.

When examining spontaneous neural activity (using fMRI), however, brain functional alterations were found to be associated with social and cognitive impairments in 16p11.2 del (Bertero et al., 2018). The brain functional alterations were reduced global prefrontal connectivity and reduced long-range prefrontal connectivity with parieto-temporal areas in 16p11.2 del (as described in detail in **Chapter 1**). As such, it is worth examining further properties and attributes of frontal resting-state signal (e.g., entropy) and its link to a range of ESSENCE traits in 16p11.2 del.

Indeed, investigating properties such as the level of entropy, or in other words, the level of irregularity and unpredictability, in neural activity has been increasingly producing interesting findings in relation to ESSENCE disorders (for a review, see Chu et al., 2017; Takahashi, 2013; Yang and Tsai, 2013). With Multi-Scale Entropy (MSE) analysis (Costa et al., 2002; Costa et al., 2005), in particular, it is possible to quantify the level of entropy (i.e., irregularity) of moment-to-moment patterns of (neural/BOLD) amplitudes across different timescales in the signal. In simple terms, higher entropy indicates higher irregularity in the

signal, while lower entropy indicates a more regular, predictable pattern. MSE analysis is 'multi-scale' because entropy is measured at different timescales, beginning with the timescale of the original signal, referred to as timescale 1, and then timescale 2 is generated by averaging two non-overlapping consecutive datapoints in the signal, and then three datapoints for timescale 3, etc, across the whole signal

To elaborate further, MSE is more accurately conceptualised as an index of signal complexity. A more complex signal conveys rich information (i.e., likely meaningful/ biological) and is in between the two extremities of randomness and order. Single-timescale-entropy-based approaches assign higher entropy values to more random signals and lower entropy to more regular signals. By considering multiple timescales, however, MSE is able to distinguish biological complex signals from random signals (i.e., white noise; Costa et al., 2002; Costa et al., 2005). This is because at lower (i.e., finer/shorter) timescales, both random and signals with an 1/f property (i.e., pink noise; a signal common in biological systems, in which the power spectral density (PSD) is inversely proportional to the signal's frequency) present with high entropy values, however at later timescales (i.e., higher/coarser/longer scales), random signals monotonically decrease in entropy compared to biological signals. Therefore, measuring entropy at multiple timescales is advantageous and appropriate for investigating neural activity.

On a conceptual level, the general consensus is that entropy, like other neural measures, relates to information processing (McDonough and Nashiro, 2014; Garrett et al., 2013). Higher entropy has been more specifically, albeit abstractly, interpreted as reflecting a less deterministic system capable of facilitating dynamic neural communication and switching between different cognitive states (Mišić et al., 2015; Mišić et al., 2011; Vakorin et al., 2011; Liang et al., 2014). Accordingly, it would be expected that entropy and functional connectivity (FC: a measure of neural synchrony between different brain regions, and therefore reflecting neural communication) are positively related: with higher entropy levels, there would be higher FC between the respective brain regions. However, studies that examined this MSE-FC relationship suggest a more complicated interpretation that is timescale dependent (**Figure 3.1**; Wang et al., 2018; Ghanbari et al., 2015; McDonough and Nashiro, 2014). In the case of MSE and FC both measured from fMRI data, a negative and positive relationship was found at lower (**Figure 3.1a**) and higher timescales (**Figure 3.1b**), respectively (McDonough and Nashiro, 2014). It is important to note that fMRI's lower temporal resolution, compared to EEG and LFP, means that fMRI entropy levels at high

timescales are equivalent to EEG/LFP entropy levels at mid or lower timescales. Hence, this should be considered when interpreting and comparing MSE-FC studies. With MSE-local field potential (LFP) and FC-fMRI correlations (**Figure 3.1c** and **Figure 3.1d**; Wang et al., 2018), a positive relationship at each respective timescale was reported. In addition, the strength of the relationship progressively increased with higher timescales ($r = 0.44$, $r = 0.51$, $r = 0.54$, $r = 0.56$, $r = 0.45$, therefore portrayed as a positive relationship across timescales in **Figure 3.1c** and **Figure 3.1d**). Using simulated neural data (i.e., neural mass modelling), a similar positive trend was observed; in addition, the MSE-FC relationship at timescales in the lower range was best described as an inverted U-shape, or a quadratic function at respective time-scale bins (in the lower range), yet the relationship could be described as positive across timescales (with the r-coefficient increasing in strength from lower to higher timescales; $r = 0.24$, $r = 0.34$, $r = 0.44$, $r = 0.72$, $r = 0.79$, $r = 0.65$ **Figure 3.1e and Figure 3.1f**; Wang et al., 2018). Interestingly, the MSE-FC relationship might be different for individuals presenting with ESSENCE disorders. For instance, a negative relationship was found between MSE-MEG and FC-MEG at any timescale and brain region in individuals with ASD (**Figure 3.1g** and **Figure 3.1h**; Ghanbari et al., 2015). For timescales in the lower range, the strength of the negative correlation progressively increases ($r = -0.46$, $r = -0.65$, $r = -0.82$). This trend is also found for timescales in the higher range although to a lesser extent as the rate of decrease is relatively lower ($r = -0.40$, $r = -0.53$). However, this trend does not form a continuum from lower to higher scales. It was not clear, however, whether a trend towards a negative MSE-FC relationship would be equally apparent across timescales (i.e., not only at individual categories of timescales but across all timescales)[4].

---

[4] Note that although essentially similar to what has been described earlier in relation to MSE analysis, some of the aforementioned studies (e.g., Wang et al., 2018) analysed MSE in the frequency domain as opposed to the time domain. As MSE is sensitive to changes in the frequency content of the signal in a predictable manner, the impact of MSE on timeseries in the time-domain and its equivalence in the frequency domain could be deduced (**Figure 3.1C** and **Figure 3.1D**). Therefore, for the sake of consistency, the relevant literature has been and will henceforth be discussed in the context of entropy at time-domain timescales rather than entropy at different frequencies.
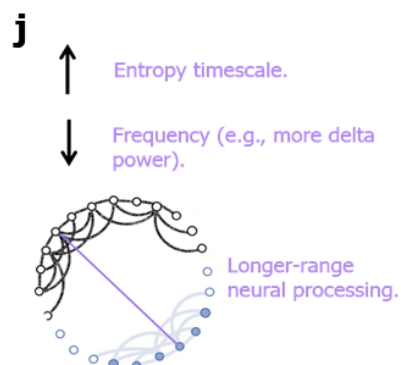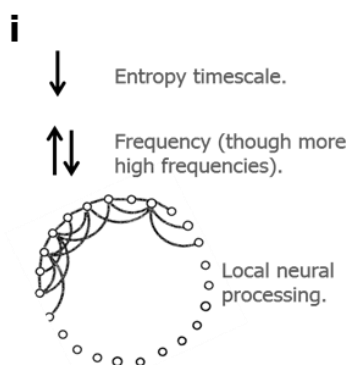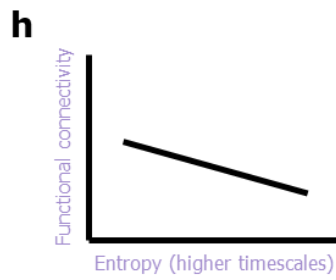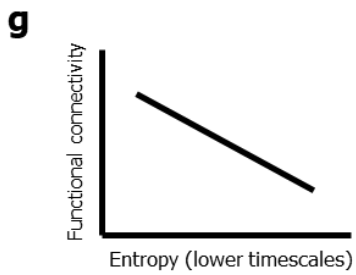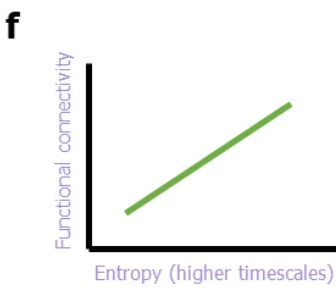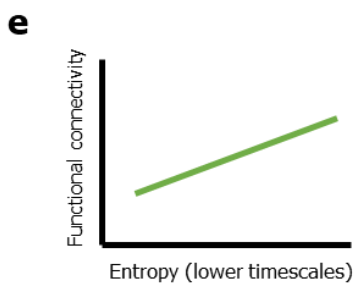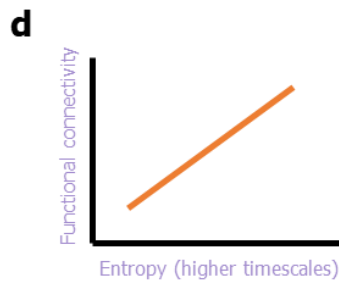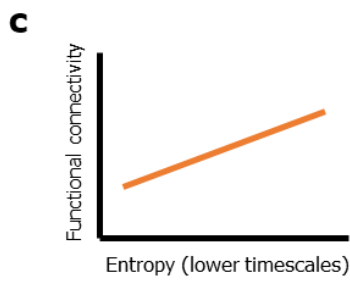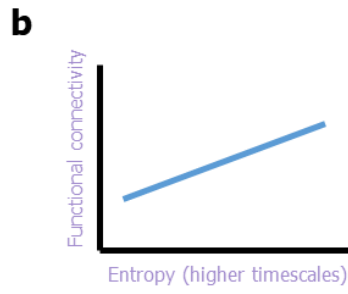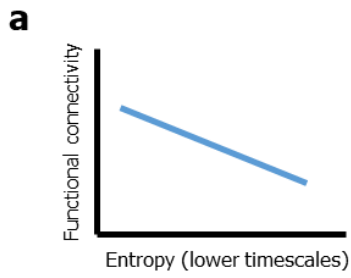
Figure 3.1: Conceptual representation of the relationship between MSE, functional connectivity, frequencies, and local and long-range neural processing.
Subfigures (a, b, c, d, e, f, g, h, i, j) show the relationship between entropy and functional connectivity for respective modalities (e.g., fMRI, LFP). Subfigures (i) and (j) describe the relationship between entropy at lower timescales and higher timescales, respectively, with power, and neural processing range (i.e., short-range vs long-range). For subfigure (i), entropy at lower timescales (downward arrow) reflects power at higher frequencies and, to a lesser extent, lower frequencies (double arrows, one upward to indicate higher frequencies and downward arrow indicates lower frequencies). Entropy at lower timescales and, hence, higher frequencies further reflect local neural processing (subfigure indicating local connections). For subfigure (j), Entropy at higher timescale (upward arrow), reflects power at lower frequencies (downward arrow), and long-range neural processing (subfigure indicating long-range activity).

Notably, MSE relates to the frequency domain as it is sensitive to changes in the frequency content of the signal (**Figure 3.1i** and **Figure 3.1j**). MSE's coarse-graining procedure, in which time-series with growing timescales are generated from the original time-series, essentially acts as a low-pass filter (i.e., a filter that passes low frequencies and attenuates higher frequencies; Courtiol et al., 2016; Govindan et al., 2007; Kaffashi et al., 2008; Valencia et al., 2009). Due to the coarse-graining effect, lower timescales contain activity from both higher frequencies and lower frequencies (**Figure 3.1i**), whereas higher timescales contain lower frequencies (**Figure 3.1j;** Courtiol et al., 2016; Takahashi et al., 2010; Mizuno et al., 2010). Therefore, it is more likely that lower timescales reflect local neural processing (**Figure 3.1i**) and higher timescales reflect longer-range neural processing (**Figure 3.1j;** Mizuno et al., 2010, Vakorin et al., 2011; McIntosh et al., 2014). This observation is supported by evidence of associations between MSE at lower timescales and higher timescales with metrics of local and distributed entropy, respectively (McDonough and Nashiro, 2014, McIntosh et al., 2014, Vakorin et al., 2011).

As mentioned earlier, atypical entropy has been implicated in various ESSENCE disorders found in 16p11.2 del (**Table 3.1**). Both resting-state and task-related paradigms showed atypical MSE patterns in the clinical group. Both higher and lower entropy have been found in ESSENCE disorders (relative to typical controls) in a manner that is task- (e.g., Mišić et al., 2015), timescale-, and brain region-dependent (e.g., Ghanbari et al., 2015). Accordingly, these studies (**Table 3.1**) suggest that whether higher or lower entropy, atypical entropy levels in ESSENCE could be indicative of a pathological state involving a dysfunction in neural temporal coordination. For example, compared to controls, higher entropy was found in ASD at higher timescales in the occipital, parietal, and temporal areas

at resting-state (Takahashi et al., 2016), while lower entropy at higher timescales was found in a face and chair detection task (Catarino et al., 2011) in the same brain areas. In addition, Milne et al., (2019) found lower overall entropy in ASD at resting-state across all timescales and brain regions. Other ESSENCE disorders that have shown atypical MSE (**Table 3.1**) include epilepsy and seizures (Bosl et al., 2017; Lu et al., 2015), ADHD (Chenxi et al., 2016), Schizophrenia (Takahashi et al., 2010), Alzheimer's (Yang et al., 2013; Mizuno et al., 2010) and Tourette's syndrome (Weng et al., 2017).

In addition to the dependence of MSE on task, timescale, and brain region, evidence showed that MSE levels are age-dependent in a manner following an inverted U-shaped curve: MSE increases at lower scales from childhood to adulthood and then decreases at higher scales in old age (McIntosh et al., 2014; Milne et al., 2019). This pattern, however, is not present in ESSENCE disorders as no relationship was found between MSE and age in ASD in one study (Milne et al., 2019), while an atypical MSE maturation was found in another study (Takahashi et al., 2016).

Other than group differences in neural entropy, several resting-state studies found that certain changes in neural entropy levels were related to psychiatric traits in ESSENCE disorders (**Table 3.1**). Overall, these studies suggest that MSE is sensitive to neural changes in ESSENCE disorders, including changes to the developmental trajectory of age-related neural change in ESSENCE disorders, and may be related to specific traits and symptoms that occur in ESSENCE disorders.

Table 3.1: MSE of M/EEG neural activity in ESSENCE disorders.

ESSENCE	Study	Analysis method	Paradigm	Key findings	MSE link with ESSENCE
ASD	Milne et al. (2019)	MSE	Resting-state	Lower entropy in ASD (MSE value computed by collapsing over scale factor and electrodes (frontal, centro-parietal, occipital)). Atypical MSE development: For controls, MSE at lower scales positively correlated with age and MSE at higher scales negatively correlated with age. Whereas for ASD, no relationship between MSE and age was found.	No relationship between MSE and psychiatric traits (SRS-2, RBQ-2A, BAIT, ASRS Screener).
	Bosl et al. (2017)	Modified MSE	Resting-state	Higher entropy in ASD at frontal, occipital, left temporal areas at all scales.	-
	Liu et al. (2017)	MSE	Motor observation task; motor imitation task.	Lower entropy in ASD (possibly across all scales) at central, parietal, occipital, and right temporal areas.	-
	Takahashi et al. (2016)	MSE	Free watching of videos without sound.	Higher entropy in ASD at higher scales over the occipital, parietal, and temporal areas. Atypical MSE development: For controls, MSE positively correlates with age at around scale 10 in occipital, temporal, parietal areas. For ASD, MSE positively (weakly) correlates with age at lower scales in central area.	MSE (at higher scales in fronto-central area) was negatively correlated with communication ability (ADOS-severity scale).
	Ghanbari et al. (2015)	MSE within frequency bands (maximum entropy along the scales).	Resting-state	Lower entropy in ASD in delta band over frontal areas, and in alpha band over occipital-parietal areas. Also, higher entropy in ASD in delta (parietal areas), theta (central and temporal areas) and gamma (frontal-central boundary areas).	MSE across frequencies was both negatively and positively correlated with symptom severity (social responsiveness scale (SRS)).

ESSENCE	Study	Analysis method	Paradigm	Key findings	MSE link with ESSENCE
	Mišić et al. (2015)	MSE	Set-shifting task designed to test mental flexibility	An interaction between task and group at many regions (e.g., prefrontal, parietal, etc.); the ASD group showed higher entropy at higher scales in one task, and higher entropy at lower scales in another task. The control group showed the opposite contrast in both tasks.	Activation of the identified regions correlated with faster reaction times in controls – but not in ASD.
	Bosl et al. (2011)	Modified MSE	Resting-state	Lower entropy in high-risk ASD group (HRA) across all scales and brain areas. A model showed 80% accuracy in identifying HRA at nine months old.	-
	Catarino et al. (2011)	MSE	Face and chair detection task.	Lower entropy in ASD at higher scales over temporal, parietal, and occipital areas.	No difference in behavioural performance.
Epilepsy and seizures	Bosl et al. (2017)	Modified MSE	Resting-state	Higher entropy in absence epilepsy across all brain areas at all scales.	-
	Lu et al. (2015)	MSE and CI (estimating area under MSE curve by integrating entropy values of all scales).	Interictal EEG (between seizures) in light sleep state.	MSE: lower entropy in most scales in neonates with later epilepsy (epilepsy group) compared to typical controls and those without later epilepsy (seizures group). (Brain areas not specified). CI: lower entropy in epilepsy group compared with controls or seizures group over central areas.	-
ADHD	Chenxi et al. (2016)	MSE within frequency bands (mean entropy along the scales).	Multi-source interference task.	Higher entropy in ADHD in delta band and lower entropy in alpha at longer scales mainly over frontal and central areas.	Longer reaction time of ADHD group compared to controls during interference trials.

ESSENCE	Study	Analysis method	Paradigm	Key findings	MSE link with ESSENCE
SZ	Takahashi et al. (2010)	MSE	Resting-state	Higher entropy in the drug-naive SZ group at higher scales in frontal, central, and temporal areas. Using antipsychotic treatment, this higher entropy in SZ was lowered to the typical controls' level in frontal and central areas. However, entropy levels in temporal areas tended to remain higher.	No relationship between MSE and psychiatric traits (BPRS) pre- and during treatment. No relationship between MSE and medication dose.
Alzheimer's	Yang et al. (2013)	MSE	Resting-state	Lower entropy in AD at lower scales over fronto-central, temporal, and occipito-parietal areas. Higher entropy at higher scales over the same areas.	MSE correlated with cognitive function (MMSE) and psychiatric traits (NPI). Over temporal, parietal, and occipital areas, MSE at lower scales was positively correlated with cognitive function, while MSE at higher scales was negatively correlated with cognitive function. Over various brain areas, MSE at lower scales was negatively correlated with psychiatric traits, while MSE at higher scales was positively correlated with psychiatric traits, especially sleep changes.
	Mizuno et al. (2010)	MSE	Resting-state	Lower entropy in AD at lower scales in frontal areas. Higher entropy at higher scales at frontal, central, parietal, and occipital areas.	MSE at higher scales was negatively correlated with cognitive function (MMSE).
Tourette's syndrome	Weng et al. (2017)	CI (estimating area under MSE curve by integrating entropy values of all scales); MSE (separate CI of scales grouped into 4 groups).	Resting-state	Lower CI in Tourette's syndrome in central, parietal, and occipital areas. Lower CI across all scales across various brain areas.	-

ASD, Autism Spectrum Disorder; ADHD, Attention Deficit Hyperactivity Disorder; SZ, Schizophrenia; AD, Alzheimer's Disorder; SRS, Social Responsiveness Scale; RBQ-2A, Adult Repetitive-Behaviours Questionnaire; BAIT, Beck Anxiety Inventory-Trait; ASRS Screener, WHO Adult ADHD Self-Report Scale Screener, Part A; ADOS, Autism Diagnostic Observation Schedule; HRA, High Risk ASD group; CI, Complexity Index; BPRS, Brief Psychiatric Rating Scale; MMSE, Mini Mental State Examination; NPI, Neuropsychiatric Inventory.

To our knowledge, no study to date investigated whether EEG neural activity is altered for 16p11.2 del at rest, whether using entropy-based approaches or complementary conventional power approaches. As fronto-parietal spontaneous neural activity has been particularly implicated in 16p11.2 del and linked with cognitive and social traits (Bertero et al., 2018), the current study will focus solely on 16p11.2 del. This will also maintain consistency with the study conducted in the next chapter on 16p11.2 del mouse model. Thus, the purpose of the current study is twofold; 1) To determine whether fronto-parietal spontaneous EEG activity is altered in 16p11.2 del, using both MSE and power analyses (including low-to-high frequency ratio (LHR)); 2) To identify changes in neural dynamics that are related to ESSENCE traits in 16p11.2 del carriers. Hence, this study tests the following hypotheses in relation to 16p11.2 del: 1) Neural activity, as reflected by entropy and power measures, is atypical; 2) There is a relationship between neural entropy and ESSENCE traits.

3.2 Methods

3.2.1 Participants

Data source is as described in **Chapter 2**, **Section 2.2.1**. Resting-state data from a total of 39 participants were obtained from the SVIP consortium for the current study. Data from five participants were excluded; these exclusions were either based on entropy values identified as extreme outliers (n = 4) or EEG files with signals greatly contaminated by artefacts on visual inspection (n = 1). The remaining 34 participants were analysed in this study: 22 del and 12 typical controls.

Participant information relating to age, sex, CNV inheritance, number of diagnoses, and IQ scores are reported in **Table 3.2**. The diagnoses in the current sample are listed in **Table 3.3**.

Table 3.2: Participant information.

Group	N	Age mean in months (SD)	Age range in months	Sex	CNV inheritance[a]			FSIQ mean (SD)[b c d]	Number of diagnoses mean [range]
					De-novo	Inherited	unknown		
del	22	67.09 (45.70)	10 - 183	M 12	7	2	3	80.95 (16.18)	2.30 [0 - 5]
				F 10	8	1	1		
Ctrl	12	69.67 (22.68)	39 - 109	M 6	-	-	-	-	-
				F 6	-	-	-	-	-

FSIQ, full-scale IQ.
[a]CNV inheritance data were obtained from the file svip_subjects.csv
[b]Missing data from del carriers (n = 2), typical group (n = 12).
[c]IQ data and the number of diagnoses were extracted from the file diagnosis_summary.csv
[d]The reported IQ scores were not adjusted for prematurity.

Table 3.3: Diagnoses in 16p11.2 del carriers.

Diagnosis	del (n = 22)
ADHD	3
Coordination disorder	12
Language disorder	9
Learning disorder	1
Intellectual disability	4
Behaviour disorder	3
Borderline intellectual functioning	2
ASD	3
Enuresis disorder	1
Articulation disorder	8

Each 16p11.2 del carrier may have more than one diagnosis.
ADHD, attention deficit hyperactivity disorder; ASD, autism spectrum disorder

Note that, the reported IQ scores were not adjusted for prematurity. Information regarding current medication was extracted from the SFARI medication questionnaire (med_child.csv); two del carriers were taking medication for anxiety and epilepsy/ seizures (i.e., diazepam (Valium) and topiramate (Topamax)).

Mann-Whitney U test revealed that there was no significant age difference between the two groups (U = 108.50, p = 0.397); and a Chi-Square test showed no association between group and sex ($\chi^2(1)$ = 0.06, p = 0.800). Other than age and sex, participant details and phenotypic data were not available for the typical control group. Therefore, IQ comparisons between del and controls were not possible.

3.2.2 Ethical approval

The current study has been ethically approved as described in **Chapter 2**, **Section 2.2.3**.

3.2.3 EEG recording and pre-processing prior to current study

EEG was recorded using a 128 channel HydroCel Geodesic Net (Electrical Geodesics Inc., Eugene, OR, USA). The signal was amplified with a NetAmps 300 amplifier and digitised at a sampling rate of 500 Hz. Spontaneous EEG was collected for 2 to 12 minutes during which participants rested and watched silent videos on a Tobii T60 eye-tracking monitor (Tobii Technology, Sweden; Note that eye-tracking data was not collected). The monitor was 34.7 cm wide and was positioned at a distance of ~ 60 cm from the participants' seat. Infant participants were seated on their caregiver's lap.

EEG data were previously pre-processed offline, using NetStation software, by collaborators of the SVIP project. A number of pre-processing steps were conducted prior to obtaining the data for the current study. The data were filtered with 1 Hz high pass and 60 Hz notch filter. Missing channels and eye channels were marked bad. Also, excessively noisy channels were marked bad and replaced using interpolation techniques. Channels (including interpolated channels) were referenced to an average reference.

3.2.4 EEG pre-processing conducted in the current study

Additional pre-processing steps were conducted by the current authors after obtaining the dataset. For each participant, a channel was identified as bad if more than 10% of its datapoints were outside of the predefined range [-150 uV, 150 uV]. If a particular channel was bad for more than 4 participants, then the channel was removed for all participants. Under this criterion, 68 channels out of 129 channels were removed for all participants. The

remaining channels that were bad for each respective participant were removed and interpolated using the ERPLAB function erplab_interpolateElectrodes (Lopez-Calderon and Luck 2014). On average, the number of channels interpolated for the respective participant was 4.44 [range: 0 - 18]. Therefore, for all participants, a montage of 61 channels was retained (15 channels at frontal, parietal, and temporal regions; 16 channels at the occipital region). For the current study, the channels selected for analyses are those corresponding to the frontal and parietal regions in order to maintain consistency with the following study described in the next chapter (**Chapter 4**). The signal was then detrended.

3.2.5 Behavioural and psychiatric assessments

Child Behaviour Checklist for ages 1.5-5 (CBCL), Social Responsiveness Scale (SRS), Autism Diagnostic Observation Schedule-Calibrated Severity Score (ADOS-CSS), and IQ participant data were accessed from the Simons VIP Phase 1 16p11.2 dataset at SFARI Base (http://www.sfari.org/resources/sfari-base).

3.2.5.1 Child Behaviour Checklist for Ages 1.5-5 (CBCL)

The CBCL/1.5-5 (Rescorla, 2005) is an assessment of parent or caregiver report of behavioural and psychiatric problems in preschool children. The assessment contains 99 statements, which describes child problems, such as 'aches or pains without medical cause' and 'acts too young for age'. The respondent is asked to indicate whether the statements are 'not true' (0), 'somewhat or sometimes true' (1), or 'very true or often true' (2), either presently or within the past two months. The CBCL/1.5-5 identifies the following seven empirically-based syndromes based on the summed scores of items of the respective syndrome: aggressive behaviour, anxious/depressed, attention problems, emotionally reactive, somatic complaints, withdrawn, and sleep problems. The CBCL/1.5-5 also yields five DSM-oriented categories: affective problems, anxiety problems, attention-deficit/hyperactivity problems, pervasive developmental problems, and oppositional defiant problems. In addition, two aggregate broad-band scales can be derived by grouping items that comprise certain syndromes; these two global groupings are labelled as internalising problems and externalising problems. Finally, the sum of all CBCL 1.5-5 items yields a 'total problems' score. The clinical range for the syndromes and DSM-oriented scales is defined as T-scores $\geq$ 70, and the borderline clinical range is T-scores between 65 and 69. For the broadband and total problems scores, the clinical range is T-scores $\geq$ 64, and the borderline range is T-scores between 60 and 63. For the current paper, T-scores of each DSM-oriented scale and T-scores of the syndromic scale 'sleep problems' were taken for correlational

analyses with the EEG measures of interest. Data from six del carriers are missing. CBCL severity in the current sample is shown in **Table 3.4**.

Table 3.4: CBCL severity in 16p11.2 del.

	Affective problems	Anxiety problems	Pervasive developmental	ADHD	Oppositional defiant	Sleep problems
	50	51	66	64	52	59
	70	50	51	52	50	88
	63	54	70	64	59	51
	56	57	66	50	52	51
	50	50	50	50	50	50
	60	60	86	57	64	56
	50	50	50	51	50	50
	60	50	68	57	59	59
	52	50	51	50	50	50
	77	57	77	67	52	70
	52	51	59	64	55	51
	70	50	66	52	51	50
	67	50	72	57	50	56
	51	50	59	54	50	62
	77	70	72	76	80	88
	72	70	72	71	73	64
Frequency of carriers in the borderline or clinical range.	**6**	**2**	**10**	**3**	**2**	**3**

Data from six deletion carriers are missing. Red indicates T-scores > 64, i.e., borderline clinical or clinical range.

3.2.5.2 The Social Responsiveness Scale (SRS)

The SRS (Costantino and Gruber, 2005) quantifies severity of social and communication difficulties related to autism spectrum disorder. It is a questionnaire designed to be administered to the parent or teacher who has routinely observed the child in a usual social setting. For 65 items, the respondent is asked to rate statements about the child's behaviour the past six months, by indicating 'not true' (0) to 'almost always true' (3). In addition to the total score, the SRS yields five subscales: social awareness, social cognition, social communication, mannerisms, and social motivation. Increasing scores indicate higher severity of social difficulties. For the correlation analyses, the T-scores of the total SRS scores were studied. Data from nine del carriers are missing.

3.2.5.3 Autism Diagnostic Observation Schedule-Calibrated Severity Score (ADOS-CSS)

As described in **Chapter 2**, **Section 2.2.4.1**. Data from nine del carriers are missing.

3.2.5.4 IQ

As described in **Chapter 2**, **Section 2.2.4.2**. Data from two del carriers are missing.

3.2.6 EEG measures

3.2.6.1 Multiscale entropy

Multiscale entropy (MSE) analysis was performed on scales 1-20 for a continuous EEG signal of 60,000 data-points (2 minutes; 500 Hz sampling rate). From the whole signal of length <10 minutes, the chosen two-minute segment range was from 8000 to 68,000 data-points. (This range allows the exclusion of the first 16 seconds of recording in order to avoid potentially contaminated data due to participant movement and other artefacts).

The following software and toolboxes were used for the analyses, MATLAB (The MathWorks Inc.), EEGlab toolbox (Delorme and Makeig, 2004), and multiscale entropy toolbox (http://www.psynetresearch.org/tools.html – Liang et al., 2014). The MSE method measures sample entropy (SampEn; Richman and Moorman, 2000) on multiple timescales (Costa et al., 2005; Costa et al., 2002). MSE consists of two main steps as follows.

1) From the original EEG time-series $\{x_1, x_2, \ldots, x_N\}$, multiple time-series, e.g., 20 timeseries, are constructed through a coarse graining process. The process involves averaging neighbouring data-points within non-overlapping windows which increase in length as per the determined scale factor (i.e., from 1 to 20 scales in the current study, where 1 signifies the original time-series and 20 refers to a window size of 20 data-points). The length of each

constructed time-series, therefore, corresponds to N/τ, where N is the length of the original time-series and τ is the scale factor. For example, for timescale 3 and N = 60,000 datapoints, then the length of the timeseries for timescale 3 is 60,000/3 = 20,000 datapoints. The below equation describes the coarse-graining process; Each element, j, of a coarse-grained time-series $\{y(\tau)\}$ is calculated as such:

$$y_j^{(\tau)} = (1/\tau) \sum_{i=(j-1)\tau+1}^{j\tau} x_i \qquad 1 \leq j \leq N/\tau$$

2) Then, SampEn is calculated for each coarse-grained time-series $\{y(\tau)\}$. SampEn measures the regularity of a signal: low entropy signifies high regularity and high entropy indicates irregularity (and possibly high complexity). SampEn is defined as the negative natural logarithm of the conditional probability that within a given time-series $\{y(\tau)\}$, similar sequences of data-points of length m will still match at m+1, while excluding self-matches. SampEn, therefore, is calculated according to the equation:

SampEn (m, r, N) = - ln (A/B)

Where *m* denotes sequence length; *r* is the similarity criterion or the tolerance range – two data-point sequences are considered matched if their amplitude falls within the similarity criterion, which is usually defined as 20 percent multiplied by the standard deviation of the original time-series; *N* is the length of the original time-series.

A = the number of matched pairs for m+1/ the number of all probable pairs for m+1

B = the number of matched pairs for m/ the number of all probable pairs for m

Based on previous M/EEG studies (e.g., Takahashi et al., 2016; Ghanbari et al., 2015) and recommendations by Richman and Moorman (2000), the following MSE parameters were chosen: *m* was set to 2 and *r* = 0.20. MSE was first determined for each channel and then averaged over frontal and parietal brain areas, in line with Takahashi et al. (2016). For each brain region, entropy of scales 1-20 was averaged into four bins: timescales of 1-5, 6-10,

11-15, and 16-20. The data was further reduced for correlation analyses; Entropy was averaged into two bins of timescales 1-10 and 11-20 per region (frontal and parietal).

3.2.6.2 Complexity index

The complexity index (CI) is another measure of entropy as described by Costa et al. (2005). For each channel, CI was computed by estimating the area under the MSE curve via integrating entropy values of all scales. A trapezoidal numerical integration was applied via the 'trapz' function in MATLAB. The average CI was calculated over channels at the frontal and parietal areas, respectively.

3.2.6.3 Power spectral density

Power Spectral Density (PSD) of each channel was computed as per Welch's method using the 'pwelch' MATLAB function. The signal was first detrended and subtracted from the mean signal amplitude. In accordance with Welch's method, the signal (60,000 data-points or 2 minutes) was divided into segments of equal length (2-second segments in this case or 1000 datapoints) with a 50% overlap. Given a sampling rate of 500 Hz and N = 1000 data-points per segment, the resultant frequency resolution was 0.5 Hz. Each segment was windowed with a Hamming window and modified periodograms (PSDs of each Hamming window) were estimated. The final PSD was obtained by averaging the periodograms of all segments.

Absolute and relative power were then computed for the following frequency bands: delta [2-4 Hz], theta [4-8 Hz], alpha [8-14 Hz], beta [14-30 Hz], and gamma [30-50 Hz]. Absolute power of each frequency band was obtained via the trapezoidal integration method, using the 'trapz' MATLAB function. Prior to obtaining the relative power, the total spectral power was defined as the entire range between 1-50 Hz (due to a notch filter applied at 60 Hz). Relative power at each frequency band was subsequently calculated as the ratio of power of the respective frequency band to the total spectral power defined earlier. Relative power of each frequency band was averaged separately over the frontal and parietal brain regions.

3.2.6.4 Low-to-high frequency ratio

Low-to-high frequency ratio (LHR) was measured by taking the ratio of absolute delta power to the absolute beta power for each the frontal and parietal regions.

3.2.7 Statistical analyses

Permutation tests (Rodgers, 1999) were conducted to investigate whether there were group differences in neural activity (for each EEG power and entropy metric described in earlier sections) in the frontal and parietal regions between del carriers and controls. This was conducted, as described in detail in **Chapter 2**, **Section 2.2.11**. To account for multiple comparisons, the false discovery rate (FDR) was controlled using the Benjamini-Hochberg procedure, with $q < 0.05$.

We also applied the permutation approach to Spearman's correlation analyses to examine whether age, IQ, and psychiatric traits (CBCL, ADOS-CSS, and SRS) impact neural responses in 16p11.2 del carriers (method as described in **Chapter 2**, **Section 2.2.11**). All the outcomes were corrected by controlling the FDR using the Benjamini-Hochberg procedure, with $q < 0.05$. As IQ, CBCL, ADOS-CSS, and SRS data were not available for the control group, permutation correlation analyses were conducted for only the del group (n = 22). However, phenotypic data for each respective assessment were missing for some participants. Namely, out of 22 participants, data for IQ, CBCL, ADOS-CSS, and SRS only included 20, 16, 13, and 13 del participants, respectively. From these participants, outliers were identified and removed. Specifically, prior to conducting permutation correlation analyses, Cook's distance was measured to indicate influential data-points (observations) that should be marked as outliers. Data-points with Cook's distance larger than three times the mean Cook's distance were marked as outliers (range: 0-3) and removed from the datasets prior to conducting correlation analyses.

3.3 Results

3.3.1 Multiscale entropy

Significant group differences ($p \leq 0.010$) were found in MSE at all the respective timescales in the frontal region (**Table 3.5; Figure 3.2**). Specifically, MSE was higher for del than controls. No group difference was found in MSE at any timescale bin for the parietal region.
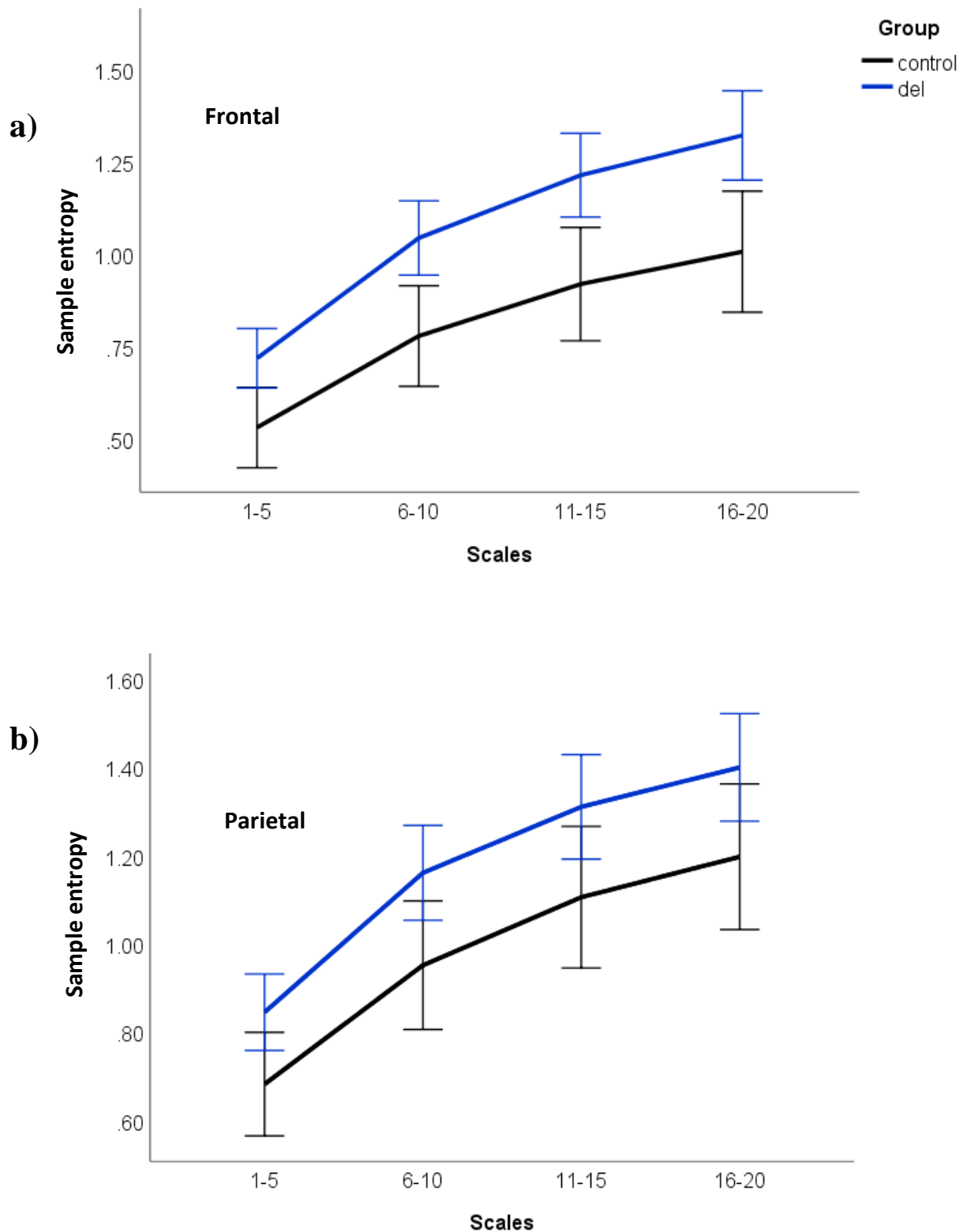
Figure 3.2: MSE group differences in the frontal and parietal regions.
a) MSE group differences in the frontal region. **b)** MSE group differences in the parietal region.
Blue indicates 16p11.2 del group; black indicates control group. Error bars: 95% confidence
intervals.

3.3.2 Complexity index

CI was compared between del and controls at the frontal and parietal regions, respectively. CI was significantly higher for del compared to controls ($p \leq 0.010$) at the frontal region (**Table 3.5**). No significant group difference in CI was found at the parietal region.

Table 3.5: Neural MSE and CI of 16p11.2 del and control groups.

		Control	del	Actual difference	P-value
Parietal	MSE scale 1-5	0.76 [0.42 0.82]	0.89 [0.3 1.13]	0.16	0.030
	MSE scale 6-10	1.02 [0.49 1.23]	1.23 [0.52 1.52]	0.21	0.022
	MSE scale 11-15	1.18 [0.55 1.41]	1.36 [0.59 1.7]	0.20	0.045
	MSE scale 16-20	1.26 [0.61 1.53]	1.45 [0.64 1.84]	0.20	0.050
	CI	20.37 [9.79 23.9]	23.94 [10.42 28.7]	3.76	0.028
Frontal	MSE scale 1-5	0.55 [0.24 0.74]	0.69 [0.3 1.09]	0.19	**0.010**
	MSE scale 6-10	0.77 [0.29 1.1]	1.07 [0.36 1.35]	0.27	**0.003**
	MSE scale 11-15	0.92 [0.34 1.26]	1.26 [0.42 1.54]	0.29	**0.003**
	MSE scale 16-20	1.04 [0.38 1.36]	1.37 [0.46 1.65]	0.31	**0.004**
	CI	15.65 [5.89 21.32]	21.21 [7.33 26.44]	5.09	**0.003**

The data are reported as median [range]. Significant group differences ($p \leq 0.010$) are in bold.

3.3.3 Power spectral density

Group differences in relative power within each frequency band (delta, theta, alpha, beta, and gamma) at each of the frontal and parietal regions were examined (**Table 3.6**). All results were non-significant.

3.3.4 Low-to-high frequency ratio

No significant group differences were found in LHR at either frontal or parietal regions (**Table 3.6**).

Table 3.6: Power (%) and LHR (%) of 16p11.2 del and control groups.

		Control	del	Actual difference	P-value
Parietal	δ	0.46 [0.36 0.78]	0.41 [0.25 0.71]	0.06	0.141
	θ	0.24 [0.16 0.37]	0.25 [0.19 0.38]	0.02	0.243
	α	0.15 [0.04 0.27]	0.15 [0.06 0.34]	0.02	0.427
	β	0.08 [0.02 0.12]	0.09 [0.02 0.21]	0.02	0.177
	γ	0.04 [0.01 0.11]	0.04 [0.01 0.19]	< 0.01	0.774
	δ/β	6.50 [3.23 67.63]	4.55 [1.78 38.76]	4.77	0.316
Frontal	δ	0.55 [0.47 0.74]	0.5 [0.36 0.7]	0.06	0.047
	θ	0.24 [0.18 0.32]	0.27 [0.19 0.38]	0.03	0.055
	α	0.1 [0.05 0.16]	0.12 [0.05 0.19]	0.02	0.082
	β	0.06 [0.02 0.1]	0.07 [0.02 0.12]	0.01	0.313
	γ	0.03 [0.01 0.1]	0.03 [0.01 0.08]	0.01	0.444
	δ/β	10.63 [5.37 64.37]	7.99 [4.29 28.77]	6.50	0.071

The data are reported as median [range]. All results are non-significant. Significance threshold at $p \leq 0.010$.

3.3.5 The impact of age on MSE, PSD, and LHR

To assess the impact of age on EEG measures of interest over the frontal and parietal regions, correlation permutation tests were performed separately for del and control groups. Specifically, correlations were performed between age and the following EEG measures: lower scale MSE and higher scale MSE; power of delta, theta, alpha, beta, and gamma bands; and LHR. No significant correlations were found between age and any of these EEG measures at the respective brain regions in either group (**Table 3.7**).

Table 3.7: Correlations between MSE, power, LHR, and age.

		Control	del
		Age	
Parietal	MSE lower scale	-0.39	0.36
	MSE higher scale	-0.56	0.31
Frontal	MSE lower scale	0.08	0.30
	MSE higher scale	-0.22	0.08
Parietal	**δ**	0.46	-0.25
	θ	0.004	-0.43
	α	0.09	-0.1
	β	0.11	0.25
	γ	-0.24	-0.14
	δ/β	0.27	-0.44
Frontal	**δ**	0.42	-0.16
	θ	0.02	0.09
	α	-0.21	-0.12
	β	-0.51	0.47
	γ	-0.23	-0.32
	δ/β	0.57	-0.55

The reported values correspond to the r_s coefficient. All results are non-significant. Significance threshold at $p < 0.014$.

3.3.6 Correlations of EEG measures with ESSENCE traits

Correlation permutation tests were performed to examine correlations between MSE, power, and LHR measures against behavioural and psychiatric assessments in the del group (**Table 3.8** and **Table 3.9**). Overall, strong correlations were found between frontoparietal EEG measures and most of the CBCL traits ($p \leq 0.006$). Entropy at lower timescales correlated positively with pervasive developmental, ADHD, and oppositional defiant problems; whereas entropy at higher timescales correlated positively with anxiety problems. In terms of power, strong correlations with anxiety, pervasive developmental, and oppositional defiant problems were found; these correlations were negative with lower-frequency power, and positive with

higher-frequency power, that is, as CBCL traits' severity increased, lower-frequency power decreased, but higher-frequency power increased, respectively. The same CBCL-subscales, i.e., anxiety, pervasive developmental, and oppositional defiant problems, showed strong negative correlations with LHR. No significant correlations were found between any of the EEG measures and CBCL-affective problems, CBCL-sleep problems, ADOS-CSS, SRS, or IQ.

Table 3.8: Correlations between MSE and ESSENCE traits in 16p11.2 del.

| | Parietal | | Frontal | |
	Lower scale	Higher scale	Lower scale	Higher scale
CBCL-affective problems [a]	0.59	0.16	0.59	0.39
CBCL-anxiety problems [a]	0.66	**0.76**	0.62	**0.75**
CBCL-pervasive developmental [a]	**0.71**	0.64	**0.69**	0.48
CBCL-ADHD [a]	0.52	0.64	**0.75**	0.63
CBCL-oppositional defiant [a]	**0.80**	0.66	0.67	0.60
CBCL-sleep problems [a]	0.40	0.26	0.36	0.21
CBCL-total problems [a]	0.22	-0.12	0.34	0.28
ADOS-CSS [b]	-0.27	-0.13	-0.11	-0.13
SRS [c]	-0.06	-0.24	0.03	-0.22
IQ [d]	0.59	0.16	0.59	0.39

The reported values correspond to the r_s coefficient. Significant results ($p \leq 0.006$) are in bold.
[a] Data from six deletion carriers are missing.
[b] Data from nine deletion carriers are missing.
[c] Data from nine deletion carriers are missing.
[d] Data from two deletion carriers are missing.

Table 3.9: Correlations between power, LHR, and ESSENCE traits in 16p11.2 del.

	Parietal						Frontal					
	δ	θ	α	β	γ	δ/β	δ	θ	α	β	γ	δ/β
CBCL-affective problems [a]	-0.30	0.19	0.19	0.63	0.62	-0.53	-0.26	0.30	0.06	0.64	0.40	-0.47
CBCL-anxiety problems [a]	**-0.78**	0.50	0.68	0.22	0.22	**-0.86**	**-0.80**	0.54	**0.77**	0.26	-0.04	**-0.78**
CBCL-pervasive developmental [a]	**-0.80**	0.56	0.59	0.50	0.52	**-0.82**	**-0.70**	**0.83**	0.63	0.24	0.01	-0.44
CBCL-ADHD [a]	-0.63	0.18	0.40	0.59	0.61	-0.68	-0.45	0.52	0.33	0.21	0.37	-0.53
CBCL-oppositional defiant [a]	-0.65	0.27	0.45	0.60	0.59	**-0.83**	**-0.72**	0.54	0.38	0.39	0.03	**-0.68**
CBCL-sleep problems [a]	-0.40	-0.04	0.24	0.65	0.43	-0.66	-0.35	0.24	0.10	0.34	0.29	-0.46
ADOS-CSS [b]	-0.14	-0.46	0.28	0.54	0.08	-0.47	-0.28	-0.24	-0.07	0.66	0.58	-0.34
SRS [c]	0.21	-0.36	-0.10	0.42	0.64	-0.52	0.15	-0.18	-0.17	0.52	0.56	-0.37
IQ [d]	0.27	-0.17	-0.21	-0.12	-0.28	0.21	0.29	0.36	-0.34	-0.12	-0.36	0.17

The reported values correspond to the r_s coefficient. Significant results ($p \leq 0.006$) are in bold.
[a] Data from six deletion carriers are missing.
[b] Data from nine deletion carriers are missing.
[c] Data from nine deletion carriers are missing.
[d] Data from two deletion carriers are missing.

3.4 Discussion

The aims of the current study were 1) to determine whether fronto-parietal spontaneous neural activity, indexed by oscillatory power and MSE, in 16p11.2 del carriers was altered compared to typical controls; and 2) to establish whether fronto-parietal spontaneous neural activity is related to ESSENCE traits in 16p11.2 del carriers. The main findings are 1) MSE and CI were higher for del than controls at all respective timescales over the frontal region, but not the parietal region; 2) No significant group differences were found in LHR or relative power within each respective frequency band and brain region; 3) Overall strong associations were found between MSE, CI, relative power in delta, theta, and alpha frequency bands, LHR[5], and several CBCL traits (e.g., anxiety problems). Together, these results suggest a specific dysfunction in frontal spontaneous neural activity that seems to strongly reflect or impact on a wide array of ESSENCE traits.

Taking the ESSENCE approach of considering interrelated psychiatric disorders together, certain commonalities emerge in neural entropy between these disorders and 16p11.2 del. Similar to 16p11.2 del, higher spontaneous entropy in fronto-central brain areas has been found in various ESSENCE disorders (**Table 3.1**). Notably, the current study found higher entropy in del at both lower and higher timescales compared to controls, as jointly reflected by CI and MSE analyses. This is reminiscent of findings previously reported in relation to ASD and absence epilepsy (Bosl et al., 2017) where an overall higher entropy at resting-state was also found compared to controls. Findings from many other studies, though, suggest that it is more common in ESSENCE disorders for there to be timescale-dependent variations in the level of entropy, compared to typical controls (**Table 3.1**). Higher spontaneous fronto-central entropy has been more frequently observed at higher timescales in particular (ASD; Ghanbari et al., 2015; Schizophrenia; Takahashi et al., 2010; Alzheimer's; Yang et al., 2013; Mizuno et al., 2010). This implies that ESSENCE disorders, in the aforementioned studies, showed atypical long-range spontaneous neural processing involving the fronto-central region, as it has been suggested that neural entropy at lower and higher timescales respectively reflect local/shorter-range and longer-range neural processing (McDonough and Nashiro, 2014, McIntosh et al., 2014, Vakorin et al., 2011). In contrast, we speculate that the findings in the current study suggest that there is a disruption in both

---

[5] Because the outcomes from relative power analyses of respective frequencies and LHR are similar, these will be mainly discussed altogether as one category.

shorter- and longer-range neural processing involving the frontal brain region and possibly affecting the default mode network and/or other resting-state networks.

In 16p11.2 del, Bertero et al. (2018) only implicated long-range neural dysfunction (equivalent of entropy at higher timescales) involving the prefrontal cortex, as revealed with functional connectivity fMRI analysis. As described earlier, Bertero et al. (2018) found reduced prefrontal long-range connectivity in 16p11.2 del. In light of the relationship between MSE and functional connectivity (**Figure 3.1**), specifically when examined using MEG, LFP, and simulated data (which arguably are more comparable to EEG data compared to fMRI in terms of temporal resolution), the higher entropy found in the current study might translate to hyperconnectivity – therefore conflicting with some of Bertero et al.'s (2018) findings. Nevertheless, it is clear, from the current study's findings together with Bertero et al.'s (2018), that functional frontal neural activity at resting-state is altered in 16p11.2 del, especially in relation to long-range neural activity.

It is unclear, however, how this altered neural activity might lead to the numerous ESSENCE traits found in 16p11.2 del. An interesting hypothesis that might explain a potential link on a conceptual level comes from Misic et al.'s (2015) ASD study. In Misic et al.'s (2015) study, ASD participants showed typical MEG entropy activity when compared to the control group in response to tasks designed to test mental flexibility; however looking more closely at MSE during the respective mental flexibility tasks, it seemed that for the ASD group, higher entropy at higher scales was employed for one task and higher entropy at lower scales for the other. While the control group showed opposite entropy activity in terms of timescales at each task. A related finding in the same study is that higher entropy at the identified task-related regions was associated with faster reaction times in controls – but not in ASD. Therefore, the authors suggested the observed findings could be due to the misappropriation of neural resources to perform the respective mental flexibility tasks. Keeping this view in mind, perhaps the current study's higher frontal entropy in del was due to a functional brain reorganisation, which altered neural networks involving the frontal region. This higher entropy might reflect a compensatory mechanism that is misallocating neural resources and therefore leading to an overall atypical information processing within resting-state networks. A compensatory mechanism that misallocates neural resources likely impacts a wide range of processes leading to numerous ESSENCE traits that vary in severity.

Indeed, neural activity (in the form of entropy and complementary LHR power metrics) might be a marker of a compensatory mechanism affecting a range of ESSENCE traits. In support of this view, neural activity was found to be strongly associated with ESSENCE traits (as measured via the Child Behaviour Checklist (CBCL)) in this study, even though most of del carriers in this sample did not reach the CBCL cut off for the clinical range (with the exception of pervasive developmental problems:10 out of 16 carriers are in the borderline or clinical range; **Table 3.4**). Notably, despite the lack of group differences in power and LHR in the current study, results from correlation analyses showed strong links between entropy, power, LHR, and CBCL traits in del. These correlations were complementary and in line with the view that higher entropy and lower LHR might reflect similar or complementary mechanisms. Specifically, with higher entropy and lower LHR (note that LHR = delta/beta power, therefore a lower LHR means delta power was lower than beta power), there was a reciprocal increase in ESSENCE traits. In other words, entropy was positively associated with CBCL severity (**Table 3.8**); while LHR was negatively correlated to CBCL severity (**Table 3.9**). Altogether, these associations signify a compensatory mechanism and possible impairment in neural processing in del, which may be impacting various ESSENCE traits that have been accounted for in the CBCL. These include pervasive developmental problems, ADHD problems, oppositional-defiant problems, and anxiety problems. It is beneficial, therefore, to take the ESSENCE approach and consider the wide spectrum of difficulties via instruments such as CBCL, as opposed to focusing on a particular disorder or trait, in this (i.e., 16p11.2 del) and other related CNVs (e.g., 1q21.1 CNV) or even idiopathic psychiatric disorders (e.g., ASD).

As mentioned earlier, entropy at lower timescales carries information from both lower and higher frequencies, while entropy at higher timescales reflects information from lower frequencies (Courtiol et al., 2016; Takahashi et al., 2010; Mizuno et al., 2010). Accordingly, it is interesting that no group differences in either relative power or LHR were found in this study while finding group differences in entropy. Especially since both entropy and LHR measures have been interpreted as reflecting cognitive flexibility at a higher conceptual level (e.g., Misic et al., 2015). Specifically, higher entropy and lower LHR, respectively, might similarly reflect the brain's adaptability to switch between cognitive states. Based on that perspective, the current study's finding of higher entropy in del, therefore, was expected to be complemented by a lower LHR in 16p11.2 del compared to controls, which was not the case. This could indicate, therefore, that entropy, relative to power, is a more sensitive measure

useful for capturing certain properties of neural information processing in 16p11.2 del, not possible by conventional power analyses alone. This view is further supported by previous studies conducting joint entropy and power analyses (Misic et al., 2015; Catarino et al., 2011). For example, distinct aspects of neural activity (e.g., activation of distinct brain regions/pathways) were revealed in the respective analyses in Misic et al.'s (2015) study. In addition, Catarino et al. (2011), similar to the current study, found no group differences in EEG power between ASD and controls, while group differences in entropy were observed (i.e., lower entropy over temporo-parietal and occipital areas in ASD).

It is worth pointing out that in most prior work, LHR has been shown to be higher in ADHD (Barry et al., 2003), though studies have also reported negative findings (Arns et al., 2018; Loo et al., 2013; Kitsune et al., 2015). As only three participants in the current study were diagnosed with ADHD (**Table 3.3**), it was not possible to examine whether the 16p11.2 del carriers with an ADHD diagnosis would show similar contrasts with typical controls in LHR to that of idiopathic ADHD. In relation to the LHR-anxiety correlation in 16p11.2 del, it was found to be negatively correlated in the current study (indicating higher levels of anxiety with lower LHR); This finding is in congruence with Putman et al.'s (2010) study that showed a negative correlation between LHR and anxiety, although in typical participants. Interestingly, LHR has been linked with the regulation of interactions between cortical-subcortical systems, i.e., frontal cognitive inhibitory processes vs. limbic motivation/reward-seeking behaviour (Knyazev et al., 2007). Relatedly, atypical spectral power in ASD has been widely interpreted as reflecting an imbalance in neural excitatory/inhibitory processes (Rubenstein and Merzenich, 2003). Keeping these concepts in mind, it is possible to assume with caution that a similar picture is the case in 16p11.2 del (whether as part of a compensatory mechanism or otherwise), even though this is a reductionist view and the overall pathophysiology is undoubtedly complex.

Evidence drawn from 16p11.2 del mouse studies suggests a possible dysregulation and interplay between multiple neurotransmitter and neuromodulator systems (Stoppel et al., 2018; Wang et al., 2018; Walsh et al., 2018; Panzini et al., 2017; Portmann et al., 2014), which could be contributing to an excitation/inhibition imbalance. Although 16p11.2 del mice showed no difference in the availability of GABAergic receptors (i.e., $GABA_A$ receptors and $GABA_A$ α5 subunit quantified using autoradiography) in any brain region compared to wild-type control mice (Horder et al., 2018), another study found that administration of R-baclofen ($GABA_B$ receptor agonist) improved cognitive and social

performance in 16p11.2 del mice (Stoppel et al., 2018). In relation to excitatory activity, glutamatergic (NMDA receptor) hypofunction in the prefrontal cortex was identified in 16p11.2 del mice, as revealed by electrophysiological recordings (Wang et al., 2018).

In addition to the aforementioned neurotransmitter systems, serotonin (5-HT; Walsh et al., 2018; Panzini et al., 2017) and dopamine (as explained in **Chapter 2**; Portmann et al., 2014) have also been implicated in 16p11.2 del and in behavioural deficits of relevance to 16p11.2 del, such as social, cognitive, and anxiety problems (Lee and Goto, 2018; Zhang and Stackman, 2015; Albert et al., 2014). Walsh et al. (2018) found that the deletion of the mouse equivalent 16p11.2 region, specifically from 5-HT neurons induced social deficits and reduced dorsal raphe 5-HT neuronal excitability, as identified via electrophysiological recordings. In addition, using optogenetic techniques, Walsh et al. (2018) bidirectionally modulated the release of 5-HT from dorsal raphe neurons projecting to the nucleus accumbens in 16p11.2 del mice, which in turn influenced social behaviour. Specifically, activation of dorsal ralphe 5-HT neurons in the nucleus accumbens rescued social deficits exhibited by 16p11.2 del mice, and vice versa. Surprisingly, reduced 5-HT activity in 16p11.2 del mice did not impact anxiety-related behaviours in Walsh et al.'s (2018) study. Nevertheless, 5-HT dysregulation could be a key driver impacting the excitation/inhibition balance, which in turn contributes towards pathology in 16p11.2 del.

Relatedly, evidence from a previous study (Takahashi et al., 2010; **Table 3.1**) suggests that higher entropy might relate to atypical dopaminergic and/or serotonergic activity (in humans). Specifically, Takahashi et al. (2010) studied EEG MSE activity in drug-naïve schizophrenia (SZ) participants pre- and post-treatment with antipsychotics (comparisons between pre-treatment SZ vs typical controls were also conducted). The treatment involved typical antipsychotics, i.e., dopamine antagonists (dopamine receptor response blocking), in addition, a few participants received atypical antipsychotics, i.e., dopamine-serotonin antagonists. Takahashi et al. (2010) found increased entropy at higher timescales in fronto-centro-temporal areas in SZ (pre-treatment) compared to controls. This is somewhat similar to the findings in the current study as higher entropy was found at higher timescales (but also lower timescales) in fronto-central areas in 16p11.2 del compared to controls. Notably, Takahashi et al. (2010) also found that this higher entropy in SZ was lowered to the control participants' level in fronto-central areas in response to antipsychotic treatment. In other words, the observed atypically high entropy observed in SZ was reversed in response to medications which act on attenuating dopaminergic and, to a lesser extent,

serotonergic activity. Thus, the identified atypical neural entropy in 16p11.2 del, in the current study, along with the observed strong links between neural activity and psychiatric traits, could, therefore, signify an excitation/inhibition imbalance, driven by multiple neurotransmitter systems including dopamine and 5HT, in 16p11.2 del.

Overall, the current study established that 16p11.2 del carriers present with atypical neural activity as revealed with entropy measures. Neural entropy levels were consistently higher in the frontal region for del relative to typical controls at all timescales. Hence, this implicates interactions between local and long-range neural processing at resting-state networks. Whether reflecting a compensatory or dysfunctional mechanism, neural activity in del was strongly associated with ESSENCE traits, including anxiety, pervasive developmental, ADHD, and oppositional defiant problems. To better interpret these results and understand the underlying pathology or compensatory system, 16p11.2 deletion animal models are valuable. Atypical neural activity on a system level, as is the case in the current study, might be reflecting atypical neural activity on a cellular level – such as the excitation/inhibition imbalance in 16p11.2 del mice, as described earlier. Accordingly, to make it more possible for future studies to draw parallels from 16p11.2 del mouse models, the following study in this thesis will repeat the same analyses already conducted in this chapter but with 16p11.2 deletion mice.

Chapter 4   Spontaneous neural activity in 16p11.2 deletion mouse model

4.1   Introduction

Parallel human and mouse studies are necessary and valuable for investigating neural activity in 16p11.2 del. The 16p11.2 del mouse model can be used to support findings relating to human 16p11.2 del. Different aspects of atypical EEG/LFP features in humans and mice were described in previous studies (as described in **Chapter 1**, in addition to the studies conducted in this thesis, **Chapters 2** and **3**). However, it is unclear whether there are common EEG/LFP features between 16p11.2 del humans and mice, due to the small number of studies and lack of studies addressing this question. Identifying the common EEG/LFP features is a means to finding reliable features that more likely reflect 16p11.2-related pathophysiology. From a different perspective, human-mouse comparisons could also determine whether the atypical EEG features are conserved across species (with a loss of 16p11.2). After identifying the conserved EEG/LFP features, the mouse model can be used to investigate the reversibility of these features and associated phenotypes. This can be done with optogenetic techniques and drug treatments, among other experimental techniques not applicable to human participants. Using optogenetic techniques, Walsh et al. (2018) showed that social deficits were rescued in 16p11.2 del mice by manipulating the activity of dorsal raphe serotonergic neurons. A similar approach could be applied to examine whether isolating and activating specific neurons in 16p11.2 del could modulate the aberrant EEG/LFP features and restore normal signal features in these mice. This would, in turn, inform future studies on possible underlying mechanisms responsible for the aberrant signal observed in 16p11.2 del humans (and mice) and their associated phenotypes/pathophysiology. As a result, these studies would improve efforts on interpreting EEG activity and related findings for 16p11.2 del humans.

Of relevance to human-mouse parallel studies is to recognise that it is feasible to compare EEG data with LFP data. This is because EEG and LFP signals have similar properties and come from relatively similar sources in the brain (Buzsaki et al., 2012; Cohen, 2017). Essentially, EEG and LFP recordings capture the extracellular electric currents resulting from the (electrochemical) interaction between neurotransmitters and receptors at the dendrites of the receiving neurons, thousands to millions of neurons. For these postsynaptic potentials to be detected, neurons need to act in synchrony and be aligned in parallel (otherwise the dipoles formed by neighbouring neurons, due to the electric positive and negative flow of ions across the membrane of each neuron, will cancel each other out).

Spatially, EEG samples a relatively large spatial area of neural activity from superficial layers of the cortex, while LFP samples neighbouring neural activity to the inserted electrode from deeper layers (i.e., down to layers V or VI). Based on the above-mentioned properties and because of their abundance, pyramidal neurons are considered to be the main contributors to the EEG/LFP signals. However, all ionic currents from cellular processes of neurons and glial cells, excitatory and inhibitory, from different areas of the brain contribute to the EEG/LFP signal. Temporally, EEG and LFP data are similar in terms of their temporal resolution, i.e., milliseconds, which is an important feature that makes parallel analyses plausible.

An obvious distinction, however, between EEG and LFP is the impact of the data-collection methodology on the signal. LFP activity is recorded invasively from within brain tissue (i.e., metal microelectrodes are inserted into the brain), whereas EEG activity is recorded at the scalp – therefore the soft and hard tissues distort the signal and act as a low-pass filter, capturing $< \sim 130$ Hz. In contrast, the former method of inserting an electrode within the brain captures a clearer broadband signal, which contains LFP activity ($< \sim 130$ Hz) and multiunit activity (MUA; $> \sim 200$ Hz). MUA activity represents action potentials or spikes (which are usually at higher frequencies relative to synaptic events) detected from neurons near the electrode. This spike activity could be clustered based on the temporal width of the spike waveforms: wide-spiking, putative excitatory neurons, and narrow-spiking, putative inhibitory interneurons (e.g., Lazaro et al., 2019). Certainly, data obtained invasively from within the brain contains more information, contrary to EEG, in relation to spike activity and the relationship between unit and system-level neural activity. However, other than in exceptional cases such as during surgery for treating epilepsy, it is not possible to collect LFP/MUA activity from humans. Hence, it is useful to conduct parallel EEG-human and LFP-mouse analyses.

The aforementioned similarities between EEG and LFP signals (i.e., similar properties and presumed electrogenesis) gives cause for expecting parallel EEG-human and LFP-mouse studies to show similar signal features. For example, if the CNV human group showed a particular atypical feature in their EEG activity, then a similar LFP feature would be expected in the CNV mouse group. These EEG-LFP features could, in turn, be interpreted in a similar way and linked with further evidence from 16p11.2 del mouse studies investigating the underlying pathology on other levels.

Based on prior work (described in detail in the introductory **Chapter 1**), prefrontal long-range (fMRI) connectivity has been implicated in both 16p11.2 del humans and mice (Bertero et al., 2018). However, the literature only consisted of two studies (Lu et al., 2019; Bertero et al., 2018) and only one of them conducted parallel analyses (Bertero et al., 2018). Thus, more studies are required to verify and expand on this finding. With this in mind, EEG neural dynamics in human 16p11.2 del was first investigated in the previous study in this thesis (**Chapter 3**), using MSE and power analyses. Briefly, there was higher entropy recorded over frontal electrodes in 16p11.2 del humans compared to typical controls, despite not finding group differences in power at any frequency band, higher entropy was found at both lower and higher timescales. It was therefore concluded that 16p11.2 del impacts short-range and long-range neural processing.

The aim of this study is to determine whether LFP entropy and power features are atypical in 16p11.2 del mice, and whether these features follow a similar pattern to that observed in 16p11.2 del humans (**Chapter 3**). Based on the human results from **Chapter 3**, the current study tests the following hypothesis: 1) no group differences will be found in power features in either electrode, i.e., frontal and retrosplenial; whereas 2) group differences will be found in entropy features, specifically, 16p11.2 del mice will show higher entropy at all timescales at the frontal electrode compared to controls.

4.2 Methods

4.2.1 Data source

Data re-analysed in the current study were obtained from Alessandro Gozzi's lab (Functional Neuroimaging Laboratory, Instituto Italiano di Tecnologia). Only a prior LFP coherence analysis of this data was previously conducted for the previous publication (Bertero et al., 2018) as such, all the analysis presented here is novel.

4.2.2 Animals

The 16p11.2 del mice (also known as 16p11.2df; Horev et al., 2011; MGI: J:176335) and control wild-type mice were obtained from Jackson Laboratories (stock no. 013128). The 16p11.2 del mouse model was engineered by the deletion of one copy (heterozygous for a deletion) of a region on mouse chromosome 7 (m7qF3; ~390 kb; Horev et al., 2011), which is homologous to the human 16p11.2 region.

The mice were bred locally (in Prof Alessandro Gozzi's lab) and housed by sex, with temperature maintained at 21±1°C and humidity at 60±10%, as described in Bertero et al. (2018).

The LFP mouse data of 16p11.2 del (n = 6; female = 1) and control littermates (n = 6; female = 3) was previously collected as described in Bertero et al. (2018) and re-analysed in the current study. The age range was 11 to 13 weeks old, corresponding to young mature adult mice, and the mean body weight was 25.3± 1.1 grams.

4.2.3 Ethical approval

All in-vivo animal studies were conducted in accordance with the Italian Law (DL 26/214, EU 63/2010, Ministero della Sanità, Roma) and the recommendations in the Guide for the Care and Use of Laboratory Animals of the National Institutes of Health. Animal research protocols were also reviewed and consented to by the animal care committee of the Istituto Italiano di Tecnologia. All surgical procedures were performed under anaesthesia.

4.2.4 In-vivo electrophysiology

LFP recordings were conducted under halothane sedation (halothane dose of 0.7% - 1%). Using two electrodes implanted in the anterior cingulate cortex (will be referred to as frontal cortex, henceforth) and retrosplenial cortex, LFP signals were recorded for approximately 10 minutes, with a sampling rate of 1500 Hz and a notch filter at 50 Hz. Details regarding animal preparation and surgery are previously described (Bertero et al., 2018).

To ensure that the sampling rate was identical to the human EEG data described in **Chapter 3**, the mouse data were resampled to 500 Hz and, as with the human EEG data, detrended (MATLAB function, 'detrend'). Thus, each animal's dataset contained 300,000 datapoints (10 min *60 sec *500 Hz). For every dataset, only artefact-free segments of a total length of two minutes (60 sec *500 Hz *2 min = 60,000 datapoints) were selected for analysis. Within the whole signal (i.e., ~10 minutes), one of the three possible 2-min ranges (i.e., 3 – 5 min (datapoints 100,000 – 160,000); 6 – 8 min (datapoints 180,000 - 240,000); or 7 – 9 min (data points 205,690 - 265,690)) were identified as artefact-free based on visual inspection of each plotted dataset (**Figure 4.1**). The respective selected 2-min range of each frontal and retrosplenial electrode was then used for analyses.

a) Frontal
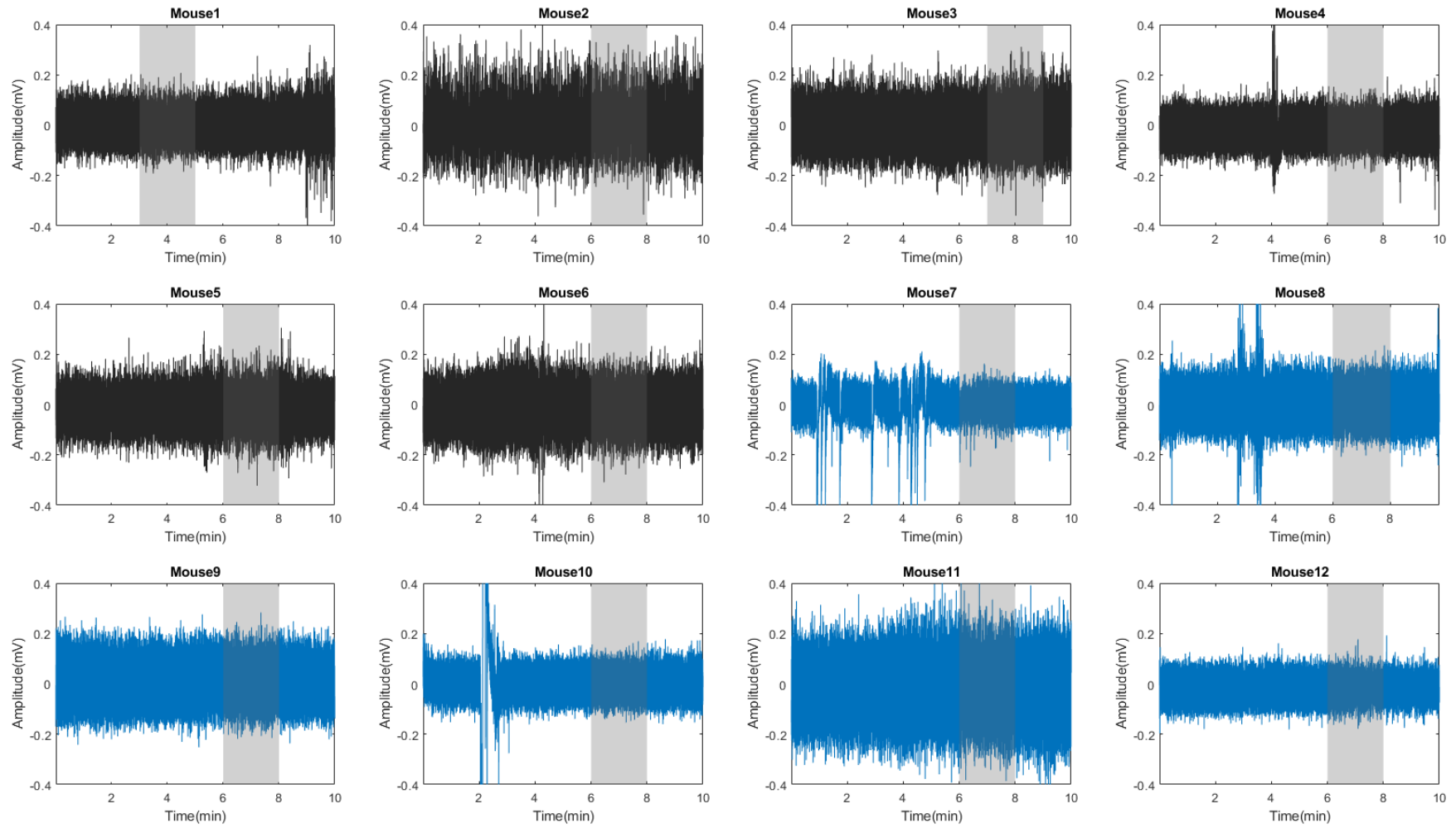
b) Retrosplenial
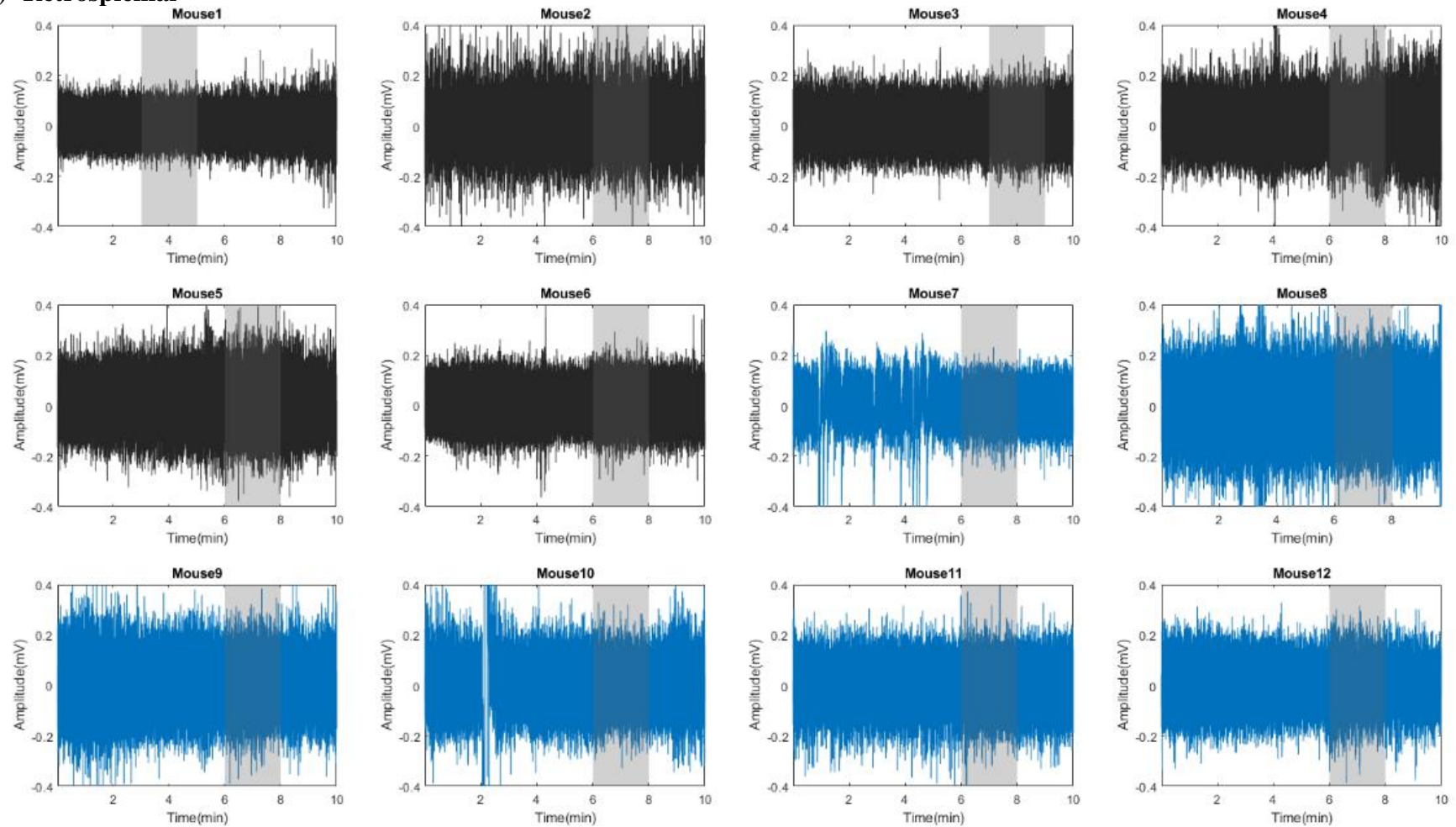
Figure 4.1: LFP signals from frontal and retrosplenial channels of 16p11.2 del and control mice.
Both subfigures show the entire timecourse of the LFP for each mouse with shading to illustrate the artefact-free portion of data that was selected for analysis. The top subfigure **(a)** specifies signal from the frontal electrode, while the bottom subfigure **(b)** specifies signal from the retrosplenial electrode. Black indicates control mice; blue indicates del mice

4.2.5 LFP measures

4.2.5.1 Multi-scale entropy

The MSE measure is previously described in **Chapter 3**. The analysis parameters were consistent with analyses carried out on human EEG (**Chapter 3**), i.e., signal length and sampling rate, number of timescales, entropy sequence length (m), and similarity criterion (r). MSE analysis (timescales 1-20) was conducted for a continuous LFP signal of 60,000 datapoints (2 minutes; 500 Hz sampling rate). Further entropy parameters were $m = 2$ and $r = 0.2$ (Takahashi et al. 2016; Ghanbari et al. 2015; Richman and Moorman, 2000). MSE of each channel, frontal and retrosplenial, were computed separately. Entropy of scales 1-20 was averaged per channel into four groups consisting of averaged entropy scales 1-5, 6-10, 11-15, and 16-20.

Secondary analyses were also conducted with the same analysis parameters as described above but with the addition of a bandpass filter (0.5 – 40 Hz) applied to the signal, as this pre-processing step was performed in Bertero et al.'s (2018) study (which conducted LFP coherence analysis on the same datasets analysed in the current study, as mentioned earlier). Because the outcome of the secondary analyses produced highly similar results, the current study reports the results of only the primary analyses.

4.2.5.2 Complexity index

The complexity index (CI) measure is previously described in **Chapter 3**. CI was computed separately for frontal and retrosplenial electrodes.

4.2.5.3 Power spectral density

Details on how Power Spectral Density (PSD) was computed and how relative power was extracted are previously described in **Chapter 3**. The frequency bands were segmented as such, delta [2-4 Hz], theta [4-8 Hz], alpha [8-14 Hz], beta [14-30 Hz], and gamma [30-40 Hz]. Prior to obtaining the relative power, the total spectral power was defined as the entire range between 1-40 Hz (due to notch filters applied at 50 Hz). Relative power of each frequency band of each channel, frontal and retrosplenial, was then computed.

4.2.6 The effect of MSE on power

As mentioned earlier, previous authors (e.g., Courtiol et al., 2016; Takahashi et al., 2010) showed evidence indicating that the MSE method essentially acts as a low-pass filter with

entropy at lower timescales mainly representing higher frequency content and entropy at higher timescales representing lower frequency content. Similar to prior work, the current study, therefore, investigated how the MSE method, specifically the step involving coarse-graining of the original signal into multiple timescales, affects power content of high and low frequencies within the signal. LFP mouse signal (n = 1; 60,000 data-points) of the frontal channel was first coarse-grained into 20-timescales. PSD of time-series at each timescale was computed as described earlier with the same parameters, i.e., window length of 2 seconds with 50% overlap. The sampling rate and the number of datapoints per segment, however, were adjusted for each coarse-grained timeseries.

4.2.7 Statistical analyses

Statistical analyses were as described in **Chapter 3**.

4.3 Results

4.3.1 MSE, CI, power, and LHR

The results of the permutation tests performed to examine group differences in MSE (**Figure 4.2**), CI, and PSD metrics are presented in **Table 4.1**. No significant results were found despite the medium to large effects sizes for some of the comparisons (**Table 4.1**). Secondary analyses similarly showed no significant results.

Table 4.1: MSE, CI, power, and LHR of 16p11.2 del and control mice comparisons.

		Frontal			Retrosplenial		
		Mean difference	P-value	Cohen's d	Mean difference	P-value	Cohen's d
MSE							
	Scale 1-5	0.14	0.267	**0.59**	0.15	0.136	**0.76**
	Scale 6-10	0.01	0.930	0.05	0.04	0.652	0.27
	Scale 11-15	0.04	0.499	0.34	< 0.01	0.940	0.04
	Scale 16-20	0.03	0.561	0.29	< 0.01	0.996	< 0.01
CI							
	CI	0.20	0.895	0.07	0.84	0.480	0.41
Power							
	δ	0.13	0.178	**0.72**	0.04	0.500	0.35
	θ	0.09	0.243	**0.59**	0.02	0.622	0.24
	α	0.03	0.155	**0.73**	0.01	0.507	0.32
	β	0.02	0.448	0.37	0.01	0.539	0.31
	γ	< 0.01	0.795	0.13	0.01	0.259	**0.59**
	δ/β	2.04	0.138	**0.79**	0.54	0.415	0.45

MSE, multiscale entropy; CI, complexity index. Large to medium effect sizes are in bold.
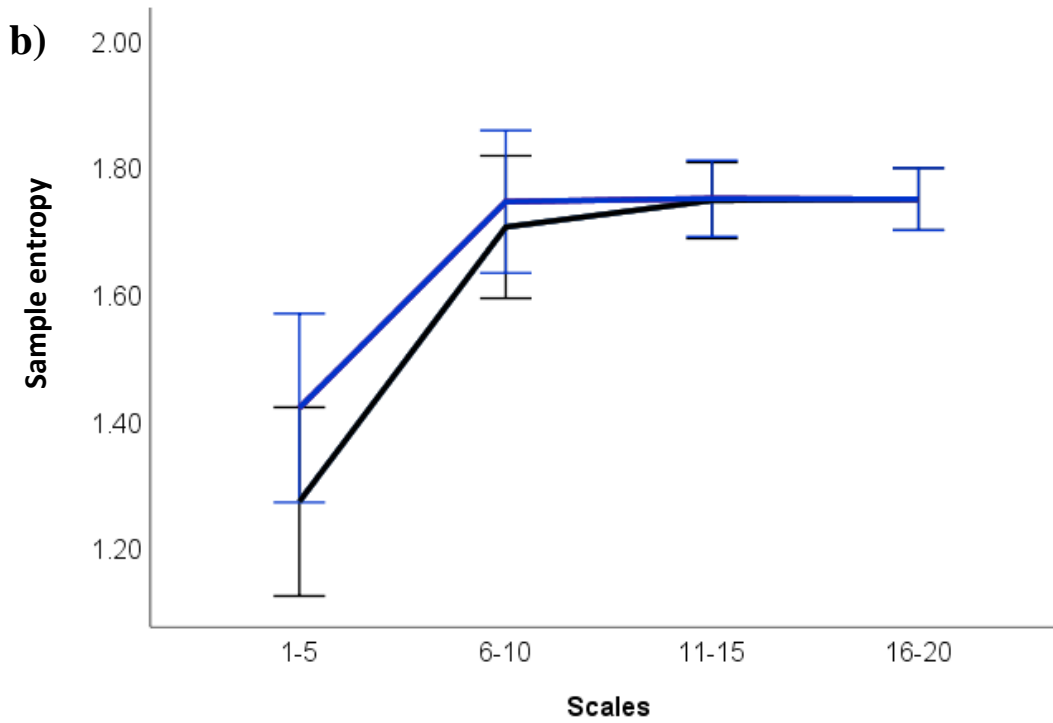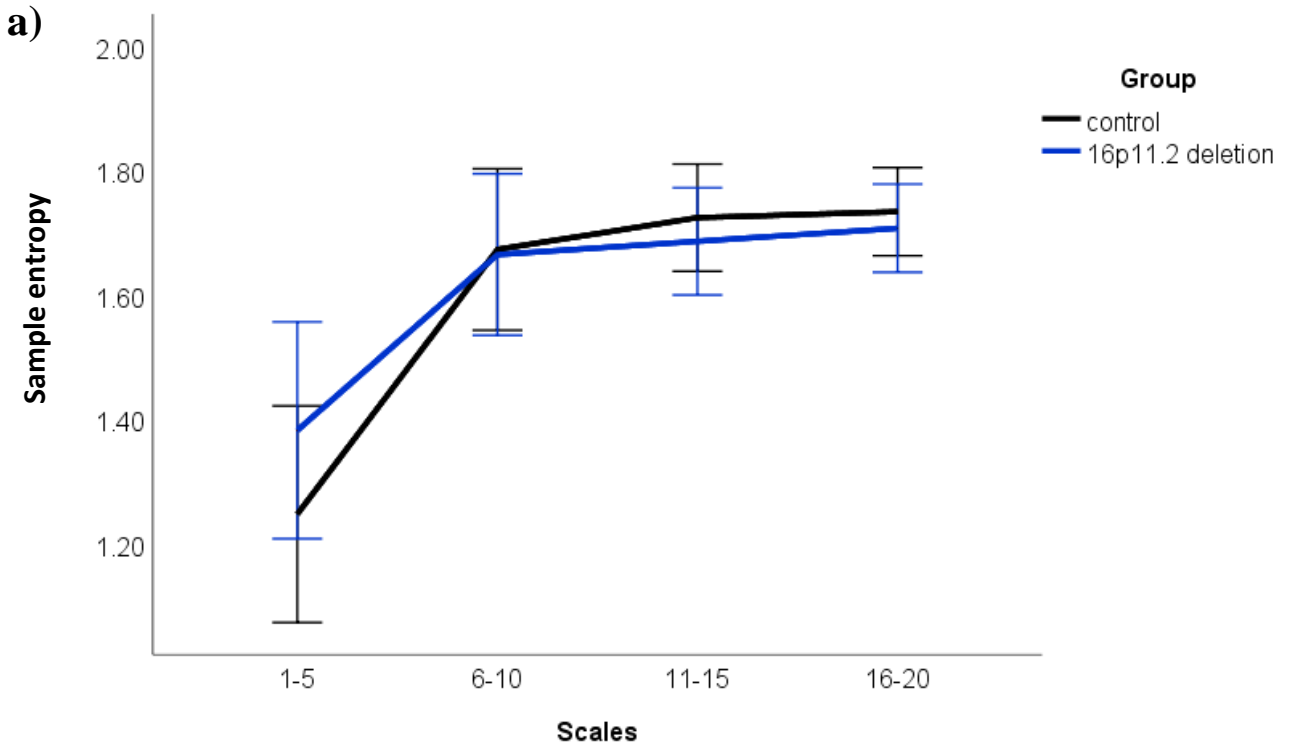
Figure 4.2: MSE group differences at frontal and retrosplenial electrodes.
a) Frontal electrode. **b)** Retrosplenial electrode. Error bars: 95% confidence intervals. Blue indicates 16p11.2 del group; black indicates control group.

4.3.2 The effect of MSE on power

To aid interpretations of power and MSE results, the current study examined the effect of MSE on power (**Figure 4.3**). By observing the power spectral density (PSD) of each timeseries (i.e., signal at each timescale), a general progressive decline in power was found as the frequency increased. More importantly, consistent with previous studies (Courtiol et al., 2016; Takahashi et al., 2010), the current study found that power at higher frequencies gradually reduces as the timescale increases (as can be seen by observing all the timeseries, **Figure 4.3**). This confirms that entropy at higher timescales mainly represents lower frequency content and vice versa.

a)
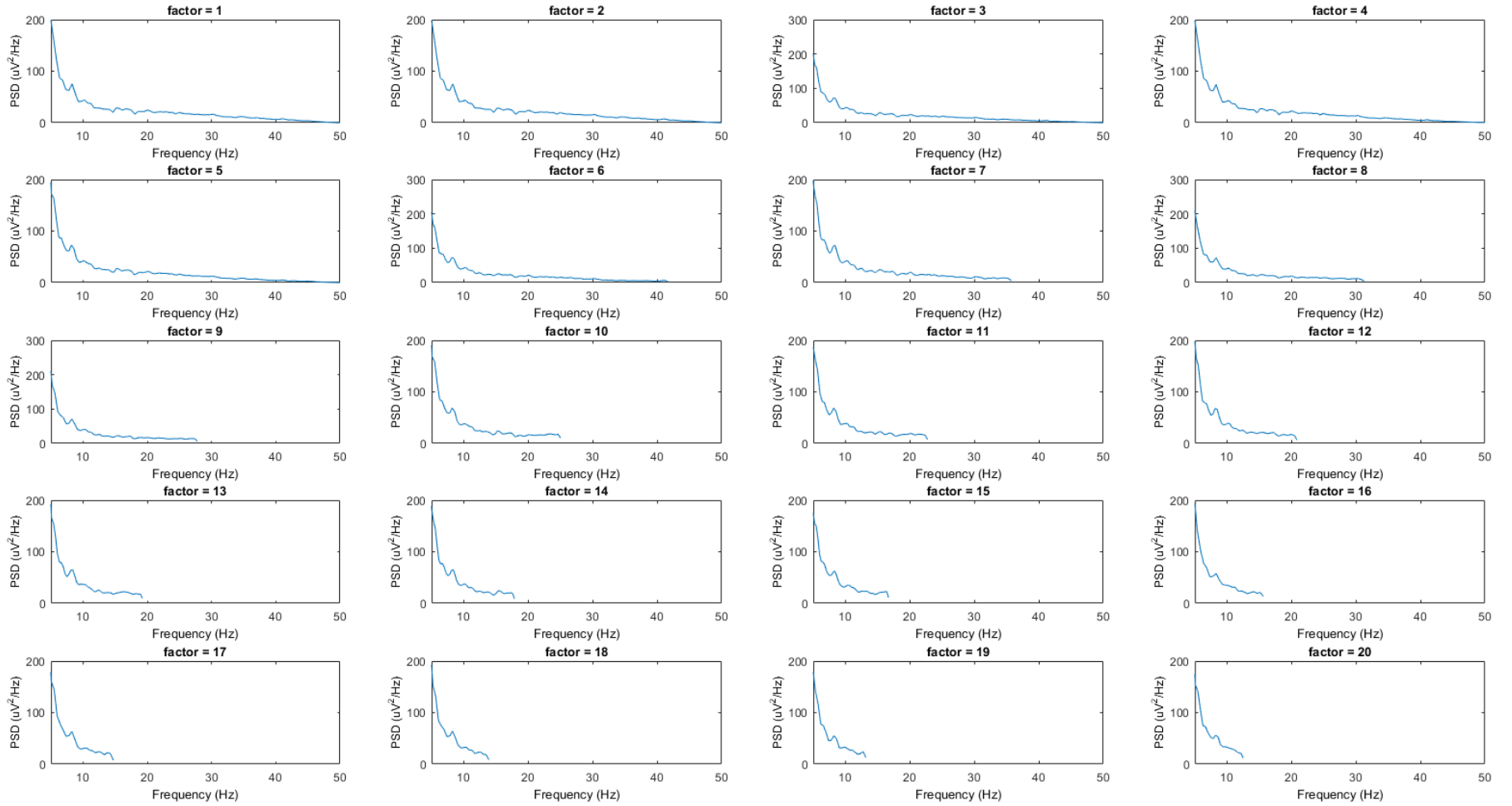
Figure 4.3:Power spectral density of each coarse-grained timeseries in units of a) microvolts and b) decibels.
This was conducted for timescale (or factor) 1 to 20.

4.4 Discussion

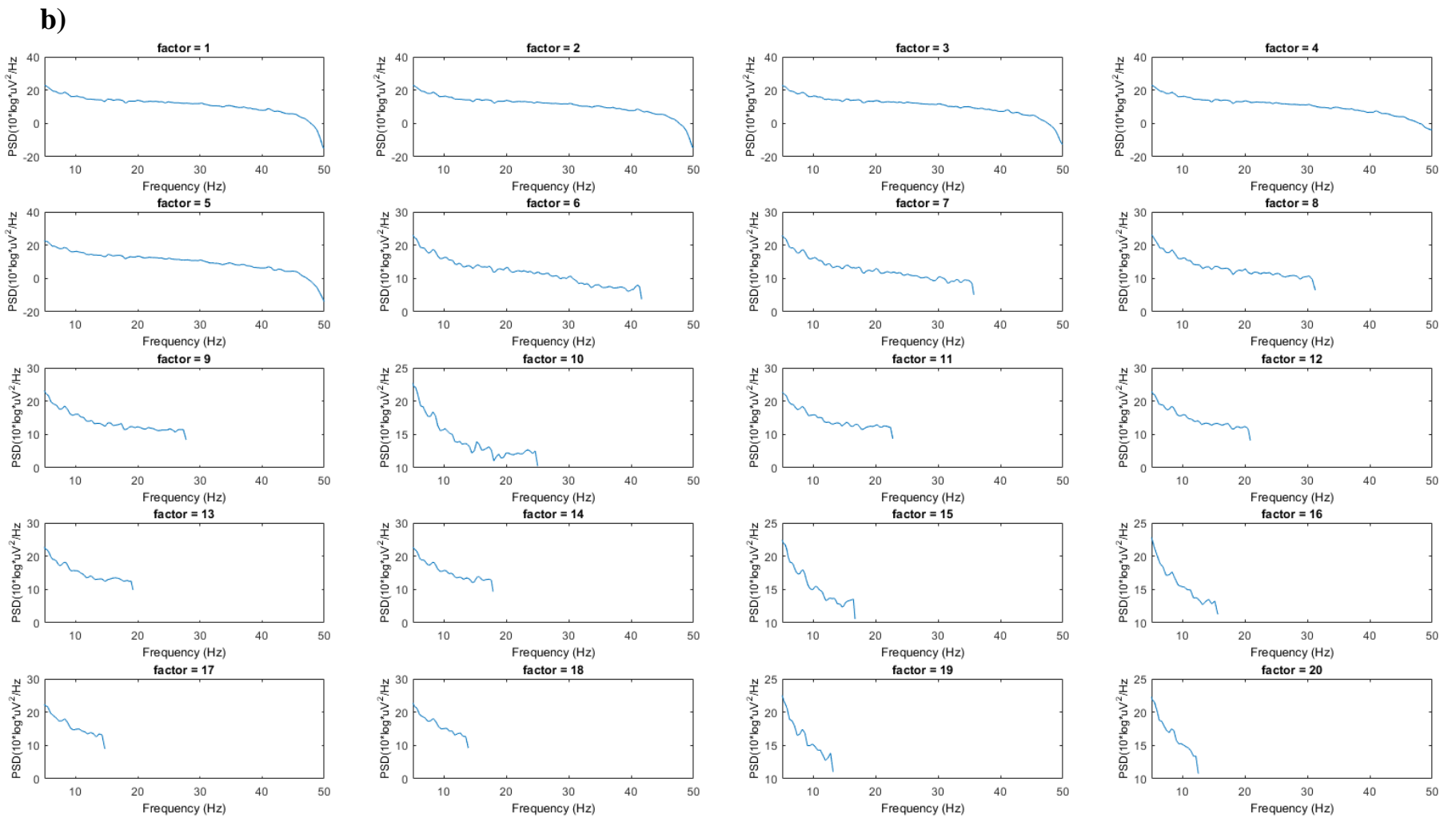A 16p11.2 del mouse model (Horev et al., 2011) was used in the current study to capture the impact of a loss of 16p11.2 on spontaneous neural activity across species. We conducted LFP analyses paralleling the human EEG analyses (**Chapter 3**) of neural entropy and spectral power. This comparative perspective would help in identifying converging evidence to the 16p11.2 human results and improving interpretations of the observed EEG alterations in humans. In this study, however, the 16p11.2 del mouse results were inconsistent with the human results; Neural dynamics, as measured by MSE and power metrics, were in the typical range in 16p11.2 del mice, as no group differences were found compared to wild-type mice.

The lack of consistency between the present study's 16p11.2 mouse results and the previously reported human results (**Chapter 3**) could be attributed to a number of factors. A hemideletion of 16p11.2 might not impact humans and mice in the same way in terms of their phenotypic profile and severity. As shown in **Chapter 1**, although 16p11.2 humans and mice share similar phenotypes (e.g., cognitive and motor deficits), there are also some differences (e.g., body weight and hearing problems). It may be the case that sensitivity to gene dosage at 16p11.2 differ between humans and mice (Hiroi, 2018). Unlike 16p11.2 del humans, nearly half of 16p11.2 del mice are expected not to survive as pups (Horev et al., 2011; Portmann et al., 2014). Perhaps, the mice that do survive engage compensatory mechanisms and exhibit mild changes in LFP entropy and power, relative to wild-type mice, that the current study was not able to detect in this sample. Consequently, EEG/LFP activity in humans and mice might not display similar patterns or reflect analogous dysfunctions in this case.

The mouse genetic background and strain might also play a role in modulating the observed neural activity and other phenotypes. 16p11.2 del mice under a hybrid genetic background of C57BL/6NxC3B displayed social interaction deficits, whereas these deficits were not found in mice with an inbred genetic background of C57BL/6N (see **Chapter 1**, **Figure 1.10**; Arbogast et al., 2016). Similarly, in a mouse model of Angelman syndrome, LFP delta power activity was dependent on the mouse genetic background (Sidorov et al., 2017); Higher delta power was found in mice under a particular genetic background (i.e., 129 background), but not in mice under the other background (i.e., C57BL/6). It is possible, therefore, that 16p11.2 del mice under a different genetic background than that in the current study, i.e., hybrid C57BL/6NxSv, would display more pronounced changes in LFP neural dynamics relative to control mice. This is in line with the notion that a deleterious CNV, such

as 16p11.2 del, may not be sufficient for the CNV-associated phenotypes to appear (Forsingdal et al., 2019; Girirajan et al., 2010). The absence, severity, and variability of phenotypes associated with 16p11.2 del could be largely influenced by genetic background (Girirajan et al., 2012; O'Donovan and Owen, 2016); This includes interactions between 16p11.2 del, single nucleotide polymorphisms, single nucleotide variants, and other CNVs.

In spite of the aforementioned considerations and limitations, two recent studies observed differences in neural activity in 16p11.2 del mice relative to controls, as described earlier (Lu et al., 2019; Bertero et al., 2018). Bertero et al. (2018) found reduced prefrontal-retrosplenial LFP coherence (i.e., a measure of functional connectivity), within the delta frequency range, in 16p11.2 del mice.

Prior work (as described in **Chapter 3** and summarised in **Figure 3.1**) suggested that there is a relationship between functional connectivity and neural entropy. For this reason (and because the LFP data re-analysed in the current study are the same as the data analysed and presented by Bertero et al. (2018)), it is surprising that the current study's findings did not show any concordance with Bertero et al.'s (2018) results. Nevertheless, evidence that connectivity and entropy features relate does not necessitate that features in relation to both measures could always be detected concurrently.

In relation to Lu et al.'s (2019) study, the authors found atypical EEG activity during awake and sleep states in delta, theta, and beta frequency bands in 16p11.2 del mice (as mentioned in **Chapter 1**). The discrepancy between the current study (i.e., no group differences in power) and Lu et al.'s (2019) findings could be due to the electrode position and depth. The current study recorded LFP activity from the anterior cingulate cortex and retrosplenial cortex, whereas Lu et al. (2019) recorded EEG activity from the parietal region. Accordingly, future studies should examine EEG/LFP mouse activity at these and other brain areas to verify whether neural activity is altered at some sites, but not others in 16p11.2 del mice.

In addition to the aforementioned considerations, future studies should take into account the testing ages of both humans and mice. Neural entropy in 16p11.2 del could impact humans and mice differently at specific ages. Prior work has shown that neural entropy dynamics are age-dependent in typically developing humans (McIntosh et al., 2014); It might be the case that disruptions of neural entropy are more pronounced at specific ages

not represented in the current mouse sample (age in the current sample ranges between 11 to 13 weeks, corresponding to young mature adults).

Although the small sample size in the current study is typical of mouse studies, it is possible that a larger sample would have been needed to reveal group differences mirroring that of humans (**Chapter 3**). Perhaps, the mouse sample (n = 6 del; n = 6 control) is not sufficiently powered to show any significant effects. This might be the case as we found medium to large effect sizes for the entropy and, surprisingly, power measures (**Table 4.1**), suggesting that group differences might become apparent with a larger sample. Interestingly, there seems to be a trend of higher entropy at lower timescales (timescale 1-5) at the prefrontal electrode as shown in **Figure 4.2**, partly supporting our human results (**Chapter 3**; although higher entropy was found at all timescales in 16p11.2 del humans). Indeed, power analysis confirmed that even with the EEG variables with large effect sizes (e.g., Frontal MSE scales 1-5: 0.59; and Frontal low to high frequency ratio (LHR): 0.79, **Table 4.1**), sample sizes of 30 and 17, respectively, for each the del and control mice groups, were required to achieve a statistical power of 60% for detecting an effect.

Notably, to further establish the link between neural activity and behavioural phenotypes in 16p11.2 del, it is essential to conduct 16p11.2 del mouse studies that investigate this link, analogous to human studies. Prior work in this thesis showed a strong neural-behaviour link (e.g., entropy and anxiety levels) in 16p11.2 del humans (**Chapter 3**). Therefore, investigating the relationship between LFP activity and anxiety behaviour (in addition to other psychiatric traits) in 16p11.2 del mice could reveal interesting results.

The presented work is the first study to investigate neural entropy in 16p11.2 del mice and directly compare 16p11.2 mouse LFP with human EEG data. The lack of group differences in neural entropy in 16p11.2 del mice, despite our previous human results reported in **Chapter 3**, should be verified and further investigated in future studies. Studying human and mouse in parallel is important for contributing converging evidence to 16p11.2 del human studies and identifying reliable and conserved EEG/LFP features across species. This enables future studies to test the reversibility of EEG/LFP features and consider potential drug treatments. Equally, future studies could form links between the shared atypical EEG/LFP activity between humans and mice, and dysfunctions observed at other levels in mouse studies. This, in turn, would help in better interpreting the EEG 16p11.2 del findings.

Chapter 5   General Discussion

5.1   Answers to the outstanding questions presented in the introductory chapter 1.

After reviewing the literature, this thesis identified key outstanding questions pertaining to neural activity in 16p11.2 CNV carriers – these questions were presented in the introductory chapter and are listed below. The aim of this thesis, therefore, was to answer the below research questions. To this end, three studies were conducted that collectively answered these questions and produced novel findings, which could inform future research on 16p11.2 CNVs.

5.1.1   Is neural activity altered, as revealed via EEG variability, power, and entropy metrics, in 16p11.2 CNV carriers?

The studies conducted in this thesis showed that neural activity was indeed altered in 16p11.2 CNV (human) carriers. Using EEG, neural activity was investigated in response to visual stimuli (i.e., black and white contrast-reversing checkerboards) and at resting-state (i.e., eyes-open condition). For the former, electrodes selected for analyses were placed on the occipital region, whereas for resting-state / spontaneous neural activity, frontal and parietal electrodes were analysed, separately. Numerous EEG metrics of neural activity, which have been previously implicated in ESSENCE disorders, were considered. For visual-evoked neural activity, metrics included variability (i.e., variability in C1, P1, and N1 single-trial amplitude and latency, and timecourse variability; alpha and beta power single-trial variability; signal-to-noise ratio (SNR)) and conventional ERP and power (i.e., mean C1, P1, and N1 amplitude and latency; mean alpha and beta power) metrics. For spontaneous neural activity, metrics included entropy (i.e., multiscale entropy (MSE) and complexity index (CI)) and power (i.e., delta, theta, alpha, beta, and gamma power; low-to-high frequency ratio (LHR)) metrics. Overall, neural activity was altered in the reciprocal 16p11.2 CNVs. For del, altered neural activity was revealed via certain variability and entropy metrics – but not power (in relation to del/ctrl comparisons). For dup, a specific alteration in power was found, with no changes in variability (in addition, entropy was not investigated for dup). Namely, neural variability (as observed via variability of timecourse amplitude and variability of P1 peak amplitude) and entropy (as observed via MSE at any timescale and CI), at occipital and frontal regions, respectively, were identified to be higher in del compared to controls. For dup, there was lower evoked alpha power compared to controls.

5.1.2 Does 16p11.2 dosage have an opposing effect on neural activity as per the additive model?

Opposing neural activity in the reciprocal 16p11.2 CNVs were not identified in the current thesis as there were no significant group differences in neural activity that were in line with the additive model (i.e., del > control and control > dup, or vice versa). Yet, it is important to acknowledge that opposing neural activity might be present in the reciprocal 16p11.2 CNVs, yet it was not revealed in this thesis due to limitations such as sample size. Non-significant trends that might suggest opposing neural activity, however, were observed via certain metrics, which showed significant group differences between del and dup groups (but not against controls). These include, P1 latency variability (del < control < dup), absolute alpha and beta variability (del > control > dup), P1 (mean) amplitude (del > control > dup), and absolute (mean) alpha and beta power (del > control > dup). Nevertheless, these trends are not sufficient evidence of an opposing effect in neural activity in the reciprocal 16p11.2 CNVs.

5.1.3 Is there a relationship between neural activity and ESSENCE traits in 16p11.2 deletion carriers?

Certain relationships were observed between neural activity and ESSENCE traits in 16p11.2 del in this thesis. Correlation analyses were conducted between resting-state neural activity (as measured via entropy, power (including LHR) metrics) and ESSENCE traits (as extracted via numerous assessments) in 16p11.2 del. For these analyses, assessment scores of IQ, autism spectrum-related traits (Autism Diagnostic Observation Schedule-Calibrated Severity Score (ADOS-CSS)), social traits (Social Responsiveness Scale (SRS)), and a range of behavioural and psychiatric problems in children (Child Behaviour Checklist for ages 1.5-5 (CBCL) subscales), were used to capture ESSENCE problems. For the latter assessment, i.e., the CBCL, five DSM-oriented subscales and one syndrome subscale were extracted: affective problems, anxiety problems, pervasive developmental problems, ADHD problems, oppositional defiant problems, and sleep problems. In relation to neural activity metrics, entropy was segmented into two categories, i.e., entropy at lower timescales and entropy at higher timescales; power was assessed at each frequency band, from delta up to gamma, in addition to LHR (delta to beta ratio). Overall, higher entropy was strongly associated with higher severity of ESSENCE problems. Specifically, entropy at lower timescales was positively correlated with pervasive developmental, ADHD, and oppositional defiant problems; whereas entropy at higher timescales was positively correlated with anxiety

problems. With regards to power-ESSENCE correlations, decreased lower-frequency power, and increased-higher frequency power, respectively, were strongly associated with increased severity of ESSENCE problems. Specifically, lower-frequency power (i.e., delta) was negatively correlated with anxiety, pervasive developmental, and oppositional defiant problems. Whereas, higher-frequency power (i.e., alpha, but also theta) was positively correlated with the same CBCL-subscales. Also, these subscales were negatively associated with LHR (as would be expected given the aforementioned power-ESSENCE correlations). Surprisingly, no significant correlations were found between neural activity and other ESSENCE traits, such as the CBCL-affective problems and sleep problems, ADOS-CSS, SRS, or IQ.

5.1.4 Is neural activity in 16p11.2 deletion mouse model similar to that of 16p11.2 deletion humans?

The current thesis did not identify similar neural activity between the 16p11.2 del mouse model and 16p11.2 del human carriers. In-vivo electrophysiological activity, captured via frontal and retrosplenial electrodes, were examined in Horev et al.'s (2011) mouse model of 16p11.2 del. Specifically, analysis of LFP entropy and power features, in line with the human 16p11.2 del analysis in this thesis, was conducted. No group differences were found in either entropy or power metrics between 16p11.2 del mice and control wild-type mice. However, it is important to note that there were medium to large effect sizes for entropy and power, indicating that there may be group differences that would become apparent with a larger sample. Trends indicated that 16p11.2 del mice showed higher entropy at lower timescales at the frontal electrode. Hence, this is partly congruent with the 16p11.2 del human results of higher entropy at all timescales at the frontal region.

5.2 Interpretation of findings

Overall, the findings from human subjects in this thesis indicate that deletion or duplication of the 16p11.2 region impacts neural activity. Despite trends suggestive of certain opposing neural activity in the reciprocal 16p11.2 CNVs, these trends were non-significant and were not representative of opposing neural activity as defined in this thesis. The results, therefore, indicate that gene-dosage impacts neural activity in 16p11.2 del vs dup carriers in unique yet non-opposing manners. Whether loss or excess of 16p11.2 dosage, neural activity at the occipital area was altered (as shown in **Chapter 2**). Therefore, this altered neural activity might involve sensory processing and, generally, cognitive processes related to learning and

adaptation to a changing environment – as EEG variability measures have been regarded as a proxy for these processes. 16p11.2 del further showed neural alterations in fronto-central areas (**Chapter 3**). This was interpreted as implicating short and long-range information processing (via atypical entropy at lower and higher timescales, respectively) involving fronto-central areas. Taken together, atypical neural activity in 16p11.2 CNV seems to be pervasive, extending to many brain regions and neural features associated with various cognitive and other processes.

Thus, the observed neural alterations could be reflecting a general dysfunction or compensatory mechanism/s that impacts a range of processes leading to various ESSENCE traits with varying severity. Indeed, this thesis showed strong links between neural activity and ESSENCE problems in 16p11.2 del, regardless of the severity level of these problems. These included anxiety, pervasive developmental, ADHD, and oppositional defiant problems. Accordingly, the observed neural alterations could be viewed as possible endophenotypes reflecting the dysfunction or compensatory mechanism/s that is impacting the mentioned ESSENCE traits.

Several lines of evidence implicate various neurotransmitter and neuromodulator systems in 16p11.2 CNV. Certainly, the dysregulation and interplay between multiple neurotransmitter systems could generate a net E/I imbalance (and might represent the above-posited compensatory mechanism or general dysfunction). Although EEG mainly captures activity from superficial cortical sources, it is also possible that certain deeper sources contributed to the observed signal (as discussed in **Chapter 4**). Therefore, the E/I imbalance reflected in the EEG might not be solely restricted to cortical E/I.

Evidence in support of this view of an overall E/I imbalance could be drawn from previous 16p11.2 CNV mouse studies (described earlier in this thesis) as multiple systems were implicated. These studies found abnormalities in the GABAergic (Stoppel et al., 2018), glutamatergic (Wang et al., 2018), dopaminergic (Portmann et al., 2014), and serotonergic systems (Walsh et al., 2018; Panzini et al., 2017).

The findings in this thesis further support this view of an overall E/I imbalance. The observed EEG features in 16p11.2 CNV carriers in this thesis, including increased neural variability and entropy (for del) and decreased alpha power (for dup), have been previously linked with dysregulation in the above-mentioned neurotransmitter systems in typical and/or ESSENCE populations (e.g., Takahashi et al., 2010; as have been described in **Chapter 2** and

Chapter 3). In addition, these neural features were associated with certain ESSENCE traits, in this thesis, such as anxiety, ADHD, and pervasive developmental problems (including ASD-related traits), which were previously linked with E/I imbalance and dysregulations in the above-mentioned systems. As such, it is possible that an overall E/I imbalance implicating multiple neurotransmitter systems are contributing to the observed EEG signal and ESSENCE traits in 16p11.2 CNV carriers.

That being said, it is important for future studies to confirm these interpretations, which, in this thesis, are meant to represent early efforts for findings links between different levels of analyses. Future parallel 16p11.2 CNV human-mouse studies should further elucidate these links and disentangle the currently-presented simplified and unifying theory of an overall E/I imbalance.

5.3   Key limitations and strengths of this thesis

Key limitations and strengths of this thesis will be acknowledged here. The small sample size is a limitation in the current thesis as it generally increases the likelihood of type I (i.e., false positives) and type II errors (i.e., false negatives) occurring in the studies conducted here. With the awareness of the trade-off between type I and type II errors, the current thesis prioritised avoiding type I errors. The rationale for this decision is the assumption that effect sizes for most of the comparisons conducted in the current thesis are sufficiently large, as group differences in neural activity especially for 16p11.2 del have been observed in prior studies with similarly small sample sizes (median sample size and range for del: 19 [8, 35]; Hinkley et al., 2019; Bertero et al., 2018; LeBlanc and Nelson, 2016; Jenkins et al., 2016; Hudac et al., 2015). Hence, it was assumed that the large effect sizes would make the occurrence of a type II error less likely. Therefore, avoiding a type I error was prioritised. To this end, the current thesis applied randomisation statistical techniques (as described in **Chapter 2**, **Section 2.2.11**) and conservative significance thresholds that vary as defined by the Benjamini-Hochberg method (computed based on the raw p-values' rank, total number of tests, and the false discovery rate, which was set at 5% in this thesis). Using this conservative approach is a strength of this thesis, as the results were narrowed down with the purpose of solely presenting significant and likely reliable results.

Conversely, it is possible that a type II error was committed, especially given that certain correlations with large effect sizes were present in this thesis (see **Chapter 2**, **Table**

2.7). For example, P1 amplitude variability was strongly correlated with ADOS-CSS for dup (r = -0.76), however, it was deemed non-significant as per the conservative significance threshold of p < 0.003 in line with the result of the Benjamini-Hochberg method. Although note that the Benjamini-Hochberg method allows for greater statistical power in the expense of increased numbers of type I errors compared to the Bonferroni correction (i.e., significance threshold divided by the number of tests) – although this depends on how the parameters are defined. In other words, compared to familywise error rate methods, such as the Bonferroni correction, the Benjamini-Hochberg method is less stringent in preventing type I errors, which makes it generally more favourable in terms of balancing the possible occurrence of type I and type II errors.

A further limitation is that datasets analysed in this thesis were not collected by the current author. Novel analyses were conducted of secondary datasets previously collected by SFARI partners and other researchers (i.e., Alessandro Gozzi's lab). Some of these datasets (i.e., EEG resting-state data analysed in **Chapter 3**) were not examined prior to this thesis. The disadvantage of studying secondary data is that various aspects relating to data collection protocol are pre-set, including study design, data length, sampling rate, quality-checks, etc. Therefore, it was not possible for the current author to alter certain data parameters and inspect data quality at the source. However, this was not an issue for the current thesis as the previous researchers involved in data collection shared their meta-data and study protocol with the current author. More importantly, the advantages of data-sharing and collaborative efforts outweigh the costs, especially in the case of rare populations such as 16p11.2 CNV carriers. Data-sharing and analysis of secondary data is a more cost-effective and efficient strategy. In addition, this strategy enables the contribution of various researchers with different skills to provide deeper analyses and converging evidence. Indeed, a strength of this thesis is that work here contributes to the deep characterisation of 16p11.2 CNV using datasets available for future efforts to test the reliability of current findings and provide converging evidence.

Another strength of this thesis is the combination of human participants and mouse model to study neural activity in 16p11.2 CNV. Parallel human-mouse studies are valuable for numerous reasons as discussed in **Chapter 4** and essential for advancing research on mechanisms implicated in 16p11.2 CNVs. However, behavioural and cognitive data for the mouse samples were not available. Therefore, analyses linking neural activity with

ESSENCE traits were not possible for the mouse samples. As such, the human-mouse comparative approach was limited to neural activity.

As the current thesis focused on analysing EEG/LFP data, the high temporal resolution provided by these neuroimaging modalities allow for interpretations of the current findings as relating to mechanisms/neurotransmitter systems that operate in similarity high temporal scales. However, the low spatial resolution relative to other neuroimaging modalities, e.g., fMRI, makes it challenging to determine links between neural pathways implicated in 16p11.2 CNV and the observed neural activity. However, EEG source localisation algorithms are increasingly improving and might be worthwhile to gain spatial information. Alternatively, future studies could incorporate parallel EEG/LFP-fMRI analyses, which collectively would be very informative.

Further limitations to the current thesis due to the small sample size include the lack of examination of possible confounding factors such as seizure susceptibility/epilepsy and current medication use. Although a minority of participants had seizure/epilepsy diagnoses (for study 1: n = 3 del and n = 1 dup) and were currently taking medications for anxiety and epilepsy (study 1: n = 2 del; study 2: n = 2 del), these factors impact the EEG signal to some extent. Nevertheless, these only represent a very small minority of the overall sample and analyses in this thesis were based on group averages and conservative significance thresholds.

Another possible limitation to this thesis was that the presented hypotheses were broad. Certainly, it was challenging to convincingly propose hypotheses with high specificity, therefore it was deemed more appropriate to do otherwise. Previous studies of neural activity in 16p11.2 CNV are only the aforementioned few, therefore, formulating specific hypotheses would not be possible in this case. Nevertheless, with broad hypotheses and a conservative approach, this thesis contributed to this literature by conducting novel analyses assessing 16p11.2 CNV neural activity using multiple metrics – which is a strength of this thesis. Based on this rationale, a recommendation would be for future studies to use a more data-driven quantitative approach to examine neural activity in 16p11.2 CNV, as will be discussed in the next section.

5.4 Future work

The natural progression from the studies conducted in this thesis would be to use more advanced analysis approaches that would address some of the main limitations mentioned above and provide advantages not possible with the current techniques. Over the past four years, there has been an exponential increase in the advancement and application of machine learning (ML) techniques, such as in research fields of robotics and medicine, but also outside of research such as in websites predicting a visitor's interests, smartphones identifying objects in images, and email platforms predicting email replies. ML entails an algorithm that develops a mathematical model with the ability to update its parameters, based on sample data (denoted training data), for the purpose of refining the model to the best possible parameters that could classify or predict patterns on a new set of data (note that this is performed without explicit instructions on how the model should learn from the training data). Among the ML techniques contributing to this boom in the use of ML is deep neural networks[6] (DNN; LeCun et al., 2015).

Novel applications of DNNs have been increasingly examined with EEG data in various research areas, e.g., seizure detection and prediction, cognitive and affective monitoring, and brain-computer interfaces (for a review see Roy et al., 2019). The increasing interest in DNN-EEG application is evident as there are more publications in the first seven months of 2018 than 2010 to 2016 altogether (Roy et al., 2019). As such, several advantages of using DNNs for EEG research were observed in these studies (Roy et al., 2019). Thus, DNNs could be especially useful for EEG research relating to 16p11.2 CNVs.

Some of the key advantages of using DNNs for 16p11.2 CNV EEG research are as follows. Based on a recent review (Roy et al., 2019), DNNs consistently outperformed conventional statistical techniques (including older ML techniques) in their classification or predictive accuracy. Of note, this was observed in research relating to ESSENCE disorders; For example, studies reported accuracies of > 80% for detecting epileptic discharges (Hao et al., 2018) and predicting ASD diagnosis (Jayawardana et al., 2019). Evidently, it would be valuable to conduct DNN-EEG analysis for 16p11.2 CNVs.

---

[6] A deep neural network (DNN) is an algorithm with multiple layers of neurons (or operations) between the input layer and output. Each layer extracts more complex information from input data and previous layers. DNN finds the best mathematical manipulation to turn the input into the output whether it be a linear relationship or non-linear.

Although the current thesis investigated various EEG features (e.g., variability, power, entropy), there are further numerous mathematical techniques for analysing EEG signals and extracting features. This makes the task of identifying the key features that most likely fit the criteria of an endophenotype for 16p11.2 CNVs and related ESSENCE traits challenging. DNNs (especially with model architectures of convolutional neural networks (CNN), recurrent neural networks (RNN), a hybrid of the two, or more advanced networks) solve this problem by automatically extracting salient features from the EEG signal. Whether using raw or pre-processed data, DNNs have been successful in extracting meaningful features and were reported to achieve good performance (Roy et al., 2019). As opposed to researchers training for years to learn how to conduct various mathematical techniques for signal analysis, DNNs automatically extract meaningful features not restricted to a particular technique. Although it is not possible to observe the features that were extracted by DNNs because of how the model operates, there is a technique (i.e., Inceptionism; Mordvintsev et al., 2015) that could be applied at a later step that shows the most impactful features. Alternatively, if researchers are solely interested in particular features extracted manually, then certain algorithms could be used to select salient features prior to feeding them as input into the DNN model. Even in this case, DNNs are more likely to find patterns within the features that are impactful for high performance on the classification/prediction task.

Although ML techniques are commonly perceived as only applicable when large datasets are available, recent advances made certain ML techniques, i.e., transfer learning involving DNNs, particularly useful for tackling the problem of small sample sizes (Tan et al., 2018). In psychology, transfer of learning (also denoted knowledge transfer) refers to the cognitive capability of humans to transfer learning from one context to another (Nokes-Malach and Richey, 2015). In other words, the notion refers to the ability to generalise what has been learned from one context and apply it to a novel context. Similarly, transfer learning in ML refers to the technique of taking a model that was refined and trained for a particular dataset and task (base model) and then re-using it as the base for a different yet related task (target model). This is possible because features extracted at early stages in the model are more generic, and hence more generalisable, as opposed to later stages where the model becomes more specialised for the particular task. This is akin to the visual system where lower visual areas (primary visual cortex; V1) processes edges and forwards this information to higher visual areas that ultimately detect complex shapes. Therefore to apply transfer learning, the lower level parameters of the base model is maintained, whereas the higher level

model parameters are altered when trained on the new dataset/ target task. Indeed, the transfer learning technique has already produced highly accurate results, e.g., dermatologist-level detection of skin cancer from images (Esteva et al., 2017; this study used a base model that was pretrained on images of 1000 object categories, e.g., person, dog, chair, etc. (http://www.image-net.org), and then for the purpose of fine-tuning the model for the target task of detecting skin cancer, the model was next trained on a smaller dataset of images of skin lesions). As opposed to requiring a large dataset in the same domain as the target task to train the model, datasets from different yet related domains (e.g., data of images) are combined to train the model in the transfer learning technique. Alternatively, if related datasets to the target task were unavailable, it is also possible to obtain a model (without acquiring the data) that was previously trained on related datasets. Indeed, researchers are increasingly sharing EEG datasets and pretrained models (e.g., GitHub, code sharing platform; See Roy et al., 2019 and Al-jawahiri and Milne, 2017 for EEG databases). Therefore, research relating to 16p11.2 CNVs and other rare CNVs or disorders, where large datasets are difficult to acquire, would greatly benefit from using transfer learning.

Thus, due to the aforementioned benefits of using DNNs (including higher performance, automatic feature extraction, and reduced demand of large datasets via transfer learning), this thesis recommends future EEG-DNN research in 16p11.2 CNVs. Using DNNs, the target task for the model would be to identify 16p11.2 CNV participants and predict their ESSENCE traits based on their EEG activity. In line with the ESSENCE framework, the (base) training datasets could include EEG signals of various ESSENCE disorders - along with 16p11.2 CNVs (for the target model)[7]. Relatedly, a recent study showed that there is a considerable overlap in the psychiatric problems observed in 16p11.2 CNVs and several other CNVs (Chawner et al., 2019), e.g., 1q21.1 (proximal duplication, and distal deletion and duplication), 2p16.3 (deletion), 15q11.2 (deletion), 15q13.3 (deletion and duplication), 16p11.2 (distal deletion), and 22q11.2 (duplication). Given this overlap, there is a strong rationale for further including these CNVs to train (possibly for the target model) a DNN model.

---

[7] Note that the main requirement for conducting transfer learning is for the base training and target training datasets to be in the same domain, i.e., EEG data.

5.5 Concluding remarks

This thesis investigated EEG activity in human 16p11.2 CNV carriers and in-vivo electrophysiological activity in 16p11.2 deletion mouse model. The studies conducted here were made possible due to data-sharing platforms and collaborators (i.e., SFARI and Dr Alessandro Gozzi's lab at the Istituto Italiano di Tecnologia). Indeed, these data-sharing initiatives are of great benefit to the advancement of research in this and other areas. Unique to this thesis is the approach of conducting parallel 16p11.2 human EEG-mouse LFP analyses. However, positive findings were not found in the latter (i.e., 16p11.2 del mice) despite the literature indicating otherwise. Overall, findings from the human subjects, in this thesis, contributed further evidence to the 16p11.2 CNV literature pertaining to the atypical nature of neural activity in 16p11.2 CNV. Using various metrics of neural activity, atypical evoked and spontaneous activity was identified in 16p11.2 CNV, and the latter was related to numerous ESSENCE traits. Future work should further verify and expand on these findings.

References

Ahtam, B., Link, N., Hoff, E., Ellen Grant, P., & Im, K. (2019). Altered structural brain connectivity involving the dorsal and ventral language pathways in 16p11.2 deletion syndrome. *Brain Imaging and Behavior, 13*(2), 430-445. doi:10.1007/s11682-018-9859-3

Al-Jawahiri, R., & Milne, E. (2017). Resources available for autism research in the big data era: a systematic review. *PeerJ, 5*, e2880. doi:10.7717/peerj.2880

Albert, P. R., Vahid-Ansari, F., & Luckhart, C. (2014). Serotonin-prefrontal cortical circuitry in anxiety and depression phenotypes: pivotal role of pre- and post-synaptic 5-HT1A receptor expression. *Front Behav Neurosci, 8*, 199. doi:10.3389/fnbeh.2014.00199

Angelakos, C. C., Watson, A. J., O'Brien, W. T., Krainock, K. S., Nickl-Jockschat, T., & Abel, T. (2017). Hyperactivity and male-specific sleep deficits in the 16p11.2 deletion mouse model of autism. *Autism Res, 10*(4), 572-584. doi:10.1002/aur.1707

Arazi, A., Censor, N., & Dinstein, I. (2017). Neural Variability Quenching Predicts Individual Perceptual Abilities. *The Journal of neuroscience : the official journal of the Society for Neuroscience, 37*(1), 97. doi:10.1523/JNEUROSCI.1671-16.2016

Arbogast, T., Ouagazzal, A.-M., Chevalier, C., Kopanitsa, M., Afinowi, N., Migliavacca, E., . . . Reymond, A. (2016). Reciprocal Effects on Neurocognitive and Metabolic Phenotypes in Mouse Models of 16p11.2 Deletion and Duplication Syndromes: e1005709. *PLoS Genetics, 12*(2). doi:10.1371/journal.pgen.1005709

Arns, M., Vollebregt, M. A., Palmer, D., Spooner, C., Gordon, E., Kohn, M., . . . Buitelaar, J. K. (2018). Electroencephalographic biomarkers as predictors of methylphenidate response in attention-deficit/hyperactivity disorder. *Eur Neuropsychopharmacol, 28*(8), 881-891. doi:10.1016/j.euroneuro.2018.06.002

Barry, R. J., Clarke, A. R., & Johnstone, S. J. (2003). A review of electrophysiology in attention-deficit/hyperactivity disorder: I. Qualitative and quantitative electroencephalography. *Clin Neurophysiol, 114*(2), 171-183.

Basalyga, G., & Salinas, E. (2006). When response variability increases neural network robustness to synaptic noise. *Neural computation, 18*(6), 1349. doi:10.1162/neco.2006.18.6.1349

Berman, J., Chudnovskaya, D., Blaskey, L., Kuschner, E., Mukherjee, P., Buckner, R., . . . Roberts, T. (2015). Abnormal auditory and language pathways in children with 16p11.2 deletion. *NeuroImage-Clin., 9*, 50-57. doi:10.1016/j.nicl.2015.07.006

Berman, J. I., Chudnovskaya, D., Blaskey, L., Kuschner, E., Mukherjee, P., Buckner, R., . . . Roberts, T. P. L. (2016). Relationship between M100 auditory evoked response and auditory radiation microstructure in 16p11.2 deletion and duplication carriers. *American Journal of Neuroradiology, 37*(6), 1178-1184. doi:10.3174/ajnr.A4687

Bertero, A., Liska, A., Pagani, M., Parolisi, R., Masferrer, M. E., Gritti, M., . . . Gozzi, A. (2018). Autism-associated 16p11.2 microdeletion impairs prefrontal functional connectivity in mouse and human. *Brain, 141*(7), 2055-2065. doi:10.1093/brain/awy111

Blackmon, K., Thesen, T., Green, S., Ben-Avi, E., Wang, X., Fuchs, B., . . . Devinsky, O. (2018). Focal Cortical Anomalies and Language Impairment in 16p11.2 Deletion and Duplication Syndrome. *Cerebral Cortex, 28*(7), 2422-2430. doi:10.1093/cercor/bhx143

Blumenthal, I., Ragavendran, A., Erdin, S., Klei, L., Sugathan, A., Guide, J. R., . . . Talkowski, M. E. (2014). Transcriptional consequences of 16p11.2 deletion and duplication in mouse cortex and multiplex autism families. *Am J Hum Genet, 94*(6), 870-883. doi:10.1016/j.ajhg.2014.05.004

Bosl, W. J., Loddenkemper, T., & Nelson, C. A. (2017). Nonlinear EEG biomarker profiles for autism and absence epilepsy. *Neuropsychiatric Electrophysiology, 3*(1), 1. doi:10.1186/s40810-017-0023-x

Brunner, D., Kabitzke, P., He, D., Cox, K., Thiede, L., Hanania, T., . . . Biemans, B. (2015). Comprehensive Analysis of the 16p11.2 Deletion and Null Cntnap2 Mouse Models of Autism Spectrum Disorder. *PLoS One, 10*(8), e0134572. doi:10.1371/journal.pone.0134572

Busch, N. A., Dubois, J., & VanRullen, R. (2009). The Phase of Ongoing EEG Oscillations Predicts Visual Perception. *The Journal of Neuroscience, 29*(24), 7869-7876. doi:10.1523/jneurosci.0113-09.2009

Butler, J. S., Molholm, S., Andrade, G. N., & Foxe, J. J. (2017). An Examination of the Neural Unreliability Thesis of Autism. *Cerebral cortex (New York, N.Y. : 1991), 27*(1), 185. doi:10.1093/cercor/bhw375

Buzsáki, G., Anastassiou, C. A., & Koch, C. (2012). The origin of extracellular fields and currents--EEG, ECoG, LFP and spikes. *Nat Rev Neurosci, 13*(6), 407-420. doi:10.1038/nrn3241

Catarino, A., Churches, O., Baron-Cohen, S., Andrade, A., & Ring, H. (2011). Atypical EEG complexity in autism spectrum conditions: a multiscale entropy analysis. *Clin*

Neurophysiol, 122(12), 2375-2383. doi:10.1016/j.clinph.2011.05.004

Chang, Y. S., Owen, J. P., Pojman, N. J., Thieu, T., Bukshpun, P., Wakahiro, M. L. J., . . . Mukherjee, P. (2016). Reciprocal white matter alterations due to 16p11.2 chromosomal deletions versus duplications. *Human Brain Mapping, 37*(8), 2833-2848. doi:10.1002/hbm.23211

Chawner, S. J. R. A., Owen, M. J., Holmans, P., Raymond, F. L., Skuse, D., Hall, J., & van Den Bree, M. B. M. (2019). Genotype–phenotype associations in children with copy number variants associated with high neuropsychiatric risk in the UK (IMAGINE-ID): a case-control cohort study. *The Lancet Psychiatry, 6*(6), 493-505. doi:10.1016/S2215-0366(19)30123-3

Chenxi, L., Chen, Y., Li, Y., Wang, J., & Liu, T. (2016). Complexity analysis of brain activity in attention-deficit/hyperactivity disorder: A multiscale entropy analysis. *Brain Res Bull, 124*, 12-20. doi:10.1016/j.brainresbull.2016.03.007

Christelle, G., Jason, W., Michael, E. T., Edwin, C. O., Yu, T., Sébastien, J., . . . Nicholas, K. (2012). KCTD13 is a major driver of mirrored neuroanatomical phenotypes of the 16p11.2 copy number variant. *Nature, 485*(7398), 363. doi:10.1038/nature11091

Chu, Y. J., Chang, C. F., Shieh, J. S., & Lee, W. T. (2017). The potential application of multiscale entropy analysis of electroencephalography in children with neurological and neuropsychiatric disorders. *Entropy, 19*(8), <xocs:firstpage xmlns:xocs=""/>. doi:10.3390/e19080428

Cohen, M. X. (2014). *Analyzing neural time series data : theory and practice*. Cambridge, Massachusetts: Cambridge, Massachusetts : The MIT Press, 2014.

Cohen, M. X. (2017). Where Does EEG Come From and What Does It Mean? *Trends Neurosci, 40*(4), 208-218. doi:10.1016/j.tins.2017.02.004

Consortium, T. B., Anttila, V., Bulik-Sullivan, B., Finucane, H. K., Walters, R. K., Bras, J., . . . Consortium, B. (2018). Analysis of shared heritability in common disorders of the brain. *Science, 360*(6395). doi:10.1126/science.aap8757

Constantino, J., & Gruber, C. (2005). The Social Responsiveness Scale Manual (Western Psychological Services, Los Angeles).

Cooper, G. M., Coe, B. P., Girirajan, S., Rosenfeld, J. A., Vu, T. H., Baker, C., . . . Eichler, E. E. (2011). A copy number variation morbidity map of developmental delay. *Nat Genet, 43*(9), 838-846. doi:10.1038/ng.909

Coskun, M. A., Varghese, L., Reddoch, S., Castillo, E. M., Pearson, D. A., Loveland, K. A., . . . Sheth, B. R. (2009). Increased response variability in autistic brains? *Neuroreport,*

20(17), 1543-1548.

Costa, M., Goldberger, A. L., & Peng, C. K. (2002). Multiscale entropy analysis of complex
physiologic time series. *Phys Rev Lett, 89*(6), 068102.
doi:10.1103/PhysRevLett.89.068102

Costa, M., Goldberger, A. L., & Peng, C. K. (2005). Multiscale entropy analysis of biological
signals. *Phys Rev E Stat Nonlin Soft Matter Phys, 71*(2 Pt 1), 021906.
doi:10.1103/PhysRevE.71.021906

Courtiol, J., Perdikis, D., Petkoski, S., Müller, V., Huys, R., Sleimen-Malkoun, R., & Jirsa,
V. K. (2016). The multiscale entropy: Guidelines for use and interpretation in brain
signal analysis. *J Neurosci Methods, 273*, 175-190.
doi:10.1016/j.jneumeth.2016.09.004

Crawford, K., Bracher-Smith, M., Owen, D., Kendall, K. M., Rees, E., Pardiñas, A. F., . . .
Kirov, G. (2019). Medical consequences of pathogenic CNVs in adults: analysis of
the UK Biobank. *Journal of Medical Genetics, 56*(3), 131. doi:10.1136/jmedgenet-
2018-105477

David, N., Schneider, T. R., Peiker, I., Al-Jawahiri, R., Engel, A. K., & Milne, E. (2016).
Variability of cortical oscillation patterns: A possible endophenotype in autism
spectrum disorders? *Neuroscience and Biobehavioral Reviews, 71*, 590-600.
doi:10.1016/j.neubiorev.2016.09.031

Degenhardt, F., Priebe, L., Herms, S., Mattheisen, M., Mühleisen, T. W., Meier, S., . . .
Cichon, S. (2012). Association between copy number variants in 16p11.2 and major
depressive disorder in a German case-control sample. *American journal of medical
genetics. Part B, Neuropsychiatric genetics : the official publication of the
International Society of Psychiatric Genetics, 159b*(3), 263-273.
doi:10.1002/ajmg.b.32034

Delorme, A., & Makeig, S. (2004). EEGLAB: an open source toolbox for analysis of single-
trial EEG dynamics including independent component analysis. *Journal of
Neuroscience Methods, 134*(1), 9-21. doi:10.1016/j.jneumeth.2003.10.009

Deshpande, A., & Weiss, L. A. (2018). Recurrent reciprocal copy number variants: Roles and
rules in neurodevelopmental disorders. *Dev Neurobiol, 78*(5), 519-530.
doi:10.1002/dneu.22587

Deshpande, A., Yadav, S., Dao, D. Q., Wu, Z.-Y., Hokanson, K. C., Cahill, M. K., . . . Weiss,
L. A. (2017). Cellular Phenotypes in Human iPSC- Derived Neurons from a Genetic
Model of Autism Spectrum Disorder. *Cell Reports, 21*(10), 2678-2687.

doi:10.1016/j.celrep.2017.11.037

Dinstein, I., Heeger, D. J., & Behrmann, M. (2015). Neural variability: friend or foe? *Trends in Cognitive Sciences, 19*(6), 322-328. doi:10.1016/j.tics.2015.04.005

Dinstein, I., Heeger, D. J., Lorenzi, L., Minshew, N. J., Malach, R., & Behrmann, M. (2012). Unreliable evoked responses in autism. *Neuron, 75*(6), 981-991. doi:10.1016/j.neuron.2012.07.026

Doherty, J. L., & Owen, M. J. (2014). Genomic insights into the overlap between psychiatric disorders: implications for research and clinical practice. *Genome Med, 6*(4), 29. doi:10.1186/gm546

Duyzend, M. H., Nuttle, X., Coe, B. P., Baker, C., Nickerson, D. A., Bernier, R., & Eichler, E. E. (2016). Maternal Modifiers and Parent-of-Origin Bias of the Autism-Associated 16p11.2 CNV. *Am J Hum Genet, 98*(1), 45-57. doi:10.1016/j.ajhg.2015.11.017

D'angelo, D., Lebon, S., Chen, Q., Martin-Brevet, S., Snyder, L. G., Hippolyte, L., . . . Chung, W. K. (2016). Defining the Effect of the 16p11.2 Duplication on Cognition, Behavior, and Medical Comorbidities. *JAMA Psychiatry, 73*(1), 20-30. doi:10.1001/jamapsychiatry.2015.2123

Edgar, J. C., Khan, S. Y., Blaskey, L., Chow, V. Y., Rey, M., Gaetz, W., . . . Roberts, T. P. L. (2015). Neuromagnetic Oscillations Predict Evoked- Response Latency Delays and Core Language Deficits in Autism Spectrum Disorders. *Journal of Autism and Developmental Disorders, 45*(2), 395-405. doi:10.1007/s10803-013-1904-x

Elliott, C. (2007). Differential Ability Scales–Second edition (DAS-II) Harcourt Assessment. *San Antonio, TX*.

Esteva, A., Kuprel, B., Novoa, R. A., Ko, J., Swetter, S. M., Blau, H. M., & Thrun, S. (2017). Dermatologist-level classification of skin cancer with deep neural networks. *Nature, 542*(7639), 115-118. doi:10.1038/nature21056

Faisal, A., Selen, L., & Wolpert, D. (2008). Noise in the nervous system. In A. Faisal (Ed.), (Vol. 9, pp. 292-303).

Fernandez, B. A., Roberts, W., Chung, B., Weksberg, R., Meyn, S., Szatmari, P., . . . Scherer, S. W. (2010). Phenotypic spectrum associated with de novo and inherited deletions and duplications at 16p11.2 in individuals ascertained for diagnosis of autism spectrum disorder. *Journal of Medical Genetics, 47*(3), 195. doi:10.1136/jmg.2009.069369

Foxe, J. J., & Simpson, G. V. (2002). Flow of activation from V1 to frontal cortex in humans. A framework for defining " early" visual processing. *Experimental brain research,*

142(1), 139. doi:10.1007/s00221-001-0906-7

Gandal, M. J., Haney, J. R., Parikshak, N. N., Leppa, V., Ramaswami, G., Hartl, C., . . . Group, i.-B. W. (2018). Shared molecular neuropathology across major psychiatric disorders parallels polygenic overlap. *Science, 359*(6376), 693-697. doi:10.1126/science.aad6469

Garrett, D. D., Samanez-Larkin, G. R., MacDonald, S. W., Lindenberger, U., McIntosh, A. R., & Grady, C. L. (2013). Moment-to-moment brain signal variability: a next frontier in human brain mapping? *Neurosci Biobehav Rev, 37*(4), 610-624. doi:10.1016/j.neubiorev.2013.02.015

Ghanbari, Y., Bloy, L., Christopher Edgar, J., Blaskey, L., Verma, R., & Roberts, T. P. (2015). Joint analysis of band-specific functional connectivity and signal complexity in autism. *J Autism Dev Disord, 45*(2), 444-460. doi:10.1007/s10803-013-1915-7

Gillberg, C. (2010). The ESSENCE in child psychiatry: Early Symptomatic Syndromes Eliciting Neurodevelopmental Clinical Examinations. *Res Dev Disabil, 31*(6), 1543-1551. doi:10.1016/j.ridd.2010.06.002

Girirajan, S., & Eichler, E. E. (2010). Phenotypic variability and genetic susceptibility to genomic disorders. *Hum Mol Genet, 19*(R2), R176-187. doi:10.1093/hmg/ddq366

Girirajan, S., Rosenfeld, J. A., Coe, B. P., Parikh, S., Friedman, N., Goldstein, A., . . . Eichler, E. E. (2012). Phenotypic heterogeneity of genomic disorders and rare copy-number variants. *N Engl J Med, 367*(14), 1321-1331. doi:10.1056/NEJMoa1200395

Gonen-Yaacovi, G., Arazi, A., Shahar, N., Karmon, A., Haar, S., Meiran, N., & Dinstein, I. (2016). Increased ongoing neural variability in ADHD. *Cortex, 81*, 50-63. doi:10.1016/j.cortex.2016.04.010

Gotham, K., Pickles, A., & Lord, C. (2009). Standardizing ADOS Scores for a Measure of Severity in Autism Spectrum Disorders. *Journal of Autism and Developmental Disorders, 39*(5), 693-705. doi:10.1007/s10803-008-0674-3

Gotham, K., Risi, S., Pickles, A., & Lord, C. (2007). The Autism Diagnostic Observation Schedule: Revised Algorithms for Improved Diagnostic Validity. *Journal of Autism and Developmental Disorders, 37*(4), 613-627. doi:10.1007/s10803-006-0280-1

Govindan, R. B., Wilson, J. D., Eswaran, H., Lowery, C. L., & Preißl, H. (2007). Revisiting sample entropy analysis. *Physica A: Statistical Mechanics and its Applications, 376*(1-2), 158-164. doi:10.1016/j.physa.2006.10.077

Green, E. K., Rees, E., Walters, J. T., Smith, K. G., Forty, L., Grozeva, D., . . . Kirov, G. (2016). Copy number variation in bipolar disorder. *Mol Psychiatry, 21*(1), 89-93.

doi:10.1038/mp.2014.174

Green Snyder, L., D'Angelo, D., Chen, Q., Bernier, R., Goin-Kochel, R. P., Wallace, A. S., . . . Hanson, E. (2016). Autism Spectrum Disorder, Developmental and Psychiatric Features in 16p11.2 Duplication. *Journal of autism and developmental disorders, 46*(8), 2734-2748. doi:10.1007/s10803-016-2807-4

Guitart-Masip, M., Salami, A., Garrett, D., Rieckmann, A., Lindenberger, U., & Bäckman, L. (2016). BOLD Variability is Related to Dopaminergic Neurotransmission and Cognitive Aging. *Cerebral Cortex, 26*(5), 2074-2083. doi:10.1093/cercor/bhv029

Guy, H., Jacob, E., Jason, P. L., Young-Eun, E. S., Lakshmi, M., Hannes, V., . . . Alea, A. M. (2011). Dosage-dependent phenotypes in models of 16p11.2 lesions found in autism. *Proceedings of the National Academy of Sciences, 108*(41), 17076. doi:10.1073/pnas.1114042108

Haigh, S. M., Gupta, A., Barb, S. M., Glass, S. A. F., Minshew, N. J., Dinstein, I., . . . Behrmann, M. (2016). Differential sensory fMRI signatures in autism and schizophrenia: Analysis of amplitude and trial-to-trial variability. *Schizophrenia Research, 175*(1-3), 12-19. doi:10.1016/j.schres.2016.03.036

Haigh, S. M., Heeger, D. J., Dinstein, I., Minshew, N., & Behrmann, M. (2015). Cortical variability in the sensory-evoked response in autism. *J Autism Dev Disord, 45*(5), 1176-1190. doi:10.1007/s10803-014-2276-6

Hanson, E., Bernier, R., Porche, K., Jackson, F. I., Goin-Kochel, R. P., Snyder, L. G., . . . Chung, W. K. (2015). The Cognitive and Behavioral Phenotype of the 16p11.2 Deletion in a Clinically Ascertained Population. *Biological Psychiatry, 77*(9), 785-793. doi:10.1016/j.biopsych.2014.04.021

Hanson, E., Nasir, R. H., Fong, A., Lian, A., Hundley, R., Shen, Y., . . . Clinicians, p. S. G. (2010). Cognitive and behavioral characterization of 16p11.2 deletion syndrome. *J Dev Behav Pediatr, 31*(8), 649-657. doi:10.1097/DBP.0b013e3181ea50ed

Hao, Y., Khoo, H. M., von Ellenrieder, N., Zazubovits, N., & Gotman, J. (2018). DeepIED: An epileptic discharge detector for EEG-fMRI based on deep learning. *Neuroimage Clin, 17*, 962-975. doi:10.1016/j.nicl.2017.12.005

Heisz, J. J., Shedden, J. M., & McIntosh, A. R. (2012). Relating brain signal variability to knowledge representation. *NeuroImage, 63*(3), 1384-1392. doi:10.1016/j.neuroimage.2012.08.018

Hinkley, L. B. N., Dale, C. L., Luks, T. L., Findlay, A. M., Bukshpun, P., Pojman, N., . . . Nagarajan, S. S. (2019). Sensorimotor Cortical Oscillations during Movement

Preparation in 16p11.2 Deletion Carriers. *J Neurosci, 39*(37), 7321-7331. doi:10.1523/JNEUROSCI.3001-17.2019

Hippolyte, L., Maillard, A. M., Rodriguez-Herreros, B., Pain, A., Martin-Brevet, S., Ferrari, C., . . . Jacquemont, S. (2016). The Number of Genomic Copies at the 16p11.2 Locus Modulates Language, Verbal Memory, and Inhibition. *Biological Psychiatry, 80*(2), 129-139. doi:10.1016/j.biopsych.2015.10.021

Hiroi, N. (2018). Critical reappraisal of mechanistic links of copy number variants to dimensional constructs of neuropsychiatric disorders in mouse models. *Psychiatry Clin Neurosci, 72*(5), 301-321. doi:10.1111/pcn.12641

Horder, J., Andersson, M., Mendez, M. A., Singh, N., Tangen, Ä., Lundberg, J., . . . Borg, J. (2018). GABAA receptor availability is not altered in adults with autism spectrum disorder or in mouse models. *SCIENCE TRANSLATIONAL MEDICINE, 10*(461), eaam8434. doi:10.1126/scitranslmed.aam8434

Hudac, C., Kresse, A., Aaronson, B., Deschamps, T., Webb, S., & Bernier, R. (2015). Modulation of mu attenuation to social stimuli in children and adults with 16p11.2 deletions and duplications. *Journal of Neurodevelopmental Disorders, 7*.

Jacquemont, S., Reymond, A., Zufferey, F., Harewood, L., Walters, R. G., Kutalik, Z., . . . Froguel, P. (2011). Mirror extreme BMI phenotypes associated with gene dosage at the chromosome 16p11.2 locus. *Nature, 478*(7367), 97-102. doi:10.1038/nature10406

Jayawardana, Y., Jaime, M., & Jayarathna, S. Analysis of Temporal Relationships between ASD and Brain Activity through EEG and Machine Learning.

Jenkins, J., Chow, V., Blaskey, L., Kuschner, E., Qasmieh, S., Gaetz, L., . . . Roberts, T. P. L. (2016). Auditory Evoked M100 Response Latency is Delayed in Children with 16p11.2 Deletion but not 16p11.2 Duplication. *Cerebral Cortex, 26*(5), 1957-1964. doi:10.1093/cercor/bhv008

Kadesjö, B., & Gillberg, C. (2001). The comorbidity of ADHD in the general population of Swedish school-age children. *J Child Psychol Psychiatry, 42*(4), 487-492.

Kaffashi, F., Foglyano, R., Wilson, C. G., & Loparo, K. (2008). The effect of time delay on Approximate & Sample Entropy calculations. *Physica D, 237*(23), 3069-3074. doi:10.1016/j.physd.2008.06.005

Kaminsky, E. B., Kaul, V., Paschall, J., Church, D. M., Bunke, B., Kunig, D., . . . Martin, C. L. (2011). An evidence-based approach to establish the functional and clinical significance of copy number variants in intellectual and developmental disabilities. *Genet Med, 13*(9), 777-784. doi:10.1097/GIM.0b013e31822c79f9

Kendall, K. M., Rees, E., Bracher-Smith, M., Legge, S., Riglin, L., Zammit, S., . . . Walters, J. T. R. (2019). Association of Rare Copy Number Variants with Risk of Depression. *JAMA Psychiatry, 76*(8), <xocs:firstpage xmlns:xocs=""/>. doi:10.1001/jamapsychiatry.2019.0566

Kesby, J. P., Eyles, D. W., McGrath, J. J., & Scott, J. G. (2018). Dopamine, psychosis and schizophrenia: the widening gap between basic and clinical neuroscience. *Transl Psychiatry, 8*(1), 30. doi:10.1038/s41398-017-0071-9

Kirov, G., Rees, E., Walters, J. T. R., Escott-Price, V., Georgieva, L., Richards, A. L., . . . Owen, M. J. (2014). The Penetrance of Copy Number Variations for Schizophrenia and Developmental Delay. *Biological Psychiatry, 75*(5), 378-385. doi:10.1016/j.biopsych.2013.07.022

Kitsune, G., Cheung, C., Brandeis, D., Banaschewski, T., Asherson, P., McLoughlin, G., & Kuntsi, J. (2015). A Matter of Time: The Influence of Recording Context on EEG Spectral Power in Adolescents and Young Adults with ADHD. *A Journal of Cerebral Function and Dynamics, 28*(4), 580-590. doi:10.1007/s10548-014-0395-1

Knyazev, G. G. (2007). Motivation, emotion, and their inhibitory control mirrored in brain oscillations. In (Vol. 31, pp. 377-395).

Kumar, R. A., KaraMohamed, S., Sudi, J., Conrad, D. F., Brune, C., Badner, J. A., . . . Christian, S. L. (2008). Recurrent 16p11.2 microdeletions in autism. *Hum Mol Genet, 17*(4), 628-638. doi:10.1093/hmg/ddm376

Kyle, M. W., & Michael, B. B. (2011). Copy number variation in the dosage-sensitive 16p11.2 interval accounts for only a small proportion of autism incidence: A systematic review and meta-analysis. *Genetics in Medicine, 13*(5), 377. doi:10.1097/GIM.0b013e3182076c0c

Lazaro, M. T., Taxidis, J., Shuman, T., Bachmutsky, I., Ikrar, T., Santos, R., . . . Golshani, P. (2019). Reduced Prefrontal Synaptic Connectivity and Disturbed Oscillatory Population Dynamics in the CNTNAP2 Model of Autism. *Cell Rep, 27*(9), 2567-2578.e2566. doi:10.1016/j.celrep.2019.05.006

Leblanc, J. J., & Nelson, C. A. (2016). Deletion and duplication of 16p11.2 are associated with opposing effects on visual evoked potential amplitude. *Molecular autism, 7*(1), 30-30. doi:10.1186/s13229-016-0095-7

LeCun, Y., Bengio, Y., & Hinton, G. Deep learning.

Lee, Y. A., & Goto, Y. (2018). The Roles of Serotonin in Decision-making under Social Group Conditions. *Sci Rep, 8*(1), 10704. doi:10.1038/s41598-018-29055-9

Liang, W. K., Lo, M. T., Yang, A. C., Peng, C. K., Cheng, S. K., Tseng, P., & Juan, C. H. (2014). Revealing the brain's adaptability and the transcranial direct current stimulation facilitating effect in inhibitory control by multiscale entropy. *Neuroimage, 90*, 218-234. doi:10.1016/j.neuroimage.2013.12.048

Loo, S. K., Cho, A., Hale, T. S., McGough, J., McCracken, J., & Smalley, S. L. (2013). Characterization of the theta to beta ratio in ADHD: identifying potential sources of heterogeneity. *J Atten Disord, 17*(5), 384-392. doi:10.1177/1087054712468050

Lopez-Calderon, J., & Luck, S. J. (2014). ERPLAB: an open-source toolbox for the analysis of event-related potentials. *Frontiers in human neuroscience, 8*(1), 213-213. doi:10.3389/fnhum.2014.00213

Loviglio, M. N., Leleu, M., Männik, K., Passeggeri, M., Giannuzzi, G., van der Werf, I., . . . Consortium, p. (2017). Chromosomal contacts connect loci associated with autism, BMI and head circumference phenotypes. *Mol Psychiatry, 22*(6), 836-849. doi:10.1038/mp.2016.84

Lu, H. C., Pollack, H., Lefante, J., Mills, A. A., & Tian, D. (2019). Altered sleep architecture, rapid eye movement sleep, and neural oscillation in a mouse model of human chromosome 16p11.2 microdeletion. *Sleep, 42*(3). doi:10.1093/sleep/zsy253

Lu, W. Y., Chen, J. Y., Chang, C. F., Weng, W. C., Lee, W. T., & Shieh, J. S. (2015). Multiscale Entropy of Electroencephalogram as a Potential Predictor for the Prognosis of Neonatal Seizures. *PLoS One, 10*(12), e0144732. doi:10.1371/journal.pone.0144732

Maillard, A., Ruef, A., Pizzagalli, F., Migliavacca, E., Hippolyte, L., Adaszewski, S., . . . Jacquemont, S. (2015). The 16p11.2 locus modulates brain structures common to autism, schizophrenia and obesity. *Molecular Psychiatry, 20*(1), 140-147. doi:10.1038/mp.2014.145

Marshall, C. R., Howrigan, D. P., Merico, D., Thiruvahindrapuram, B., Wu, W., Greer, D. S., . . . Consortium, C. N. V. a. S. W. G. o. t. P. G. (2017). Contribution of copy number variants to schizophrenia from a genome-wide study of 41,321 subjects. *Nature Genetics, 49*(27-35).

Martin-Brevet, S., Rodríguez-Herreros, B., Nielsen, J. A., Moreau, C., Modenato, C., Maillard, A. M., . . . Jacquemont, S. (2018). Quantifying the Effects of 16p11.2 Copy Number Variants on Brain Structure: A Multisite Genetic-First Study. *Biological Psychiatry, 84*(4), 253-264. doi:10.1016/j.biopsych.2018.02.1176

Mathewson, K. E., Lleras, A., Beck, D. M., Fabiani, M., Ro, T., & Gratton, G. (2011). Pulsed

out of awareness: EEG alpha oscillations represent a pulsed-inhibition of ongoing cortical processing. *Front Psychol, 2*, 99. doi:10.3389/fpsyg.2011.00099

McCarthy, S. E., Makarov, V., Kirov, G., Addington, A. M., McClellan, J., Yoon, S., . . . Consortium, W. T. C. C. (2009). Microduplications of 16p11.2 are associated with schizophrenia. *Nat Genet, 41*(11), 1223-1227. doi:10.1038/ng.474

McDonnell, M. D., & Abbott, D. (2009). What Is Stochastic Resonance? Definitions, Misconceptions, Debates, and Its Relevance to Biology. *PLoS Computational Biology, 5*(5), e1000348. doi:10.1371/journal.pcbi.1000348

McDonough, I. M., & Nashiro, K. (2014). Network complexity as a measure of information processing across resting-state networks: evidence from the Human Connectome Project. *Front Hum Neurosci, 8*, 409. doi:10.3389/fnhum.2014.00409

McIntosh, A. R., Vakorin, V., Kovacevic, N., Wang, H., Diaconescu, A., & Protzner, A. B. (2014). Spatiotemporal dependency of age-related changes in brain signal variability. *Cereb Cortex, 24*(7), 1806-1817. doi:10.1093/cercor/bht030

McLoughlin, G., Palmer, J. A., Rijsdijk, F., & Makeig, S. (2014). Genetic Overlap between Evoked Frontocentral Theta- Band Phase Variability, Reaction Time Variability, and Attention- Deficit/ Hyperactivity Disorder Symptoms in a Twin Study. *Biological Psychiatry, 75*(3), 238-247. doi:10.1016/j.biopsych.2013.07.020

Miller, D. T., Chung , W., Nasir , R., Shen , Y., Steinman, K. J., Wu, B.-L., & Hanson, E. (2009). 16p11.2 Recurrent Microdeletion. In. GeneReviews [Internet].

Milne, E. (2011). Increased intra-participant variability in children with autistic spectrum disorders: evidence from single-trial analysis of evoked EEG. *Front Psychol, 2*, 51. doi:10.3389/fpsyg.2011.00051

Milne, E., Gomez, R., Giannadou, A., & Jones, M. (2019). Atypical EEG in autism spectrum disorder: Comparing a dimensional and a categorical approach.

Mizuno, T., Takahashi, T., Cho, R. Y., Kikuchi, M., Murata, T., Takahashi, K., & Wada, Y. (2010). Assessment of EEG dynamical complexity in Alzheimer's disease using multiscale entropy. *Clin Neurophysiol, 121*(9), 1438-1446. doi:10.1016/j.clinph.2010.03.025

Mišić, B., Doesburg, S. M., Fatima, Z., Vidal, J., Vakorin, V. A., Taylor, M. J., & McIntosh, A. R. (2015). Coordinated Information Generation and Mental Flexibility: Large-Scale Network Disruption in Children with Autism. *Cereb Cortex, 25*(9), 2815-2827. doi:10.1093/cercor/bhu082

Mišić, B., Vakorin, V. A., Paus, T., & McIntosh, A. R. (2011). Functional embedding

predicts the variability of neural activity. *Front Syst Neurosci, 5*, 90. doi:10.3389/fnsys.2011.00090

Mordvintsev, A., Olah, C., & Tyka, M. (2015). Inceptionism: Going Deeper into Neural Networks. Retrieved from https://ai.googleblog.com/2015/06/inceptionism-going-deeper-into-neural.html

Mullen, E. M. (1995). *Mullen scales of early learning*: AGS Circle Pines, MN.

Myatchin, I., Lemiere, J., Danckaerts, M., & Lagae, L. (2012). Within- subject variability during spatial working memory in children with ADHD: an event- related potentials study. *European Child & Adolescent Psychiatry, 21*(4), 199-210. doi:10.1007/s00787-012-0253-1

Niarchou, M., Chawner, S. J. R. A., Doherty, J. L., Maillard, A. M., Jacquemont, S., Chung, W. K., . . . Bree, M. B. M. v. D. (2019). Psychiatric disorders in children with 16p11.2 deletion and duplication. *Translational psychiatry, 9*(1), 8-8. doi:10.1038/s41398-018-0339-8

Nokes-Malach, T., & Richey, E. (2015). Knowledge Transfer. In *Emerging Trends in the Social and Behavioral Sciences* (pp. 1-15).

O'Connor, C. (2008). Fluorescence In Situ Hybridization (FISH). In (Vol. 1, pp. 171). Nature Education.

O'Donovan, M. C., & Owen, M. J. (2016). The implications of the shared genetics of psychiatric disorders. *Nat Med, 22*(11), 1214-1219. doi:10.1038/nm.4196

Owen, D., Bracher-Smith, M., Kendall, K. M., Rees, E., Einon, M., Escott-Price, V., . . . Kirov, G. (2018). Effects of pathogenic CNVs on physical traits in participants of the UK Biobank 11 Medical and Health Sciences 1103 Clinical Sciences. *BMC Genomics, 19*(1), <xocs:firstpage xmlns:xocs=""/>. doi:10.1186/s12864-018-5292-7

Owen, J. P., Bukshpun, P., Pojman, N., Thieu, T., Chen, Q., Lee, J., . . . Sherr, E. H. (2018). Brain MR Imaging Findings and Associated Outcomes in Carriers of the Reciprocal Copy Number Variation at 16p11.2. *Radiology, 286*(1), 217-226. doi:10.1148/radiol.2017162934

Owen, J. P., Chang, Y., Pojman, N., Bukshpun, P., Wakahiro, M., Marco, E., . . . Mukherjee, P. (2014). Aberrant White Matter Microstructure in Children with 16p11.2 Deletions. *J. Neurosci., 34*(18), 6214-6223. doi:10.1523/JNEUROSCI.4495-13.2014

Panzini, C. M., Ehlinger, D. G., Alchahin, A. M., Guo, Y., & Commons, K. G. (2017). 16p11.2 deletion syndrome mice perseverate with active coping response to acute stress - rescue by blocking 5-HT2A receptors. *J Neurochem, 143*(6), 708-721.

doi:10.1111/jnc.14227

Pernet, C. R., Sajda, P., & Rousselet, G. A. (2011). Single-trial analyses: why bother? *Front Psychol, 2*, 322. doi:10.3389/fpsyg.2011.00322

Portmann, T., Yang, M., Mao, R., Panagiotakos, G., Ellegood, J., Dolen, G., . . . Dolmetsch, Ricardo e. (2014). Behavioral Abnormalities and Circuit Defects in the Basal Ganglia of a Mouse Model of 16p11.2 Deletion Syndrome. *Cell Reports, 7*(4), 1077-1092. doi:10.1016/j.celrep.2014.03.036

Pucilowska, J., Vithayathil, J., Tavares, E. J., Kelly, C., Karlo, J. C., & Landreth, G. E. (2015). The 16p11.2 deletion mouse model of autism exhibits altered cortical progenitor proliferation and brain cytoarchitecture linked to the ERK MAPK pathway. *The Journal of neuroscience : the official journal of the Society for Neuroscience, 35*(7), 3190-3200. doi:10.1523/JNEUROSCI.4864-13.2015

Putman, P., van Peer, J., Maimari, I., & van der Werff, S. (2010). EEG theta/beta ratio in relation to fear-modulated response-inhibition, attentional control, and affective traits. *Biol Psychol, 83*(2), 73-78. doi:10.1016/j.biopsycho.2009.10.008

Qureshi, A. Y., Mueller, S., Snyder, A. Z., Mukherjee, P., Berman, J. I., Roberts, T. P. L., . . . Buckner, R. L. (2014). Opposing brain differences in 16p11.2 deletion and duplication carriers. *The Journal of neuroscience : the official journal of the Society for Neuroscience, 34*(34), 11199-11211. doi:10.1523/JNEUROSCI.1366-14.2014

Rescorla, L. A. (2005). Assessment of young children using the Achenbach System of Empirically Based Assessment (ASEBA. *Mental Retardation and Developmental Disabilities Research Reviews, 11*(3), 226-237. doi:10.1002/mrdd.20071

Richman, J. S., & Moorman, J. R. (2000). Physiological time-series analysis using approximate entropy and sample entropy. *Am J Physiol Heart Circ Physiol, 278*(6), H2039-2049. doi:10.1152/ajpheart.2000.278.6.H2039

Rodgers, J. L. (1999). The Bootstrap, the Jackknife, and the Randomization Test: A Sampling Taxonomy. *Multivariate Behavioral Research, 34*(4), 441-456. doi:10.1207/S15327906MBR3404_2

Rosenfeld, J., Coppinger, J., Bejjani, B., Girirajan, S., Eichler, E., Shaffer, L., & Ballif, B. (2010). Speech delays and behavioral problems are the predominant features in individuals with developmental delays and 16p11.2 microdeletions and microduplications. *Advancing Interdisciplinary Research, 2*(1), 26-38. doi:10.1007/s11689-009-9037-4

Roy, Y., Banville, H., Albuquerque, I., Gramfort, A., Falk, T. H., & Faubert, J. (2019). Deep

learning-based electroencephalography analysis: a systematic review. *J Neural Eng, 16*(5), 051001. doi:10.1088/1741-2552/ab260c

Rubenstein, J. L., & Merzenich, M. M. (2003). Model of autism: increased ratio of excitation/inhibition in key neural systems. *Genes Brain Behav, 2*(5), 255-267.

Sanders, S. J., Ercan-Sencicek, A. G., Hus, V., Luo, R., Murtha, M. T., Moreno-De-Luca, D., . . . State, M. W. (2011). Multiple recurrent de novo CNVs, including duplications of the 7q11.23 Williams syndrome region, are strongly associated with autism. *Neuron, 70*(5), 863-885. doi:10.1016/j.neuron.2011.05.002

Shin, K. S., Kim, J. S., Kim, S. N., Hong, K. S., O'Donnell, B. F., Chung, C. K., & Kwon, J. S. (2015). Intraindividual neurophysiological variability in ultra-high-risk for psychosis and schizophrenia patients: single-trial analysis. *NPJ schizophrenia, 1*, 15031-15031. doi:10.1038/npjschz.2015.31

Shinawi, M., Liu, P., Kang, S.-H. L., Shen, J., Belmont, J. W., Scott, D. A., . . . Lupski, J. R. (2010). Recurrent reciprocal 16p11.2 rearrangements associated with global developmental delay, behavioural problems, dysmorphism, epilepsy, and abnormal head size. *Journal of Medical Genetics, 47*(5), 332. doi:10.1136/jmg.2009.073015

Sidorov, M. S., Deck, G. M., Dolatshahi, M., Thibert, R. L., Bird, L. M., Chu, C. J., & Philpot, B. D. (2017). Delta rhythmicity is a reliable EEG biomarker in Angelman syndrome: a parallel mouse and human analysis. *J Neurodev Disord, 9*, 17. doi:10.1186/s11689-017-9195-8

Sinclair, A. (2002). Genetics 101: cytogenetics and FISH. *CMAJ, 167*(4), 373-374.

Steinman, K. J., Spence, S. J., Ramocki, M. B., Proud, M. B., Kessler, S. K., Marco, E. J., . . . Sherr, E. H. (2016). 16p11.2 deletion and duplication: Characterizing neurologic phenotypes in a large clinically ascertained cohort. *American Journal of Medical Genetics Part A, 170*(11), 2943-2955. doi:10.1002/ajmg.a.37820

Stoppel, L. J., Kazdoba, T. M., Schaffler, M. D., Preza, A. R., Heynen, A., Crawley, J. N., & Bear, M. F. R-Baclofen Reverses Cognitive Deficits and Improves Social Interactions in Two Lines of 16p11.2 Deletion Mice.

Sørensen, L., Eichele, T., van Wageningen, H., Plessen, K. J., & Stevens, M. C. (2016). Amplitude variability over trials in hemodynamic responses in adolescents with ADHD: The role of the anterior default mode network and the non- specific role of the striatum. *NeuroImage: Clinical, 12*, 397-404. doi:10.1016/j.nicl.2016.08.007

Takahashi, T. (2013). Complexity of spontaneous brain activity in mental disorders. *Prog Neuropsychopharmacol Biol Psychiatry, 45*, 258-266.

doi:10.1016/j.pnpbp.2012.05.001

Takahashi, T., Cho, R. Y., Mizuno, T., Kikuchi, M., Murata, T., Takahashi, K., & Wada, Y. (2010). Antipsychotics reverse abnormal EEG complexity in drug-naive schizophrenia: A multiscale entropy analysis. *NeuroImage, 51*(1), 173-182. doi:10.1016/j.neuroimage.2010.02.009

Takahashi, T., Yoshimura, Y., Hiraishi, H., Hasegawa, C., Munesue, T., Higashida, H., . . . Kikuchi, M. (2016). Enhanced brain signal variability in children with autism spectrum disorder during early childhood. *Hum Brain Mapp, 37*(3), 1038-1050. doi:10.1002/hbm.23089

Tan, C., Sun, F., Kong, T., Zhang, W., Yang, C., & Liu, C. (2018). *A Survey on Deep Transfer Learning*. arXiv e-prints. Retrieved from https://ui.adsabs.harvard.edu/abs/2018arXiv180801974T

Theisen, A. (2008). Microarray-based Comparative Genomic Hybridization (aCGH). In (Vol. 1, pp. 45). Nature Education.

The simons vip consortium. (2012). Simons Variation in Individuals Project (Simons VIP): A Genetics- First Approach to Studying Autism Spectrum and Related Neurodevelopmental Disorders. *Neuron, 73*(6), 1063-1067. doi:10.1016/j.neuron.2012.02.014

Tian, D., Stoppel, L. J., Heynen, A. J., Lindemann, L., Jaeschke, G., Mills, A. A., & Bear, M. F. (2015). Contribution of mGluR5 to pathophysiology in a mouse model of human chromosome 16p11.2 microdeletion. *Nature Neuroscience, 18*(2), 182-184. doi:10.1038/nn.3911

Vakorin, V. A., Lippé, S., & McIntosh, A. R. (2011). Variability of brain signals processed locally transforms into higher connectivity with brain development. *J Neurosci, 31*(17), 6405-6413. doi:10.1523/JNEUROSCI.3153-10.2011

Valencia, J. F., Porta, A., Vallverdu, M., Claria, F., Baranowski, R., Orlowska-Baranowska, E., & Caminal, P. (2009). Refined Multiscale Entropy: Application to 24-h Holter Recordings of Heart Period Variability in Healthy and Aortic Stenosis Subjects. *IEEE Transactions on Biomedical Engineering, 56*(9), 2202-2213. doi:10.1109/TBME.2009.2021986

Varcin, K. J., Nelson, C. A., Ko, J., Sahin, M., Wu, J. Y., & Jeste, S. S. (2016). Visual Evoked Potentials as a Readout of Cortical Function in Infants With Tuberous Sclerosis Complex. *Journal of Child Neurology, 31*(2), 195-202. doi:10.1177/0883073815587328

Walsh, J. J., Christoffel, D. J., Heifets, B. D., Ben-Dor, G. A., Selimbeyoglu, A., Hung, L. W., . . . Malenka, R. C. (2018). 5-HT release in nucleus accumbens rescues social deficits in mouse autism model. *Nature, 560*(7720), 589-594. doi:10.1038/s41586-018-0416-4

Walters, R. G., Jacquemont, S., Valsesia, A., Smith, A. J. D., Martinet, D., Andersson, J., . . . Beckmann, J. S. (2010). A new highly penetrant form of obesity due to deletions on chromosome 16p11.2. *Nature, 463*(7281), 671. doi:10.1038/nature08727

Wang, D. J. J., Jann, K., Fan, C., Qiao, Y., Zang, Y. F., Lu, H., & Yang, Y. (2018). Neurophysiological Basis of Multi-Scale Entropy of Brain Complexity and Its Relationship With Functional Connectivity. *Front Neurosci, 12*, 352. doi:10.3389/fnins.2018.00352

Wang, W., Rein, B., Zhang, F., Tan, T., Zhong, P., Qin, L., & Yan, Z. (2018). Chemogenetic Activation of Prefrontal Cortex Rescues Synaptic and Behavioral Deficits in a Mouse Model of 16p11.2 Deletion Syndrome. *Journal of Neuroscience, 38*(26), 5939-5948. doi:10.1523/JNEUROSCI.0149-18.2018

Wechsler, D. (1999). Wechsler abbreviated intelligence scale. *San Antonio: The Psychological Corporation*.

Weinger, P. M., Zemon, V., Soorya, L., & Gordon, J. (2014). Low-contrast response deficits and increased neural noise in children with autism spectrum disorder. *Neuropsychologia, 63*, 10-18. doi:10.1016/j.neuropsychologia.2014.07.031

Weiss, L. A., Shen, Y., Korn, J. M., Arking, D. E., Miller, D. T., Fossdal, R., . . . Consortium, A. (2008). Association between microdeletion and microduplication at 16p11.2 and autism. *N Engl J Med, 358*(7), 667-675. doi:10.1056/NEJMoa075974

Weng, W. C., Chang, C. F., Wong, L. C., Lin, J. H., Lee, W. T., & Shieh, J. S. (2017). Altered resting-state EEG complexity in children with Tourette syndrome: A preliminary study. *Neuropsychology, 31*(4), 395-402. doi:10.1037/neu0000363

Wise, R. A. (2004). Dopamine, learning and motivation. *Nature reviews neuroscience, 5*(6), 483.

Woltering, S., Jung, J., Liu, Z., & Tannock, R. (2012). Resting state EEG oscillatory power differences in ADHD college students and their peers. *Behavioral and brain functions : BBF, 8*, 60. doi:10.1186/1744-9081-8-60

Yang, A. C., & Tsai, S.-J. (2013). Is mental illness complex? From behavior to brain. *Progress in Neuropsychopharmacology & Biological Psychiatry, 45*, 253-257. doi:10.1016/j.pnpbp.2012.09.015

Yang, A. C., Wang, S. J., Lai, K. L., Tsai, C. F., Yang, C. H., Hwang, J. P., . . . Fuh, J. L. (2013). Cognitive and neuropsychiatric correlates of EEG dynamic complexity in patients with Alzheimer's disease. *Prog Neuropsychopharmacol Biol Psychiatry, 47*, 52-61. doi:10.1016/j.pnpbp.2013.07.022

Yang, M., Lewis, F. C., Sarvi, M. S., Foley, G. M., & Crawley, J. N. (2015). 16p11.2 Deletion mice display cognitive deficits in touchscreen learning and novelty recognition tasks. *Learning & memory (Cold Spring Harbor, N.Y.), 22*(12), 622-632. doi:10.1101/lm.039602.115

Yang, M., Mahrt, E. J., Lewis, F., Foley, G., Portmann, T., Dolmetsch, R. E., . . . Crawley, J. N. (2015). 16p11.2 Deletion Syndrome Mice Display Sensory and Ultrasonic Vocalization Deficits During Social Interactions. *Autism Res, 8*(5), 507-521. doi:10.1002/aur.1465

Zhang, G., & Stackman, R. W. (2015). The role of serotonin 5-HT2A receptors in memory and cognition. *Front Pharmacol, 6*, 225. doi:10.3389/fphar.2015.00225

Zhou, W., Shi, Y., Li, F., Wu, X., Huai, C., Shen, L., . . . Qin, S. (2018). Study of the association between Schizophrenia and microduplication at the 16p11.2 locus in the Han Chinese population. *Psychiatry Res, 265*, 198-199. doi:10.1016/j.psychres.2018.04.049

Zufferey, F., Sherr, E. H., Beckmann, N. D., Hanson, E., Maillard, A. M., Hippolyte, L., . . . Jacquemont, S. (2012). A 600 kb deletion syndrome at 16p11.2 leads to energy imbalance and neuropsychiatric disorders. *Journal of Medical Genetics, 49*(10), 660. doi:10.1136/jmedgenet-2012-101203